

Fluorine-containing ferroelectric polymers: applications in engineering and biomedicine

Valentin V. Kochervinskii,^a Oleg V. Gradov,^b Margarita A. Gradova^b

^a JSC Scientific Research Institute of Chemical Technology,
Electrodnyaya ul. 2, stroenie 1, 111524 Moscow, Russian Federation

^b N.N.Semenov Federal Research Center for Chemical Physics, Russian Academy of Sciences,
ul. Kosygina 4, 119991 Moscow, Russian Federation

Highly polar fluorine-containing ferroelectric polymers based on vinylidene fluoride refer to the class of electroactive polymers suitable for various engineering applications. Under usual crystallization conditions, polycrystalline texture is formed, while after high-voltage polarization, it is transformed into a non-centrosymmetric structure, which gives rise to high piezoelectric and pyroelectric responses. Such materials can be used for pyroelectric energy conversion. Owing to high impact strength, ferroelectric polymers can serve as materials for alternative energy sources that convert dynamic impact energy into electricity. The non-linearity of electric response (owing to ferroelectricity) and high breakdown fields offer opportunity of using them in capacitive charge storage devices. The intense dynamics of the amorphous phase provides a rapid discharge of the stored energy into an external circuit. In view of the considerable fraction of the amorphous phase (~50%) in fluorine-containing ferroelectric polymers and high dielectric permittivity of the amorphous phase, it is possible to change the system entropy by applying an electric field. In the case of pulsed field, this provides a temperature drop; therefore, these materials (especially as composites) are promising for the design of solid-state refrigerators. The high thermoplasticity of these polymers is useful for the design of sensors (*e.g.*, microphones) with a patterned active membrane surface and enhanced characteristics. Biocompatibility and low acoustic impedance (close to the impedance of biological tissues) accounts for the possibility of using these polymers as biosensors. When domains are present in a ferroelectric film, strong local electric fields appear, which can affect the activity of living cells. Using the direct and reverse piezoelectric effect, it is possible to stimulate and control the functions of various tissues, including the nervous tissue.

The bibliography includes 463 references.

Contents

1. Introduction	1	8.2. Scaffolds for nervous tissue regeneration	21
2. Renewable energy sources	2	8.3 Scaffolds for bone and muscle tissue regeneration	22
3. Capacitive energy storage devices	5	8.4. Materials used in cardiology	23
4. Electrocaloric effect	9	8.5. Materials used in urology	24
5. Piezoelectric sensors based on ferroelectric polymers	12	8.6. Materials for connective tissue regeneration	25
6. Pyroelectric sensors and electrochromic energy converters	15	8.7. Artificial muscles	25
7. Materials for memory cells	19	8.8. Fabrication of fully functional tissue prostheses	26
8. Physical grounds for application of polyvinylidene fluoride-based materials in various fields of biomedicine	20	9. Conclusion	26
8.1. Smart scaffolds for non-invasive piezoelectric theranostics	21	10. List of abbreviations and symbols	27
		11. References	28

1. Introduction

Ferroelectric polymers represent a relatively new class of electroactive materials, which have recently attracted attention of both scientists and applied engineers.^{1–6} This is due to the specific properties of these materials caused by the chain nature of this type of condensed matter. These properties give rise to conditions needed to implement energy converters that cannot be obtained using inorganic crystals or oxide ceramics such as PZT (PbZrTi), PMN (PbMnNb), *etc.* There are data on appearance of ferroelectricity in a number of polymers such as polyurethanes,⁷ odd nylons⁸ and copolymers of vinylidene cyanide and

vinyl acetate.⁹ Materials based on fluorine-containing flexible-chain crystalline polymers are also ferroelectric. These compounds arouse the greatest interest, since the piezo(pyro)electric activity of polarized films based on them proved to be sufficient for practical implementation of energy converters.

This review addresses characteristics of the devices that use vinylidene fluoride (VDF) based polymers as active elements. These polymers (their molecular structure is schematically shown in Fig. 1) have non-classical piezo- and pyroelectricity mechanisms.^{5,6}

The structural organization of flexible-chain crystalline polymers involves folded crystals with the longitudinal

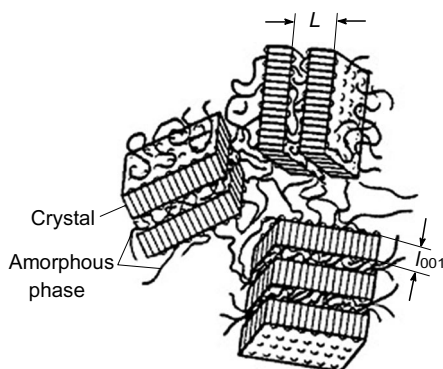


Figure 1. Schematic view of the molecular structure of crystalline polymers. The Figure was created by the authors on the basis of Ref. 3.

dimension l_{001} , which are packed in stacks with a large period L . These materials are structurally heterogeneous, since they contain amorphous regions without long-range order, along with the crystals. These flexible-chain polymers have glass transition temperatures $T_g \approx -40$ °C. This means that at room temperature (and above), the amorphous phase exhibits liquid-like dynamics, which is absent in crystals, that is, under these conditions, the polymers have both structural and dynamic heterogeneity. This feature, together with the high chemical stability, allows these polymers to be used for the formation of membranes and as matrices in the gel polymer electrolytes of lithium ion batteries.¹⁰ The liquid-like dynamics provides high ductility of the amorphous phase and, consequently, a non-classical piezoelectricity mechanism^{5, 6, 11, 12} and also gives rise to a huge electrostriction.^{5, 6, 13} The structure shown in Fig. 1 could also be useful for the design of new types of energy converters based on the ferroelectric polymers.

2. Renewable energy sources

After polarization, ferroelectric polymers become piezoactive. This means that applying a dynamic load to the material gives rise to a voltage between the electrodes. This effect underlies the operation of devices for conversion of mechanical impact energy to electric field energy.^{14–30} Below we consider some results obtained in this field using particularly ferroelectric polymers.

V.V.Kochervinskii. Doctor of Sciences (Physics and Mathematics), Chief Researcher at the Laboratory of Polymer Composite Materials, SRICT. E-mail: kochval@mail.ru

Current research interests: mechanisms of ferroelectricity, piezoelectricity and pyroelectricity in polymers; structural changes in the crystalline polymers under the electric fields; new energy sources and sensors based on triboelectricity effect and electrostriction in ferroelectric polymers; mechanisms of the influence of ferroelectric polymers on biological systems.

O.V.Gradov. Senior researcher at the Department of Dynamics of Chemical and Biological Processes, FRC CP RAS. E-mail: o.v.gradov@gmail.com

Current research interests: reaction-diffusion processes, biomimetic active scaffolds, membrane mimetic chemistry, microfluidics, soft matter physics.

M.A.Gradova. Ph.D (physical chemistry), Senior Researcher at the same Department, FRC CP RAS. E-mail: m.a.gradova@gmail.com

Current research interests: physical chemistry of tetrapyrroles, photoactive biomimetic systems, stimuli-responsive smart polymer materials, supramolecular nanocontainers for targeted drug delivery and theranostics.

The ferroelectric polymer films (like inorganic piezoceramics) have polar crystal planes randomly distributed throughout the bulk. After polarization, these planes assume a predominant direction, and the films thus acquire high piezo- and pyroresponse levels.

Currently, there is active search for renewable energy sources, and the considered polymers are of interest in this respect. They can be used, for example, for conversion of energy of the dynamic load encountered in the everyday life. Ferroelectric polymers are appropriate materials for this purpose for the following reasons. The presence of the amorphous phase in the polymer results in low Q -factors, *i.e.*, the materials are characterized by a broad dynamic range, which would produce a piezoresponse to a broad range of external dynamic load frequencies. Furthermore, due to the liquid-like dynamics of the amorphous phase at room temperature, these polymers have a high impact strength. Therefore, energy converters based on these polymers can be operated at very high amplitudes of external dynamic load, which is impossible in the case of inorganic piezoelectrics. In our opinion, such energy converters would be most efficient for harvesting and storage of the dynamic impact energy at busy highways, or for the ocean and sea wave energy.^{31–36}

The film area has a primary significance for the magnitude of the generated charge. To date, the problem of obtaining crystalline polymer film materials with a large surface area has been solved. The piezoelectric coefficients (d_{ij})[†] of this type of polymers are more than an order of magnitude lower than those of inorganic materials; however, large-area active elements based on the latter are either impossible or economically unfeasible. The effect of the area of a polyvinylidene fluoride (PVDF) active element on characteristics of a converter of a dynamic load to electricity is depicted in Fig. 2. According to Markose *et al.*,³⁷ the effect of the film size is most pronounced in the case of high dynamic load frequency. In this case, a twofold increase in the area leads to an almost two orders of magnitude increase in the generated energy. The lattice symmetry of fluorinated ferroelectric polymers results in non-zero piezoelectric coefficients d_{24} and d_{15} .^{5, 6, 12} An example of a device in which these coefficients operate was noted by Schweisinger *et al.*³⁴ It was shown that flow turbulence (in air or in water) gives rise to film bending and, hence, charges on the electrodes.

The large area and high flexibility of piezoactive polymer films open up the possibility of quite unexpected applications of these films. For example, growth of simple biological structures (biofouling) takes place on the marine

[†] For names and designations of the piezoelectric coefficients, see, for example Refs 5 and 6.

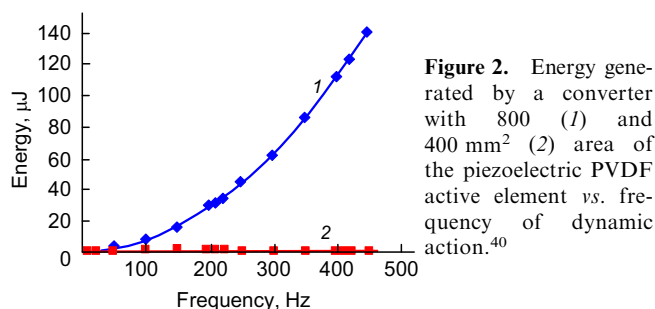


Figure 2. Energy generated by a converter with 800 (1) and 400 mm² (2) area of the piezoelectric PVDF active element vs. frequency of dynamic action.⁴⁰

ship hulls with time; this changes the flow hydrodynamics and increases the fuel consumption. In order to overcome this problem, Latour and Murphy^{38,39} proposed an anti-fouling sonar made of a piezoelectric PVDF film, which was attached to the ship bottom. The film flexibility provided a good acoustic contact between the ship hull and water. When an alternating voltage was applied to the film, the film generated acoustic waves of a certain frequency. The authors compared the volumes of fouling growth in the control sample and in the sample with the sonar. It was found that the acoustic near field generated in the latter case sharply decreased the fouling growth. It is known that acoustic impedance, which depends on the density of the medium (ρ) and on the speed of sound (v_s) in the medium, for fluorine-containing ferroelectric polymers is close to that of water. This means that wave processes at the interface between the two media are characterized by a minimum reflection; thus, the conversion coefficient is higher for a piezoelectric PVDF film, other things being equal.

Polarized polymers exhibit a pyroelectric effect, which implies generation of surface charge induced by thermal heating. Therefore, large-area pyroelectric elements, first, can serve for simply designed security alarm systems (intrusion detection sensors, protection panels, *etc.*) and, second, may be useful for the design of pyroelectric converters, which would convert thermal energy into electricity.^{40–43} According to Olsen *et al.*,⁴⁰ an external electric field with the strength $E = 50 \text{ MV m}^{-1}$ applied to a pyroelectric VDF – trifluoroethylene (TrFE) copolymer film at a temperature step of 20° resulted in a generated energy density of 0.1 J cm^{-3} , which is half that generated using PZT ceramics. However, ferroelectric polymers are characterized by high coercive fields; therefore, it can be expected that an increase in the field strength in these experiments would affect the amount of stored energy. Indeed, it was shown in relation to PVDF that, as the field increases up to 75 MV m^{-1} , the stored energy density (at a temperature step of 60°) increases to 0.5 J cm^{-3} . Hence, in the design of pyroelectric converters, preference should be given to polymeric pyroelectric materials, as they can provide greater areas of the active elements.

Great surface areas can be attained for fluorinated ferroelectric polymers by using them as microfibres, which are manufactured by electrospinning. These polymers were used to design nanogenerators in which polarized microfibres of PVDF or its copolymers served as active elements.⁴⁴ It is of interest to compare the energy conversion efficiency (η) in PVDF films of different thickness and in nanogenerators based on microfibres of various diameters. This value was calculated as the ratio of the generated electric field energy to the mechanical strain energy.

In the case of solid films, the generated charge density is markedly lower at the same strain (Fig. 3). This implies that the η value is approximately an order of magnitude higher for microfibres than for films. Transition from films to microfibres is accompanied by an increase in the effective area; therefore, the obtained data are in qualitative agreement with the results of Markose *et al.*³⁷ A similar conclusion was drawn by Wu *et al.*,⁴⁵ who found that the piezoelectric coefficient d_{33} for a solid PVDF film was 50% lower than that for microfibres. The piezoelectric coefficient e_{ij} was also higher for microfibres

$$e_{ij} = \left(\frac{\partial D_i}{\partial x_j} \right)^E \quad (1)$$

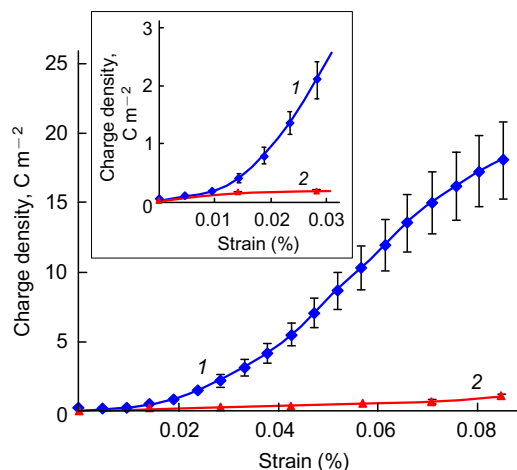


Figure 3. Strain-induced charge density vs. strain in polarized PVDF fabricated as microfibres (1) and thin films (2).⁴⁴ Published with permission from the American Chemical Society.

Here D is the electric displacement, x is strain, and the superscript E means that the electric field is zero.

One more important circumstance is the non-linearity of variation of e_{ij} in microfibres with increasing strain; this is especially obvious for low strains (see the inset in Fig. 3). Most likely, this effect is related to the electrostriction constant, which differs between isotropic and oriented samples.^{12,46,47} Drawing more substantiated conclusions requires detailed investigation of the structure of polymer microfibres at the nanoscale level with the possibility of monitoring structural changes induced by strain.

Triboelectric electronanogenerators (TENG) are of interest to address the problem of mechanical impact energy utilization. These are energy converters based on triboelectricity,^{48,49} *i.e.*, charge generation on the surface of a moving dielectric due to the friction force. For thin PVDF films at a periodic compressive force of 50 N, an output power of 3.74 mW was obtained.⁴⁹ If PVDF microfibres were used, by appropriate adjustment of experimental conditions, it was possible to attain a power density of 26.6 W m^{-2} (Ref. 49). Microfibres bear a negative charge; with allowance for this fact, a TENG design was proposed, which produced a voltage of 210 V at a working area of $6 \times 5 \text{ cm}^2$ (Ref. 50). An increase in the roughness of micro-fibre surface (which increases the friction coefficient) in this nanogenerator was accompanied by an increase in the generated voltage. It is evident that the above-mentioned triboelectricity is not directly connected with ferroelectricity, but is a consequence of the strong electron-withdrawing effect of fluorine atoms. Indeed, a device with an output voltage of 200 V and a circuit current of $10 \mu\text{A}$ was implemented on the basis of a non-ferroelectric copolymer of tetrafluoroethylene (TFE) with hexafluoropropylene (HFP) shaped as nanowires as a result of arising triboelectricity.⁵¹

The heat released on friction (usually, this is a parasitic effect) is expected to decrease the efficiency of these devices. Zi *et al.*⁵² proposed to recover this heat by introducing a polarized PVDF film into the hybrid nanogenerator. The pyroelectric effect in the film would result in generation of an additional electrical energy.⁵² The diagram of this device is depicted in Fig. 4.

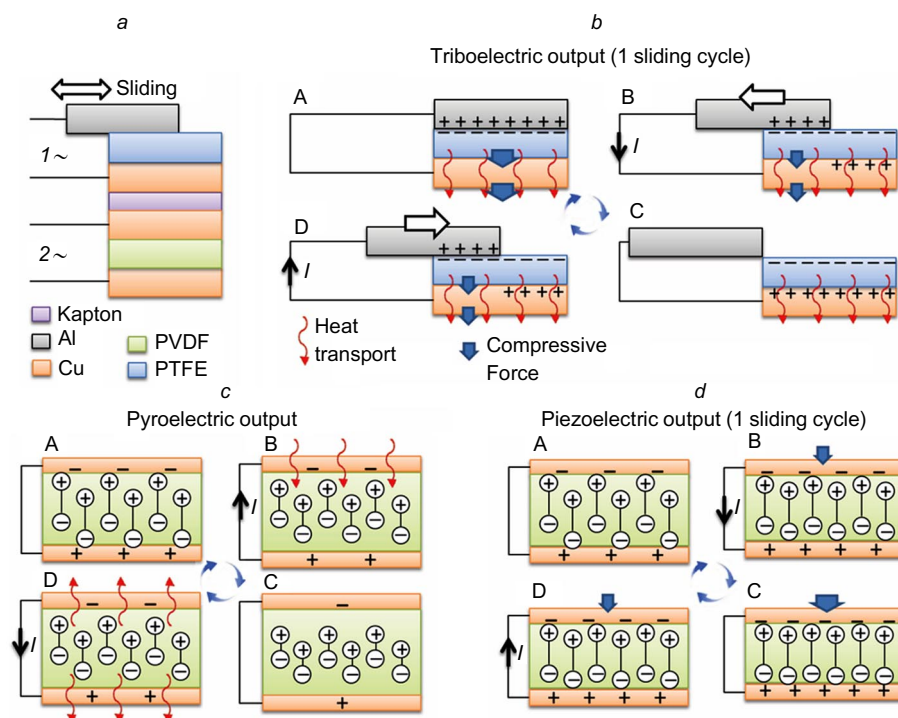


Figure 4. Diagrams of the multilayer design of a hybrid nanogenerator (a), operation mechanisms and stages (A–D) of triboelectric (b), pyroelectric (c) and piezoelectric (d) parts of the hybrid cell circuit.⁵² For 1, 2, see the text. Published with permission from John Wiley and Sons.

Two mechanisms of energy generation operate in the considered multilayer system made of different materials (see Fig. 4a):

- the proper triboelectric effect (cycle 1);
- pyro(piezo)electric effect (cycle 2).

The surface of the polytetrafluoroethylene (PTFE) film with a one-side copper coating bears a negative charge, which is balanced by the charge of the covering metal (aluminium). The choice of PTFE is due to the fact that it possesses a good electret effect, since it steadily retains the arising triboelectric charge owing to low conductivity. When the aluminium plate slides, the Teflon layer is heated due to friction, and the heat is transferred through a Kapton (polyimide) layer with high heat conductivity to the polarized PVDF layer, in which pyroelectricity is generated. Simultaneously, upon this sliding, the normal component of the force would induce a piezoelectric effect in the PVDF film; the response gives rise to a piezoelectric coefficient d_{33} . As a result of these processes, the periodic motion of the upper electrode would give rise to open-circuit voltage V and the short-circuit current I in the hybrid nanogenerator of cycle 2 (see Fig. 4a). According to the conclusions drawn by Wang and co-workers,^{53,54} both values depend on the area of the active element, which may be rather large for the considered materials.

The influence of the triboelectric effect on the characteristics of the hybrid nanogenerator as a result of periodic load is reflected in Fig. 5. It can be seen that the peak open-circuit voltage reaches 1200 V, which is several-fold greater than in the case of active element based on PVDF microfibre.⁵⁰ Presumably, due to higher conductivity, the latter is less efficient as an electret. When the external load resistance varies, the current and voltage vary in opposite directions (see Fig. 5c). The peak power density generated with a 140 MOhm load is 146 mW m^{-2} .

It is of interest to compare the voltages and currents generated by a device that operates as either a triboelectric or piezo(pyro)electric nanogenerator (PPENG) with those

generated by a combined operation of these devices (see Fig. 4).

When a periodic load is used, the currents generated by the hybrid circuit and separately by TENG and PPENG are 0.59, 0.32 and 0.26 μA , respectively. The current generated in a circuit with a capacitive load was used to charge a supercapacitor with the capacitance C , which reached 41.9 μF . The higher currents for the hybrid circuit should be accompanied by an increase in the derivative dV/dt according to the relation

$$I = \frac{dq}{dt} = C \frac{dV}{dt} \quad (2)$$

where q is charge, t is time.

The data presented in Fig. 6 confirm this conclusion. Indeed, the above derivative is approximately twice as large for the hybrid circuit than for TENG or PPENG circuit. This means that the described hybrid circuit can provide a higher charging rate of the supercapacitor.

Yet another sort of a hybrid nanogenerator based on PVDF microfibrils was proposed by Chen *et al.*;⁵⁵ the design of this device implies complete encapsulation of the active elements. This made it possible to fabricate a nanogenerator for conversion of the energy of rain water drops into electric field energy. When the dropping rate was relatively high, the maximum voltage amplitude reached 20 V, and it varied linearly as a function of the dropping rate. Modification of the design of this nanogenerator opened up the possibility of measuring the aerodynamic characteristics of the air flow. It was shown that an increase in the wind velocity from 3.4 to 15.4 m s^{-1} led to an increase in the output voltage amplitude from 4 to 15 V, also following a linear dependence. Thus, fluorine-containing ferroelectric polymers can be used to manufacture electric nanogenerators with rather high parameters. This is a highly important conclusion, since the considered materials are biocompatible, and nanogenerators based on them can be inserted into

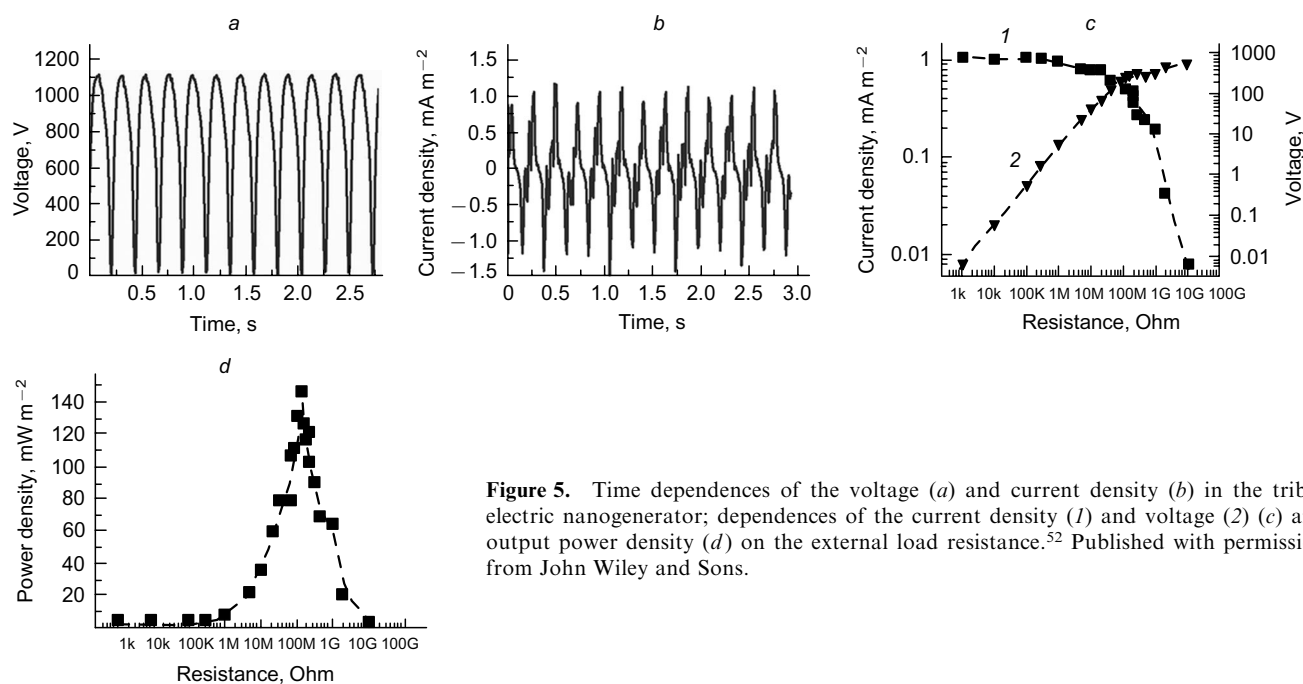


Figure 5. Time dependences of the voltage (a) and current density (b) in the triboelectric nanogenerator; dependences of the current density (1) and voltage (2) (c) and output power density (d) on the external load resistance.⁵² Published with permission from John Wiley and Sons.

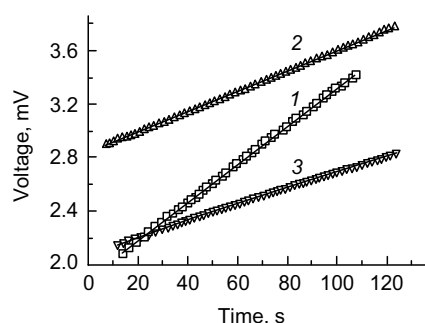


Figure 6. Voltage of a supercapacitor plotted vs. time of action of periodic load in a hybrid circuit (1) and separate circuits of tribo- (2) and piezo(pyro)electricity (3). dV/dt , mV s⁻¹: (1) 0.01418, (2) 0.00755, (3) 0.00609.⁵² Published with permission from John Wiley and Sons.

living organisms and support the life cycle of cells of various tissues.

3. Capacitive energy storage devices

Radio engineering components such as capacitors^{56–80} can operate at high voltage. They are often fabricated using dielectric polymers^{59–61} such as polyethylene (PE), polypropylene (PP),^{62–65} polyethylene terephthalate (PETF)⁶⁶ or polyimide (PI).⁶⁷ The first three polymers are crystalline; Umemura *et al.*⁶⁸ noted the effect of the supramolecular structure on the high-voltage characteristics of the polymers. One of the problems solved by using polymer dielectrics is energy accumulation in a capacitor followed by its transfer to an external circuit. The general expression for the volumetric energy density stored in a capacitor (W_e) with an applied electric field of strength E has the form

$$W_e = \int D(E)dE \quad (3)$$

It can be seen that the stored energy is mainly determined by the fields that are tolerated by the above polymers; the breakdown fields for them are relatively high, ranging from 300 to 700 MV m⁻¹ (Refs 62–67). The energy stored in the capacitors in which the insulator is represented by a linear dielectric polymer (polycarbonate, polyphenylene sulfide, PETF or PI) is approximately 0.5–1.5 J cm⁻³; for biaxially oriented polypropylene (BOPP), this value reaches 5 J cm⁻³ (Ref. 65). The modern technology requires materials with higher W_e values; therefore, for this purpose, it is appropriate to use non-linear materials, in particular, ferroelectric polymers.

The stored energy in a ferroelectric capacitor can be estimated from relation (3) and from the size of areas highlighted in violet in Fig. 7; the area confined by the hysteresis curve characterizes the energy that is converted to the internal energy. The amount of stored energy can be increased by converting the ferroelectric into the relaxor state. This is accomplished by a targeted chemical or physical modification of the structure of a ferroelectric polymer that would decrease the area encompassed by the hysteresis curve.

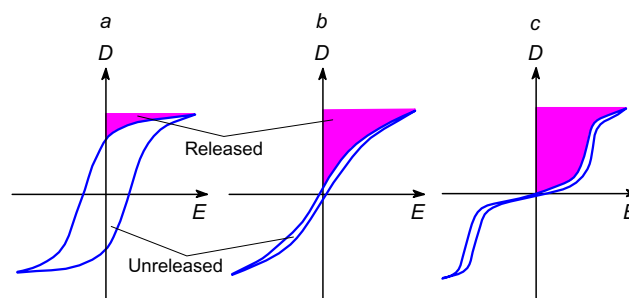


Figure 7. Schematic view of dielectric hysteresis curves for conventional (a) and relaxor ferroelectrics (b) and antiferroelectric (c).⁷⁹ Published with permission from ACS.

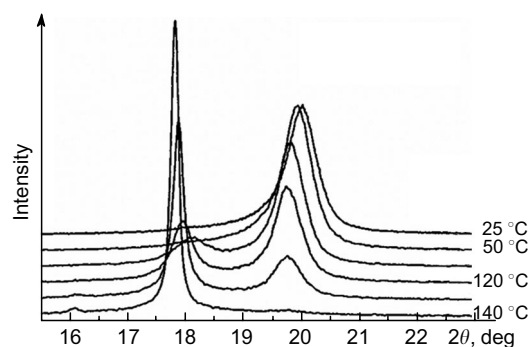


Figure 8. Temperature dependences of X-ray diffraction curves for the P(VDF–TrFE) copolymer (80 : 20 ratio).⁶⁹ Published with permission from AIP Publishing.

Ferroelectric materials (including polymers) are characterized by the Curie point (T_C) at which domains pass to the paraelectric state and spontaneous polarization regions are destroyed. This structural transition is reflected in Fig. 8 for the P(VDF–TrFE) copolymer. It can be seen that a temperature rise induces transition of the ferroelectric phase (with a reflection at greater angles) into a less densely packed paraelectric phase. A capacitor based on this copolymer is expected to have a rather high stored energy density at high temperature. However, in this case, it is impossible to ensure high fields due to increased conductivity; therefore, it is desirable to select conditions for an external stimulus that would promote this transition without heat treatment. In our opinion, a promising approach is the radiation-induced chemical modification of polymers. This is evidenced by the results of some studies (e.g.,^{69–74}). The X-ray diffraction patterns for the initial P(VDF–TrFE) samples and those irradiated with accelerated electrons are shown in Fig. 9a. It can be seen that at a particular irradiation dose, ferroelectric \rightarrow paraelectric solid-phase transition takes place (cf. Fig. 8).

Also, the data presented in Fig. 9b demonstrate the expected decrease in the remanent polarization (P_r) and, correspondingly, a potential increase in the stored energy. The mentioned radiation-induced phase transition was confirmed independently by other researchers.^{69,70,74} Apparently, in these transitions, it is necessary to take into account the radiation-induced chemical reactions that take place under irradiation of the polymers. This is indicated by

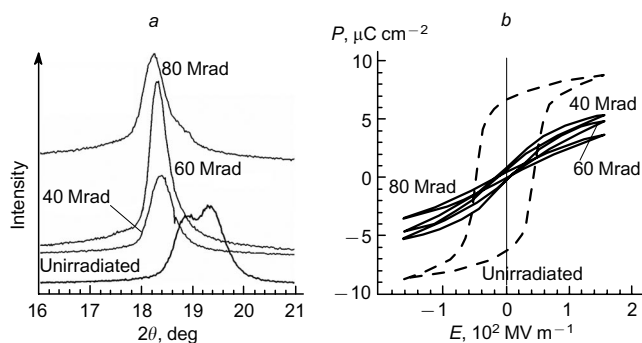


Figure 9. X-Ray diffraction (a) and dielectric hysteresis (b) curves for isotropic samples of the P(VDF–TrFE) copolymer (50 : 50) in the pristine state (dashed lines) and after irradiation with electrons with an energy of 2.55 MeV up to different doses.⁷³ P is polarization. Published with permission from AIP Publishing.

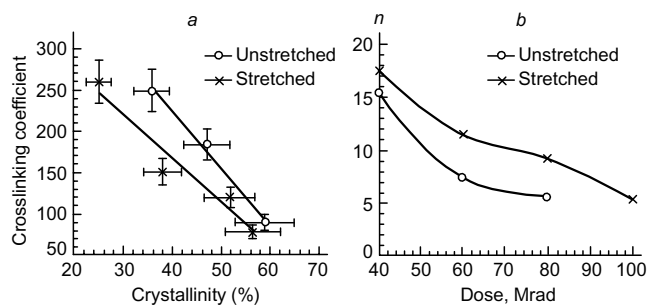


Figure 10. Crosslinking coefficient vs. degree of crystallinity (a) and number of repeating units between neighbouring crosslinks vs. irradiation dose at 95 °C (b) for the P(VDF–TrFE) copolymer (50 : 50).⁷³ Published with permission from AIP Publishing.

the data pointing to the appearance of various radicals upon irradiation of PVDF and its copolymers (see review¹³ and references cited therein).

Manifestation of these effects is depicted in Fig. 10. The crosslinking coefficient between the neighbouring chains was found from experiments on swelling of irradiated polymers and then used to estimate the average number (n) of repeated units between the crosslinks. It was shown that n decreases with increasing irradiation dose. The decrease in the crosslinking coefficient with increasing crystallinity indicates that the crosslinks occur between chains of the amorphous phase. At room temperature, this phase of the considered polymers (as noted above) exists in the liquid-like state in terms of dynamics. Presumably, characteristics of the cooperative mobility of these chains should influence the radiation-induced chemical reactions that give rise to crosslinks.

One more approach to the conversion of ferroelectric polymers into the relaxor state includes chemical modification during the polymer synthesis. It is necessary to consider copolymerization of VDF (major component) with other comonomers. It is known that VDF polymerization is always accompanied by the appearance of defects that result from head-to-head (tail-to-tail) attachment of monomer units; the defects have a certain influence on the resulting structure of the polymer.^{5,6,75} Copolymerization of VDF with tetrafluoroethylene is actually reduced to accumulation of these defects, which is manifested, in particular, as an increase in the fraction of chains in the planar zigzag conformation in the PVDF microstructure. A special role in VDF copolymerization belongs to the TrFE comonomer, which (unlike TFE) is polar. In the presence of TrFE, the fraction of planar zigzag conformations in VDF chains increases most appreciably; as a result, the dipole moment of the polar crystals increases.^{5,6,75} The highest remanent polarization was inherent in particularly these copolymers (see, for example, Fig. 9b). In our case, conversely, P_r needs to be decreased without a noticeable decrease in the breakdown voltage. This is done by using asymmetric comonomers containing, for example, chlorine atoms or hexafluoropropylene units. In both cases, the long-range order along the PVDF chain is disrupted and the capability for crystallization and formation of the domain structure decreases.

The films formed by the vinylidene fluoride–chlorotri-fluoroethylene (CTFE) copolymer⁷⁶ were actually noted to form a hysteresis loop with a small area (like that shown in Fig. 9b). This is characteristic of relaxor ferroelectrics. A

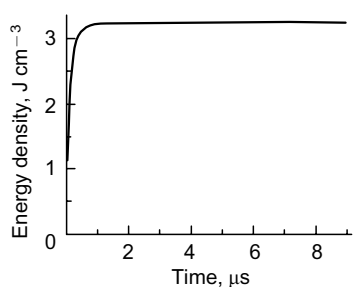


Figure 11. Time dependence of the discharge energy density at 1 kΩ load (charging with a field of 253.5 MV m⁻¹) for a capacitor involving films of the P(VDF–CTFE) copolymer (91:9).⁷⁶ Published with permission from the American Association for the Advancement of Science.

practically important conclusion follows from analysis of the time dependence of the discharge energy density, which is shown in Fig. 11. It can be seen that discharge of the stored energy to the indicated external load takes place over ~1 μs. This corresponds to output power of ~3 MW per unit volume of the copolymer. The same order of magnitude for these values was established for capacitors with oriented PVDF and VDF–hexafluoropropylene copolymer films.⁷⁷ The above value of ~1 μs is also characteristic of the average relaxation time of the cooperative chain mobility in the amorphous phase at room temperature.^{5, 6, 75} Hence, particularly the above-noted form of motion in the polymer controls the rate of discharge of the stored energy to an external circuit.

Copolymers of VDF with HFP can also serve as materials for the capacitive energy storage devices.^{77–79} Films of these copolymers are characterized by very high breakdown fields (~700 MV m⁻¹) and, as a consequence, the stored energy density reaches ~25 J cm⁻³ (Fig. 12). It is worth noting that upon temperature rise to 90 °C, the breakdown voltage decreases, but only slightly.

The data shown in Fig. 12 were obtained for a copolymer with a low HFP content. As the HFP concentration increased from 3.2 to 15.4 mass %, the film crystallinity decreased from 46 to 25% (with the film preparation conditions being the same). No significant changes were noted in the breakdown voltage, and the hysteresis loss (see Fig. 7) proved to be lower for the film with a low crystallinity.⁷⁹ Qualitatively similar results were also obtained in a later study⁷⁷ in which the crystallinity (and, hence, the proportion of the α-phase) was shown to decrease twofold for an HFP content of 4.5%. This sample oriented in a 850 MV m⁻¹ field stored 27.7 J cm⁻³ of energy; in the opinion of the authors,⁷⁷ this makes these materials promising for supercapacitors.

One more way of chemical modification of the PVDF backbone is the preparation of terpolymers by introducing CTFE or HFP comonomer, apart from TrFE.^{76, 80} In this

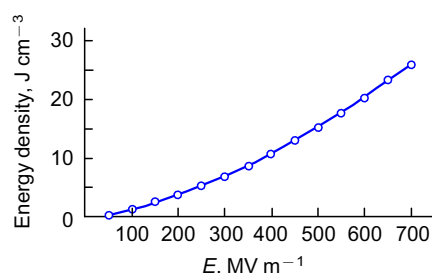


Figure 12. Dependence of the stored energy density vs. field strength for the P(VDF–HFP) copolymer.⁷⁸ Published with permission from AIP Publishing.

case, the stored energy obtained in 400 MV m⁻¹ field was close to that observed for P(VDF–HFP) copolymer films.^{77, 78}

Finally, the last method for chemical modification of PVDF is related to grafting of polystyrene (PS)^{81, 82} or polymethacrylic^{83–85} blocks to the VDF copolymer backbone. In the case of grafting of PS blocks to the terpolymer, the hysteresis loss decreased only at high fields; grafting of 14% PS blocks to the terpolymer during crystallization gave rise to a morphology composed of stacks of lamellar crystals (see Fig 1). A specific feature is that this morphology was retained at a temperature of 180 °C, which is above the melting point (*i.e.*, the crystals are already melted). The cause for this feature is not discussed, although its consequences may be of interest. When methacrylic blocks were grafted to the same terpolymer, the hysteresis loss energy of all graft terpolymers was lower. In the case of graft terpolymer, an almost linear $D(E)$ dependence was observed, which is indicative of a low hysteresis loss energy (Fig. 13).

It is known that methacrylic polymers are readily miscible with the considered fluorine-containing ferroelectric polymers.^{5, 6, 75} It cannot be ruled out that exactly this feature is responsible for the fact that the polymers obtained after grafting withstand higher operating voltages than the starting terpolymers. The breakdown characteristics were studied in detail in relation to graft terpolymers with a PEMA block. Figure 14 reflects the results of treatment of experimental data (obtained in terms of the two-parameter

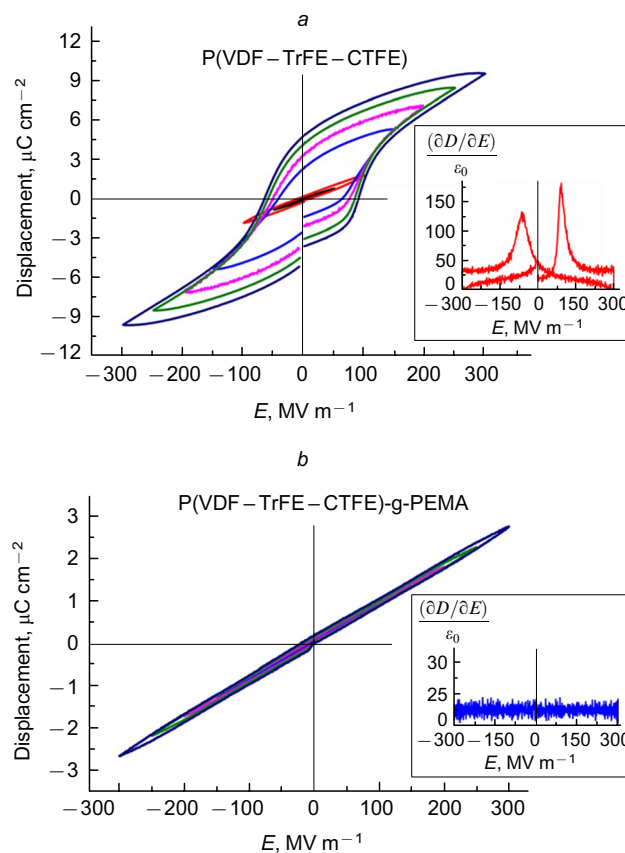


Figure 13. Hysteresis curves in different fields for the initial terpolymer (a) and after grafting of poly(ethyl methacrylate) (PEMA) (b); the insets show the experimental data for the highest applied field.⁸⁵ Published with permission from AIP Publishing.

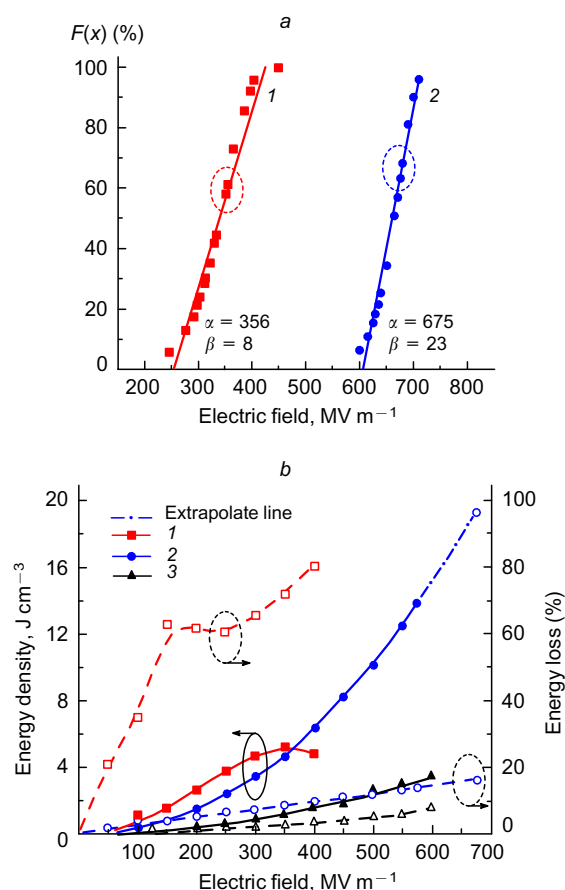


Figure 14. Breakdown characteristics in the Weibull coordinates (a) and field dependences of the stored energy (continuous lines and dark points) and energy loss (dashed lines and light points) (b) in the capacitors based on films of the initial terpolymer and after PEMA grafting.⁸⁵ (1) P(VDF–TrFE–CTFE), (2) P(VDF–TrFE–CTFE)-g-PEMA, (3) BOPP. The ellipses mark characteristic fields. Published with permission from AIP Publishing.

Weibull model),⁶⁶ according to which a statistical set of a large number of breakdown field values (E_b) can be described by the function

$$F(x) = 1 - \exp\left[-\left(\frac{x}{\alpha}\right)^{\beta_b}\right] \quad (4)$$

where x is the current E_b value, α is some characteristic field at which at least 63.2% of the test samples are broken down; β_b characterizes the variance of E_b around the mean value. For the graft terpolymer, the most probable breakdown

field is twice as high as that for the initial sample (Fig. 14 a). For the latter sample, β_b is ~ 3 times lower; this indicates that the distribution function $F(x)$ around the mean value is more narrow in the graft terpolymer.

According to relation (3), this pronounced difference in the breakdown characteristics of the samples should result in a marked difference in the stored energy, which is confirmed experimentally (Fig. 14 b). Owing to high breakdown voltage, the stored energy is several-fold higher in the graft terpolymer. A biaxially oriented polypropylene film was chosen as the linear dielectric reference sample. The breakdown field for this sample was comparable with that of the graft terpolymer; however, in the latter case, the stored energy was ~ 4 times higher. Thus, it follows that ferroelectric polymers are preferred for the capacitive energy storage devices based on polymer dielectrics.

One more method for increasing the energy stored in a capacitor is based on the preparation of PVDF blends.^{86,87} In one case, PVDF was blended with the P(VDF–HFP) copolymer by co-crystallization in the α -phase from a common solvent. Characteristics of these films with various component ratios are summarized in Table 1. It can be seen from the presented data that an increase in the PVDF fraction (up to 50:50 ratio) is accompanied by increase in some characteristics such as dielectric permittivity, elastic modulus, breakdown voltage and heat of melting and by increase in the energy stored in the capacitor, which can reach (according to published data) 30 J cm^{-3} . Unfortunately, the authors^{86,87} did not give a convincing explanation to these facts.

In another case, the same authors obtained a material based on a PVDF blend with VDF oligomer by co-crystallization (in the polymorphic α -phase) of the components from a common solvent. When the PVDF content in the blend increased to 40%, the energy stored in the capacitor was very high (27 J cm^{-3}). The model proposed by Rahimabady *et al.*⁸⁷ can be stated as follows. It is believed that oligomer molecules are located in the amorphous phase of PVDF and increase its density. This hypothesis could be verified, for example, by small-angle X-ray diffraction. It remains unknown why oligomer molecules, which have the same chemical structure as PVDF, do not enter the crystals formed by long polymer macromolecules. It was noted that at high voltage, D reaches 162 mC m^{-2} , which is higher than the theoretically predicted value of 130 mC m^{-2} (Refs 5, 6, 75).

The response of the sample to an external electric field is called macroscopic, as it characterizes averaging over a large volume including both crystals and amorphous regions. It is believed that this response is mainly provided by the polar crystals of the β -phase; therefore, there are very

Table 1. Physical characteristics of PVDF mixtures with P(VDF–HFP) copolymer.⁸⁶

Composition (%)		Dielectric permittivity		Elastic modulus, GPa	Breakdown field, MV m^{-1}	Heat of melting, J g^{-1}	Volumetric energy density, J cm^{-3}
P(VDF–HFP)	PVDF	in low fields	in high fields				
100	0	8.4	16.1	2.40	720	46.0	19.3
90	10	8.5	16.7	2.65	740	46.2	20.1
80	20	8.7	17.1	2.71	751	47.5	21.9
60	40	8.9	18.3	2.78	807	48.1	23.5
50	50	9.1	19.6	2.90	854	48.2	30.1
40	60	9.0	–	2.10	560	45.5	12.8
0	100	8.0	–	1.84	370	–	4.9

few studies addressing high-voltage polarization of isotropic PVDF and its copolymer samples crystallized in the non-polar α -phase. The publication by Rahimabady *et al.*⁸⁷ is one of such studies. It can be assumed that high-voltage polarization of the hysteresis type in these materials occurs by a different mechanism.⁸⁸ Unlike the permanent dipoles in the β -phase crystals, the appearance of macroscopic dipoles is due to the field-initiated specific motion in the non-polar α -phase crystals. The proposed mechanism can explain (at least qualitatively) the contradiction between the calculated and experimental⁸⁷ values of D , but a quantitative explanation is still missing.

The formation of a texture in crystalline thermoplastic polymers makes it possible to increase the remanent polarization by means of uniaxial stretching. This was noticed, for example, for VDF copolymers with tetrafluoroethylene⁸⁹ or trifluoroethylene.⁷³ As shown in relation to VDF copolymers with chlorotrifluoroethylene⁷⁶ and tetrafluoroethylene⁸⁹ and to the P(VDF–TrFE–CTFE) terpolymer,⁹⁰ this texture increases the breakdown voltage. For isotropic terpolymer films, it was found that the breakdown voltage can be increased by a factor of two by narrowing the molecular-mass distribution.

The breakdown fields are important for ferroelectric polymers. Usually, the breakdown characteristics are calculated in terms of the Stark–Garton model,^{91–93} according to which

$$E_b = 0.6 \left(\frac{Y}{\varepsilon_0 \varepsilon_r} \right)^{0.5} \quad (5)$$

where Y is the Young's modulus; ε_0 and ε_r are the dielectric permittivity of vacuum and relative dielectric permittivity of the medium, respectively. This relationship shows that dielectrics with high Young's modulus can resist the Maxwell stress that appears due to the action of electrostatic forces from the electrodes. However, the application of this relationship to the considered polymer dielectrics is not quite correct for a number of reasons. In practice, relationship (5) holds for the brittle fracture mechanism. The polymers discussed here demonstrate a viscoelastic behaviour, and the ultimate tensile strength corresponds to very high strains where the structure of the material has markedly changed with respect to the initial one. The situation is aggravated by the fact that both chemical⁹⁴ and solid-phase polymorphic transformations^{5,6,95} can take place in fluorine-containing ferroelectric polymers (which may be polymorphic in the crystalline phase^{5,6,75}) under the action of strong fields. Obviously, this is expected to influence the Young's modulus. The structural changes that take place in these fields are indirectly indicated by the great electrostrictive strains particularly in the relaxor ferroelectrics in question.^{5,6,13}

4. Electrocaloric effect

When a dielectric is placed in an electric field, its entropy changes. According to the laws of thermodynamics, ferroelectrics (in the general case, dielectrics) are cooled upon depolarization under adiabatic conditions. This principle may underlie the operation of the solid-state cooling systems.^{96,97} The entropy ΔS and temperature ΔT changes taking place upon field switching on and off can be written as follows:

$$\Delta S = - \int_{E_1}^{E_2} \left(\frac{\partial D}{\partial T} \right)_E dE \quad (6)$$

$$\Delta T = - \frac{T}{\rho} \int_{E_1}^{E_2} \frac{1}{C_E} \left(\frac{\partial D}{\partial T} \right)_E dE \quad (7)$$

where C_E is the heat capacity of the material.

The contribution of ferroelectric polymers to the electrocaloric effect (ECE) can be found by analyzing ECE characteristics for a number of inorganic ferroelectric materials. For example, for ferroelectric ceramics and single crystals (KH₂PO₄, SrTiO₃ and PZT of various compositions), $\Delta S < 2.9 \text{ J}(\text{kg K})^{-1}$ and $\Delta T < 2.5 \text{ }^\circ\text{C}$.^{98,99} As follows from relations (6) and (7), the small entropy and temperature changes are mainly caused by low breakdown fields ($< 3 \text{ MV m}^{-1}$) in these materials.

Higher values, $\Delta T = 9\text{--}12^\circ$, were obtained for thin films of antiferroelectric ceramics at room temperature, but entropy changes were insufficiently large: 8 and $9.7 \text{ J}(\text{kg K})^{-1}$ (Refs 100, 101). This is a considerable drawback, since practical use of this effect requires greater entropy changes.^{102,103}

In terms of a phenomenological description of ferroelectric materials, relations (6) and (7) can be written in the form

$$\Delta S = - \frac{1}{2} \beta D^2 \quad (8)$$

$$\Delta T = - \frac{1}{2C_E} \beta T D^2 \quad (9)$$

where β is the coefficient of expansion of the Gibbs energy in terms of the even powers of D .

The D value is measured, while β can be calculated. Hence, using relations (8) and (9), it is possible to predict ECE for various ferroelectric materials. It is known that the parameter D is several times higher for inorganic materials than for ferroelectric polymers. Meanwhile, the β value for the latter is of the order of $\sim 10^7$, while that for inorganic materials is $\sim 10^5$. If the experiment is carried out near the ferroelectric \rightarrow paraelectric phase transition temperature, it is necessary to take into account the heat of the transition (Q), as it makes a contribution to the entropy ($Q = T\Delta S$). Consider the relevant estimates for a classical ferroelectric, triglycine sulfate. According to Jona and Shirane,¹⁰⁴ the heat of this transition is 2 kJ kg^{-1} , which corresponds to an entropy change of $6.1 \text{ J}(\text{kg K})^{-1}$. Meanwhile, for example, for the P(VDF–TrFE) copolymer (68 : 32 ratio), the heat of phase transition is 21 kJ kg^{-1} , which corresponds to an isothermal entropy change of $56 \text{ J}(\text{kg K})^{-1}$ (Ref. 105), *i.e.*, it is approximately an order of magnitude higher than that for triglycine sulfate.

In view of the above, it is interesting to analyze the experimental results concerning ECE in the fluorine-containing ferroelectric polymers, for example, the P(VDF–TrFE) 55 : 45 copolymer (Fig. 15), for which characteristics of the ferroelectric \rightarrow paraelectric transition were studied in detail. In the vicinity of this phase transition, the maximum entropy change and decrease in the temperature take place, and a considerable change in $\partial D/\partial T$ is detected (see Fig. 15*a*). According to equations (8) and (9), this should lead to the experimentally observed increase in ΔS and ΔT .

The considered polymers are partly crystalline and contain a large portion of amorphous phase (see Fig. 1 and the comment to it); therefore, the question arises of how

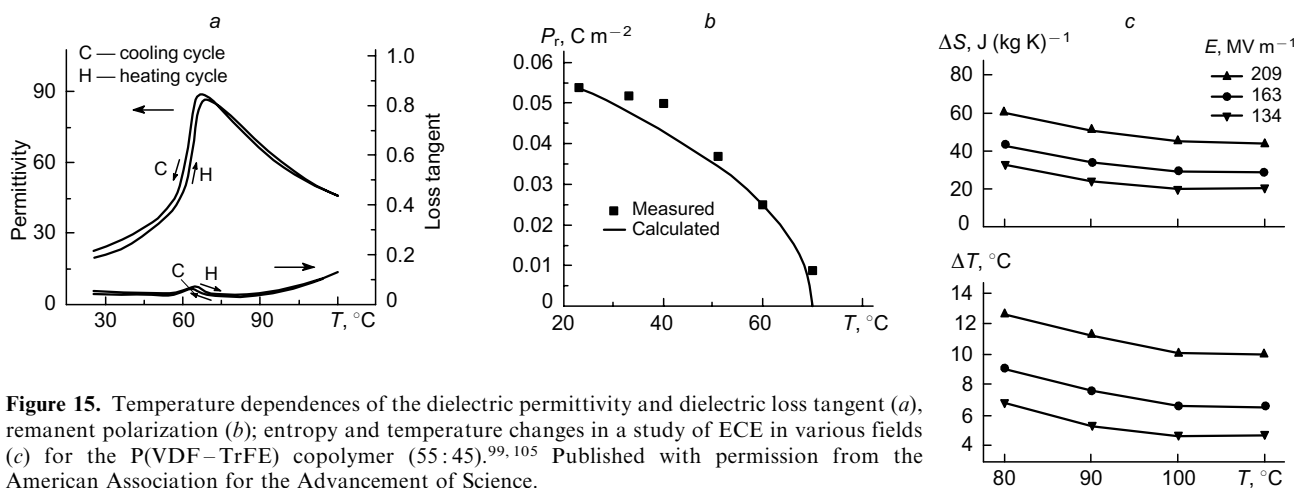


Figure 15. Temperature dependences of the dielectric permittivity and dielectric loss tangent (a), remanent polarization (b); entropy and temperature changes in a study of ECE in various fields (c) for the P(VDF-TrFE) copolymer (55:45).^{99,105} Published with permission from the American Association for the Advancement of Science.

the degree of crystallinity affects the ECE characteristics.¹⁰⁶ This question was addressed by studying blends of the P(VDF-TrFE) copolymer with polymethyl methacrylate (PMMA), which is almost fully compatible with PVDF.^{5,6,75} According to differential scanning calorimetry (DSC) data, when the PMMA content in the blend increased to 30 mass %, the degree of crystallinity decreased from 68 to 20%; under the same conditions of ECE observation (initial temperature and field), this resulted in a decrease in both ΔS and ΔT by a factor of 3.8. Among other reasons, this is due to a decrease in the concentration of copolymer crystals in the amorphous matrix. The PVDF and PMMA chains in the amorphous phase are compatible, since the DSC data detect one glass transition process.¹⁰⁷ The glass transition temperature for PVDF is approximately -40 °C, and that for PMMA is about 110 °C. Therefore, an increase in the PMMA content in the blend leads to increasing relaxation time of the cooperative micro-Brownian dynamics in the amorphous phase, which can participate in high-voltage polarization processes.¹¹ The amorphous phase of PVDF can contribute to the formation of the domain structure. This was proved by comparing the average size of the domain (according to the piezoresponse force microscopy data) with the average size of the polar crystal (determined from the reflection width in X-ray reflection patterns).¹⁰⁸⁻¹¹⁰ In all cases, the latter was at least an order of magnitude smaller than the average domain size. This means that a domain includes also an amorphous phase region. A contribution of amorphous phase regions to the domain structure can also be

assumed from the data for the P(VDF-TrFE) copolymer (68:32 ratio).¹¹¹ From this it follows that the slight decrease in ΔS in the considered blend is largely due to the decrease in the fraction of the PVDF amorphous phase. It is evident that the increase in the relaxation times of PMMA and copolymer amorphous phase segments may also account for weakening of ECE in these materials.

Data on the temperature changes related to studying ECE have been obtained by electrophysical measurements.^{99,105,106} The results were discussed in terms of the Maxwell equations, which are based on thermodynamics of equilibrium processes. Since it is unknown whether these equations hold for the polymers in question, researchers made repeated attempts to experimentally measure the changes in temperature. This was done using direct temperature measurement,⁹⁸ calorimetry^{111,112} or infrared imaging.¹¹² The results obtained by various methods were comparable,¹¹² although the use of a thermal resistor showed that direct measurement gives a greater ΔT value than the calculation by relations (6) and (7).⁹⁸

Figure 16 reflects the signals generated by a calorimeter for two P(VDF-TrFE) 65:35 samples. One of the samples was subjected to radiation treatment, which changed the type of phase transition. It can be seen that the signal of the irradiated sample is almost an order of magnitude higher. A qualitatively similar result was obtained for the copolymer with 55:45 monomer ratio (see Fig. 15).

Usually, by normal ECE is meant the effect according to which a dielectric is heated under the action of an external field and is cooled down when the field is removed.

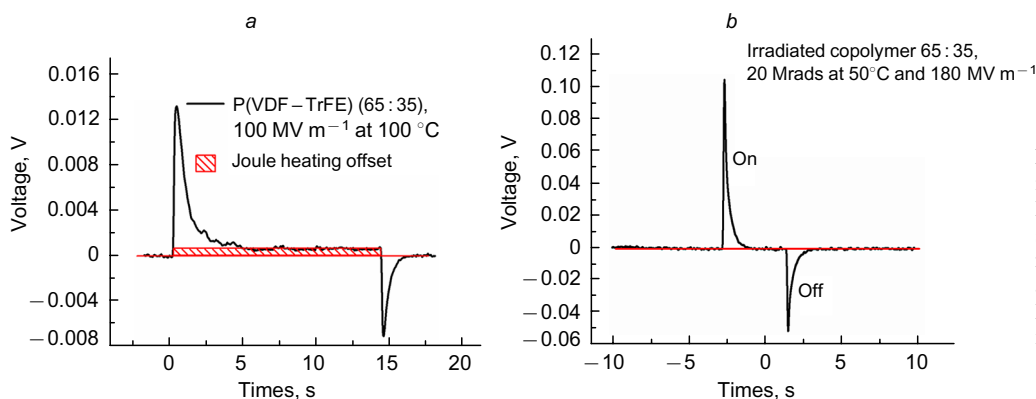


Figure 16. Signal of the calorimeter for ECE in the initial P(VDF-TrFE) copolymer sample (65:35) (a) and after its irradiation (b) with accelerated electrons (20 Mrad).¹¹¹ Published with permission from AIP Publishing.

However, for some technological applications, it is necessary to eliminate the first part of the cycle and leave only cooling (anomalous ECE). This can be done by fabrication of a hybrid material composed of conventional ferroelectric copolymer P(VDF–TrFE) and relaxor ferroelectric copolymer P(VDF–TrFE–CFE) (where CFE is chlorofluoroethylene);¹¹³ selection of the optimal composition for the hybrid material; and selection of the field lower than the coercive field of one of the components. In this case, the sample is not heated as the field is switched on, while the cooling stage is preserved. This results in isothermal entropy change to $11.5 \text{ J}(\text{kg K})^{-1}$. According to published data,^{5,6,75} ferroelectricity is retained in the considered films down to very low film thickness. An adiabatic decrease in temperature of $\sim 24^\circ$ at an operating voltage of only 27 V was attained for a 90 nm-thick film of the P(VDF–TrFE) copolymer (70 : 30 ratio).¹¹⁴

It is of interest to consider the results of some publications in which ECE was studied using composites of ferroelectric polymers with inorganic fillers. A study by Chen *et al.*¹⁵ is devoted to the effect of surface-modified ZrO_2 nanoparticles of 25 nm size on the ECE characteristics in relaxor ferroelectric terpolymer P(VDF–TrFE–CFE) with a monomer ratio of 62.5 : 29 : 8.5. As the terpolymer was crystallized, the added ZrO_2 was displaced to disordered regions with an increased free volume. The introduction of ZrO_2 led to decreasing constant β in equations (8) and (9), which are valid for domains in the crystalline phase. This indirectly proves once again that the amorphous phase is involved in the formation of the domain structure. All the above is manifested as an increase in ΔS in ECE.¹¹⁵

It is of interest to analyze characteristics of a composite material in which both components (organic and inorganic) are relaxor ferroelectrics. Li *et al.*¹¹⁶ used the P(VDF–TrFE–CFE) terpolymer (59.4 : 33.4 : 7.2) as the matrix. The inorganic relaxor ferroelectric $(1-x)\text{Pb}(\text{Mg}_{1/3}\text{Nb}_{2/3})\text{O}_3-x\text{PbTiO}_3$, where $x = 0.1$, (PMN-PT) was introduced into the terpolymer as 300 nm nanoparticles. According to low-voltage electric characteristics, both the terpolymer and the inorganic filler were relaxor ferroelectrics with a broad phase transition. The transition in this composite was implemented as a second-order phase transition, which may be attributed to the interaction of PMN-PT particles with the chains of the amorphous phase of the terpolymer, which indirectly influenced the type of the formed domains. This also applies to

ECE characteristics: the temperature and entropy changes were much greater in the composites than in the initial terpolymer. It is important that even for the PMN-PT fraction of 37.5%, it is possible to attain $\sim 180 \text{ MV m}^{-1}$ fields. This composite is characterized by a broad phase transition, which expands the temperature range of its applicability. For the highest fields, it was found that $\Delta T \approx 30^\circ$ and $\Delta S \approx 275 \text{ kJ m}^{-3} \text{ K}^{-1}$. Detailed analysis showed that the inorganic filler particles interact with chains of the amorphous terpolymer phase, which actively participates in the formation of the domain structure of this composite and other ferroelectric polymers. The authors emphasized that for a 1 μm -thick composite film, the above-mentioned ECE characteristics can be attained by applying a voltage of only 75 V. It follows from the presented data that the efficiency of the ECE cycle is markedly higher for the composite than for pristine P(VDF–TrFE).

The ferroelectric BST ceramics ($\text{Ba}_x\text{Sr}_{1-x}\text{TiO}_3$), for which the ferroelectric \rightarrow paraelectric transition temperature is changed by varying x , can also serve as a filler for the polymers used to study ECE. Zhang *et al.*¹¹⁷ used the P(VDF–TrFE–CFE) terpolymer (62.3 : 29.9 : 7.8) as the matrix and introduced BST nanoparticles from a solution. It was found that the temperature and entropy changes are 2–3 times higher for the composite than for the polymer matrix (all other factors being equal). The introduction of ferroelectric ceramics into the terpolymer results in some decrease (from 350 to 270 MV m^{-1}) in the breakdown field, which naturally restricts the increase in the ECE characteristics of the composite. For increasing the E_b values, boron nitride nanosheets (BNNS) were introduced into the composite, together with BST. Boron nitride has $E_b = 800 \text{ MV m}^{-1}$; it is a good insulator with band gap of $\sim 6 \text{ eV}$. This ternary composite (containing, for example, 6 vol.% BST and 9 vol.% BNNS) was characterized by a breakdown field of 450 MV m^{-1} (Ref. 117). Data on ECE for this material are depicted in Fig. 17. It can be seen that for the optimal BST content and a field of 250 MV m^{-1} , the temperature change reaches 50.5° and the entropy change can be $426 \text{ kJ m}^{-3} \text{ K}^{-1}$. These are the highest values found in the literature.

For the composites, the frequency dependences of the cooling power density taken off from the medium were calculated, as is done for calculation of refrigeration systems (see Fig. 18). In this case, apart from the heat per cycle, high heat conductivity of the composite was

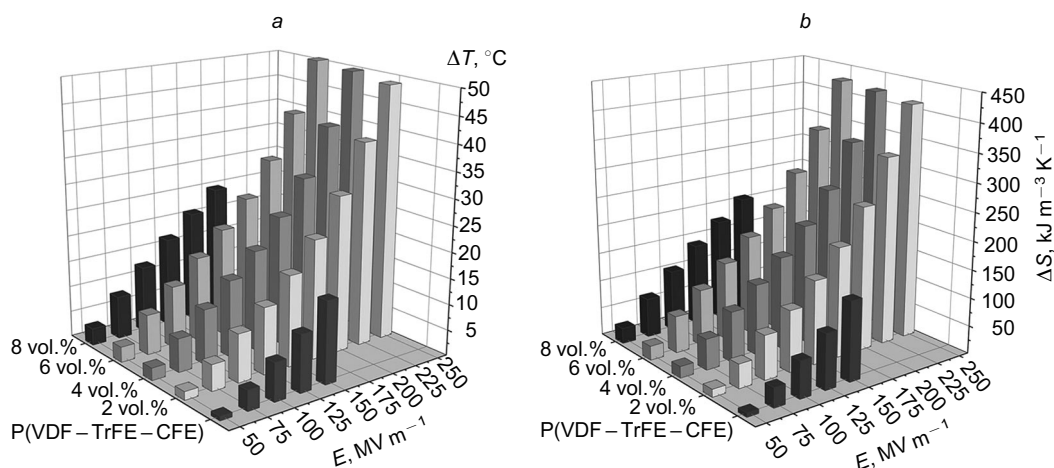


Figure 17. Diagrams reflecting the field and concentration (for BST ceramics) dependences of ΔT (a) and ΔS (b) for ECE of the P(VDF–TrFE–CFE)–BNNS–BST composite containing 9 vol.% BNNS.¹¹⁷ Published with permission from John Wiley and Sons.

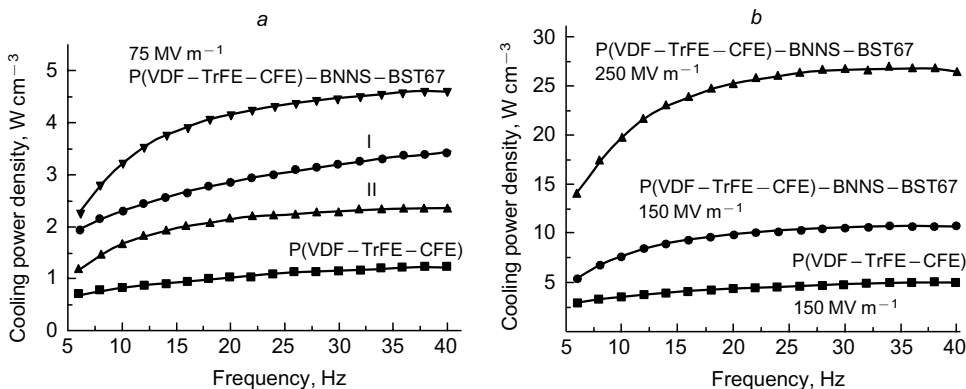


Figure 18. Frequency dependences of the cooling power density at room temperature for the polymer matrix and the P(VDF-TrFE-CFE)-BNNS-BST composite at an external field of 75 (a) and 150 and 250 MV m^{-1} (b); I and II are curves calculated with the assumption that the heat conductivity and the released heat for the composite and the polymer matrix are equal.¹¹⁷ Published with permission from John Wiley and Sons.

required. It was found that heat conductivity sharply increased (~ 5 -fold with respect to that of the polymer matrix) upon the introduction of particularly the BNNS particles. The resulting values proved to be much higher than those for vapour compression refrigeration systems.

The optimal concentration of BST ceramic particles did not exceed 8 vol.%. Higher concentrations resulted in decreasing breakdown fields; therefore, ECE characteristics of the composites would decrease. Meanwhile, the modern capabilities of ceramic synthesis make it possible to change the particle shape and produce nanocubes, nanorods and nanotubes. On the basis of theoretical estimates, it is possible to model and calculate the distribution of the local electric fields upon implantation of these particles into the polymer matrix.¹¹⁸ The lowest local fields were observed for one-dimensional nanostructures; this corresponded to higher breakdown voltages of the composites.^{119–122} In view of this fact, Zhang *et al.*¹¹⁸ prepared and studied composites based on the P(VDF-TrFE-CFE) terpolymer with BST particles of various shapes. It was shown that with equal fields and equal concentrations of the filler, the composite containing nanowires had higher D and $\partial D/\partial T$ values in the vicinity of phase transition. According to equations (6) and (7), the increase in the latter value implies improved ECE characteristics, which is supported by experimental data (Fig. 19).

In view of the above and considering the reported^{123,124} characteristics of fluorinated ferroelectric polymers and composites based on them, these materials hold promise for the fabrication of solid-state refrigeration systems.

5. Piezoelectric sensors based on ferroelectric polymers

It was shown above that fluorinated ferroelectric polymers become piezo-active after polarization; hence, they are applicable for manufacturing pressure sensors. These materials are relatively new compared with the typical inorganic ferroelectric materials such as BaTiO_3 or PZT piezoceramics. Comparison of their characteristics (Table 2) demonstrated that PVDF-based piezo sensors possess a number of advantages: high g_{ij} values, chemical and radiation stability, low density, high impact strength, *etc.*^{6,75} Therefore, PVDF-based sensors have found a variety of applications.^{126,127}

Owing to high thermoplasticity of these polymers, it is possible to produce uniaxially or biaxially stretched films with a large surface area, which are used for radiofrequency measurements.¹²⁸ Some examples of using PVDF-based sensors are presented below. An electron beam image converter using PVDF film as the active sensor element was reported.¹²⁹ The PVDF sensor provided a higher sensitivity than a quartz sensor. The resolution of the PVDF-based converter (with a lower Q -factor) was also at least two times higher.¹²⁹ Another application of these materials is for sensors for laser ablation processes. A plasma cloud is formed near the surface of the irradiated material; The pressure changes in this cloud were measured with a PVDF sensor.¹³⁰ The recorded signal was used to estimate the translational temperature and the particle drift velocity. For a tungsten target, these values were $8.8 \times 10^4 \text{ K}$ and $4.73 \times 10^5 \text{ cm s}^{-1}$, respectively.

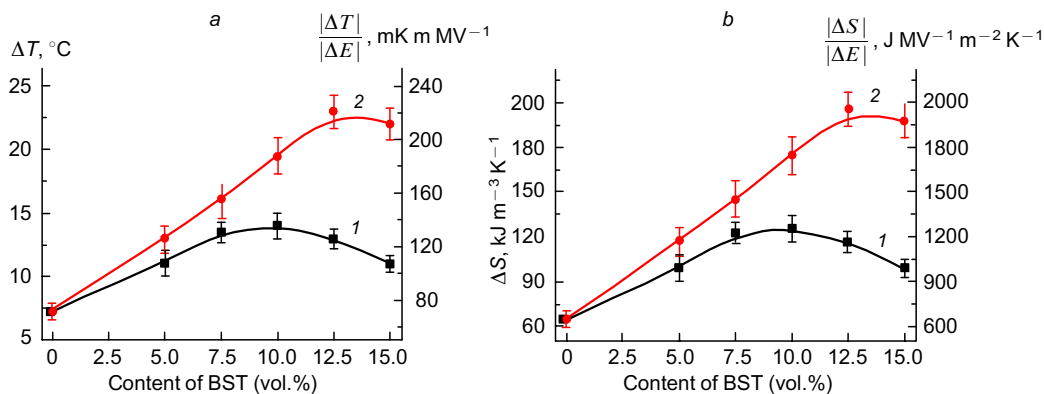


Figure 19. Concentration dependences of the absolute and normalized ΔT (a) and ΔS (b) values derived in a study of ECE for the P(VDF-TrFE-CFE)-BST composite with a filler consisting of nanoparticles in which the three dimensions are approximately equal (1) and nanoparticles stretched in one direction (2) at an external field of 100 MV m^{-1} (Ref. 118). Published with permission from American Chemical Society.

Table 2. Characteristics of inorganic and organic piezoelectrics.¹²⁵

Parameter	Designation	Unit of measurement	PZT	BaTiO ₃	PVDF
Density	ρ	10 ³ kg m ⁻³	7.5	5.7	1.78
Relative dielectric permittivity	ϵ_r	—	1200	1700	12
Piezoelectric coefficient					
voltage	d_{31}	10 ⁻¹² C N ⁻¹	110	78	23
strain	g_{31}	10 ⁻³ V m N ⁻¹	10	5	216
Electromechanical coupling coefficient	k_{31}	—	0.3	0.2	0.12
Acoustic impedance	ρv_s	10 ⁶ kg m ² N ⁻¹	30	30	2.7

De Matos *et al.*¹³¹ used a similar sensor to address somewhat different problems. It is known that laser ablation of materials is used for the radioisotope separation; for this purpose, it is important to determine the ratio of neutral and ionized products in the plasma. This was done using PVDF sensors of two types, non-polarized and polarized ones. In the latter, a charge was formed on the surface. The signals from the two sensors were compared under identical ablation conditions. It was shown that an increase in the fluence of incident radiation results in signal growth; however, the signal proved to be several times higher in the case of ionogenic products of ablation.

In the design of microphones based on piezoelectric materials, it is important to enhance the material sensitivity. According to calculations,¹³² the sensitivity can be changed by replacing the traditional flat membrane by micro-pillars, which were fabricated using piezo-active PVDF (Fig. 20).¹³² The highest sensitivity was attained for patterned electrodes with partial covering.

Taking account of the real surface of the active element (see Fig. 20 *b*), a microphone was designed. The calculated piezoelectric coefficients of the microphone were as follows: $d_{33} = 110$ pC N⁻¹ and $g_{33} = 1092$ mV m⁻¹ N⁻¹. These values are nearly three times greater than those for standard (flat) PVDF film, which amount to 33 pC N⁻¹ and 330 mV m⁻¹ N⁻¹. The value $d_{31} = 110$ pC N⁻¹ attained upon the indicated change in the surface topography proved to be equal to this value for PZT ceramics (see Table 2).

Thus, change in the surface geometry of the active element of piezoelectric polymer, apart from the electrode appearance, can considerably influence the sensitivity of the piezo-active membrane and, hence, the microphone sensitivity (the dynamic range of this microphone reached 181 dB, and the upper frequency band was not less than 100 kHz).

Since surface patterning of the active element is an efficient procedure that improves the performance of sensors based on ferroelectric polymers, it is appropriate to consider other methods used to change the surface topography. One method is related to the effect of high-power optical radiation on organic polymers.¹³³ The PVDF surface was treated with plasma produced by a pulsed UV laser.¹³⁴ The laser radiation wavelength range was 9 to 70 nm with the maximum spectral density at $\lambda = 11$ nm. For fluence of 60 mJ cm⁻², the surface photo-etching rate was approximately 70 nm per pulse. According to mass spectrometry data, low-molecular-mass fragments such as H₂, CH₂, HF, CF, *etc.* were emitted from the irradiated surface. The surface pattern thus formed is shown in Fig. 21. The smooth walls of the holes and the X-ray photoelectron spectroscopy data indicate that the photo-etching was local and, owing to the low heat conductivity of the polymer, the neighbouring areas remained intact.¹³⁴

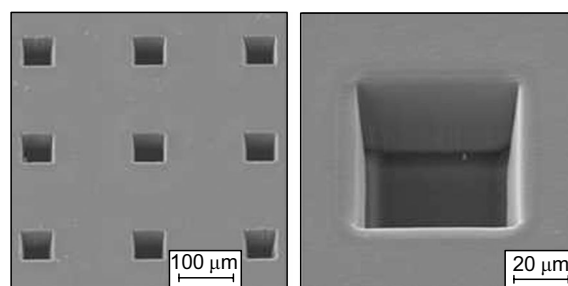


Figure 21. Micrographs of the surface of PVDF film formed under the action of plasma.¹³⁴ Published with permission from Springer Nature.

A modified etching method includes low-temperature irradiation of PVDF with a heavy ion beam.¹³⁵ This opens up the possibility of fabricating membranes the performance of which can be controlled by varying the electric field.

One more method for patterning of the surface with applied electrodes is exposure to femtosecond laser pulses.¹³⁶ By varying the laser fluence, the authors selected

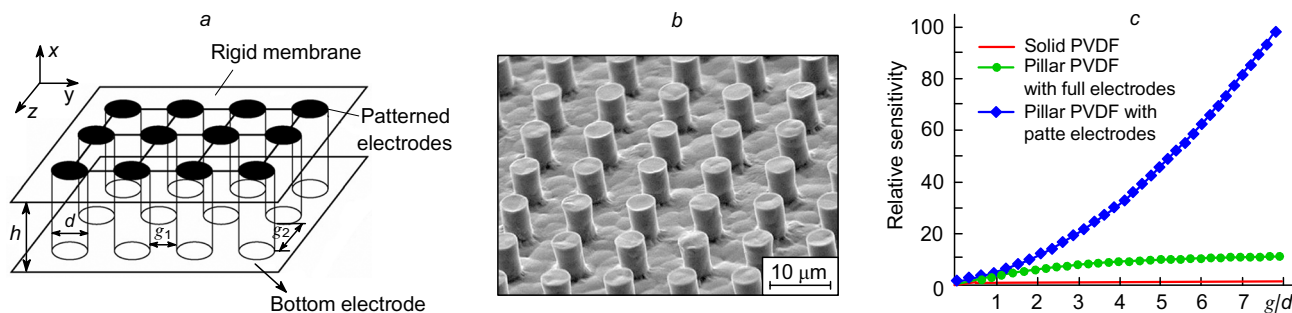


Figure 20. Acoustic sensor based on a pillar-shaped PVDF membrane (*a*), micrograph of a real surface of the active element (*b*) and calculated (with the assumption that $g_1 = g_2 = g$) dependences of the relative sensitivity of membranes made of a solid film and a pillar film with a full or patterned upper electrode (*c*).¹³² Published with permission from Elsevier.

conditions under which film ablation together with the electrodes took place. This gave rise to a vibration micro-sensor, which was tested by recording the white noise generated by compressed air. These microsensors could be used in telecommunication systems and in biomedicine.

In view of the possibility of surface micropatterning of fluorinated ferroelectric polymers, it is of interest to consider issues related to their destruction.¹³⁷ It is known that the destruction is preceded by the excitation of surface acoustic waves. Certainly, piezoceramic sensors are characterized by higher d_{ij} than PVDF sensors;¹²⁵ nevertheless, there are a few studies (see, e.g.,^{138–143}) in which PVDF sensors were used for both excitation and recording of these waves. It was noted that the signal recorded by a sensor based on PZT ceramics is markedly higher than that recorded by the PVDF sensor.¹²⁵ However, the signal amplification problem is solved by adjustment of amplifier characteristics; meanwhile, if it is necessary to endow the sensor with a certain configuration (that cannot be implemented for piezoceramics), preference is given particularly to PVDF.

Tactile sensors are widely used in robotics technology.¹⁴⁴ Most often, they require piezo-active materials, in particular, those based on ferroelectric polymers.^{145–150} Among these studies, mention should be made of the publication by Dargahi,¹⁴⁶ who considered a practically important problem involved in obtaining signals of a PVDF tactile sensor. When the sensor gets in contact with human fingers, which have quite a definite temperature differing from the sensor material temperature, the resulting signal would include both piezo- and pyroelectric responses. If the thickness mode (d_{33}) is used, the pyro- and piezoelectric responses have the same sign, which should be taken into account in the sensor design. As a type of PVDF tactile sensor, consider the use of such sensors in liquid flow meters.^{151,152}

A separate class of PVDF-based sensors are hydrophones. It follows from the general acoustic equations that the reflection coefficient (R) for a wave that passes from a medium with acoustic impedance Z_2 to a medium with acoustic impedance Z_1 is written as follows¹⁵³

$$R = \frac{Z_2 - Z_1}{Z_2 + Z_1} \quad (10)$$

If Z_2 and Z_1 are acoustic impedances of water and PVDF, then, with all other conditions being equal, the signal arising in the PVDF active element is determined by the difference ($Z_2 - Z_1$).

The acoustic impedance is an order of magnitude lower for PVDF than for inorganic materials (see Table 2). For a pressure wave with an arbitrary profile, the voltage generated by the active element is determined by the piezoelectric coefficient g_{33} , which is 20 times as high for PVDF as for PZT; therefore, the use of ferroelectric polymers in hydrophones is reasonable. Sullivan and Powers¹⁵⁴ described the design of a disk hydrophone based on PVDF, which operated at a pressure of up to 4 MPa and had a sensitivity of $-200 \text{ dBV}^{-1} \mu\text{m Pa}^{-1}$. Later, mathematical models were developed describing characteristics of this type of hydrophones.^{155–157}

It is noteworthy that these fluorinated ferroelectric polymers are characterized by high breakdown fields and, therefore, they can be applied at high operating voltages. In the case of reverse piezoelectric effect, this feature can be used to generate ultrasonic waves;^{158–160} for this purpose,

electrode characteristics should be taken into account.¹⁶¹ The increased operating electric voltage of PVDF, together with the similarity of the acoustic impedances of water (or biological fluids) and PVDF, create conditions for using PVDF as a sonar¹⁶² or for shock wave detection.^{163,164} Low acoustic Q -factor, determining the width of the dynamic response, is yet another important feature, which should be considered for the use of PVDF for lithotripsy. It follows from the cited studies that PVDF is promising for the development of a lithotripter for biological media. According to the results of Granz,¹⁶³ by using these devices, it is possible to generate ultrasonic shock pulses with a pressure of $> 20 \text{ MPa}$ in $< 50 \text{ ns}$ time. This polymer was also used to design a sensor for measuring shock waves, which provides a sensitivity of 20 mV MPa^{-1} at 3 mm size of active element.¹⁶³

Needle hydrophones are used in biomedicine.^{165,166} The capabilities of these devices were demonstrated by Crazzolara *et al.*;¹⁶⁷ the choice of experimental conditions was based on the data obtained earlier.¹⁶⁸ The block diagram of the facility for detection of ablation products of human body tissues is shown in Fig. 22*a*. The authors compared acoustic signals from two types of blood vessels on exposure to pulsed UV laser radiation on XeCl at 308 nm wavelength. When the needle microphone diameter was 500 μm , comparison of the signals revealed noticeable differences (Fig. 22*b*): for a normal vessel, the signal duration was 120 ns with a pressure maximum of 1.2 MPa, while for a calcified vessel, these values were 80 ns and 2.8 MPa, respectively. Thus, the appearance of calcium on the surface of, for example, aorta leads to a change in the ablation parameters of the tissue on exposure to an UV laser pulse. The results of most recent studies of this series

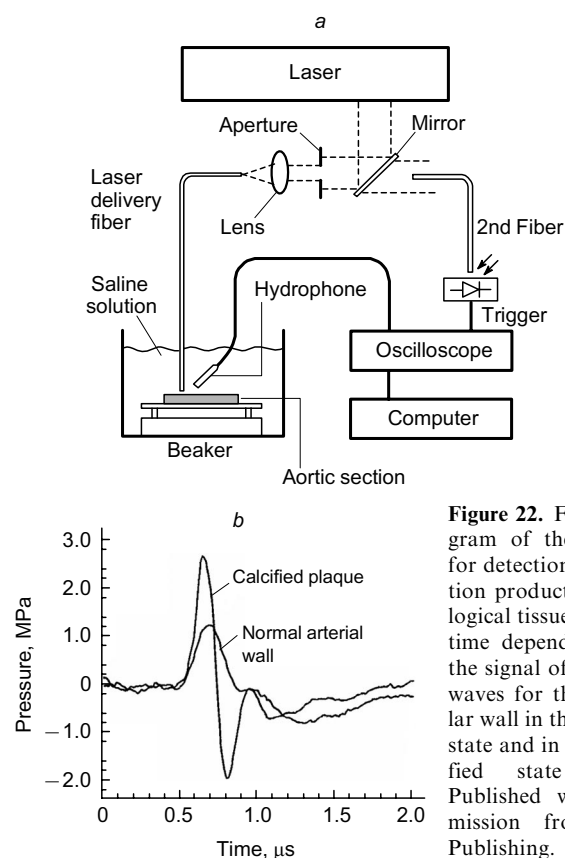


Figure 22. Flow diagram of the facility for detection of ablation products of biological tissues (*a*) and time dependences of the signal of acoustic waves for the vascular wall in the normal state and in the calcified state (*b*).¹⁶⁷ Published with permission from AIP Publishing.

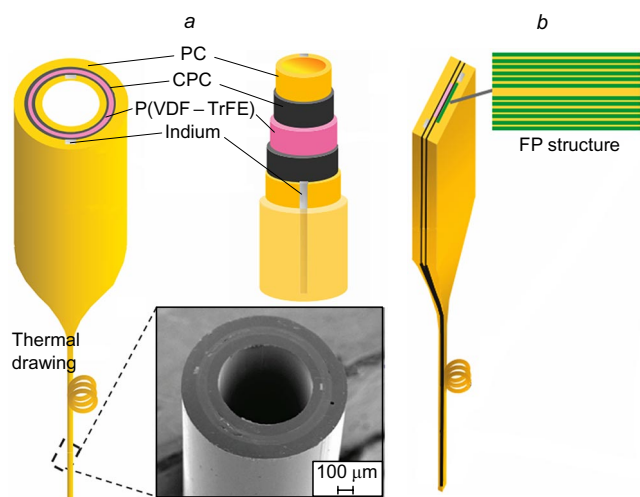


Figure 23. Scheme of formation of Fabry–Perot interferometer from the P(VDF–TrFE) copolymer (70:30) based on optical fibre with axial symmetry (a) and multilayer single crystal texture (b).¹⁸² PC is polycarbonate; CPC is carbon-filled polycarbonate; FP structure is composed of a sequence of flat active elements as uniaxially stretched films. Published with permission from Springer Nature.

demonstrated that the sensitivity of PVDF-based hydrophones and other sensors can be increased by creating PVDF composites containing either inorganic (PZT, ZnO) or organic materials, in particular, graphene.^{169–176}

The sensors considered above are based on the use of direct piezoelectric effect in the polymer active element. It follows from electromechanical equations that applying an electric voltage to a piezoelectric film leads to film distortion; hence, the film can work as an actuator. One of actuator applications of PVDF films¹⁷⁷ is concerned with the design of frequency modulators for the transmitted (reflected) light.^{178–180} Using ferroelectric polymers possessing high thermoplasticity, it is possible to simplify the manufacturing process of active element with a desired shape. Large areas of PVDF active elements characterized by a high chemical and radiation stability can potentially be used in space engineering.¹⁸¹

Owing to good thermoplasticity of PVDF and its copolymers, they can be used to manufacture a piezoelectric shell for optical fibres. When electric voltage is applied to the shell, it acts an actuator, thus changing the geometric dimensions of the optic fibre. Hence, the light wave characteristics also change. Therefore, these materials can be used to design optoacoustic converters, which are implemented, most often, as Fabry–Perot interferometers.¹⁸² The active element in this converter can have either an axial symmetry (Fig. 23 a) or a multilayer single crystal texture (Fig. 23 b). The latter configuration is preferable, since the signal to noise ratio at the characteristic points of the audio frequency modulation is higher in this case, with other factors being equal.

6. Pyroelectric sensors and electrochromic energy converters

Polarization of fluorinated ferroelectric polymers gives rise to not only piezoelectric, but also pyroelectric properties, i.e., a temperature change gives rise to electric charges on

the surface of a material. This prompts the idea of using this effect in thermal sensors. The discussed polymers are soluble and can be fabricated as ultrathin films, with the ferroelectricity being retained.^{5,6,75} Due to the low heat capacity of the active element, these films are promising for the use in pyroelectric sensors meant for detection of short heat pulses.

Below, the pyroelectric properties of fluorinated ferroelectric polymers are discussed in terms of the dipole model taken by researchers. The attention is focused on new data on the polymer microstructure. By definition, pyroelectricity is a change in the polarization with a change in the sample temperature. The general expression for this change along the x direction has the form

$$\frac{\partial P_x}{\partial T} = \frac{\partial P_{0x}}{\partial T} + \varepsilon_0 E_k \frac{\partial \varepsilon_{xk}}{\partial T} + \frac{\partial (d_{xkl} \sigma_{kl})}{\partial T} + \partial \left(\mu_{xijk} \frac{\partial u_{jk}}{\partial x_i} \right) / \partial T \quad (11)$$

where E_k is a component of the electric field vector, ε_{xk} is the dielectric permittivity tensor, P_0 is the spontaneous polarization of crystals, which are separated in the polymers by amorphous regions, x_i is a component of the strain tensor (see Fig. 1).

The first term characterizes the primary (dipole) pyroelectric effect,¹⁸³ which makes a minor contribution to the overall pyroelectric effect.^{5,6} The other terms of the equation refer to the secondary pyroelectric effect. The third term reflects the appearance of piezoelectric effect in a material with the piezoelectric coefficient d_{xkl} due to the arising stress σ_{kl} . The fourth term characterizes the flexoelectric effect (with the tensor μ_{ijkl}) where polarization arises under the action of strain gradient (with the tensor u_{jk}). In the fluorinated ferroelectric polymers containing a liquid-like amorphous phase, the probability of the appearance of strain gradient is low; therefore, the flexoelectric effect can be neglected. Low d_{kl} values indicate that the contribution of the third term to the change in polarization should also be moderate.

The second term actually characterizes the electrostriction, the contribution of which may be very high due to low crystallinity.¹³ If the amorphous phase makes a contribution to pyroelectricity, then the pyroelectric coefficient should depend on the characteristic point for disordered regions, that is, glass transition temperature. Figure 24 shows the temperature dependences of the pyroelectric properties of PVDF films. It can be seen that the charge density (current) is significantly higher in the first heating cycle (see Fig. 24 a) than in the second one (cf. q_1 , q_3 and q_2). This is due to the fact that the first heating cycle measures an irreversible process related to thermal depolarization. The temperature dependence of the reversible pyroelectric current monitored in the second heating cycle^{187–189} has two characteristic points in which the course of the curve changes (Fig. 24 b). One point is just the glass transition temperature, below which the pyroelectric response virtually does not change. It follows that freezing of the chain mobility in the amorphous phase leads to decreasing pyroelectric coefficient (see Fig. 24 c). Freezing of the orientational polarization of the chains in the amorphous phase upon glass transition is accompanied by a decrease in $\partial \varepsilon_{xk} / \partial T$; therefore, the predominant contribution in Eqn (11) is made by the second term.

The second characteristic point (Fig. 24 b,c) falls approximately to room temperature^{185,186} (or a somewhat higher temperature)¹⁸⁷ where characteristics such as the

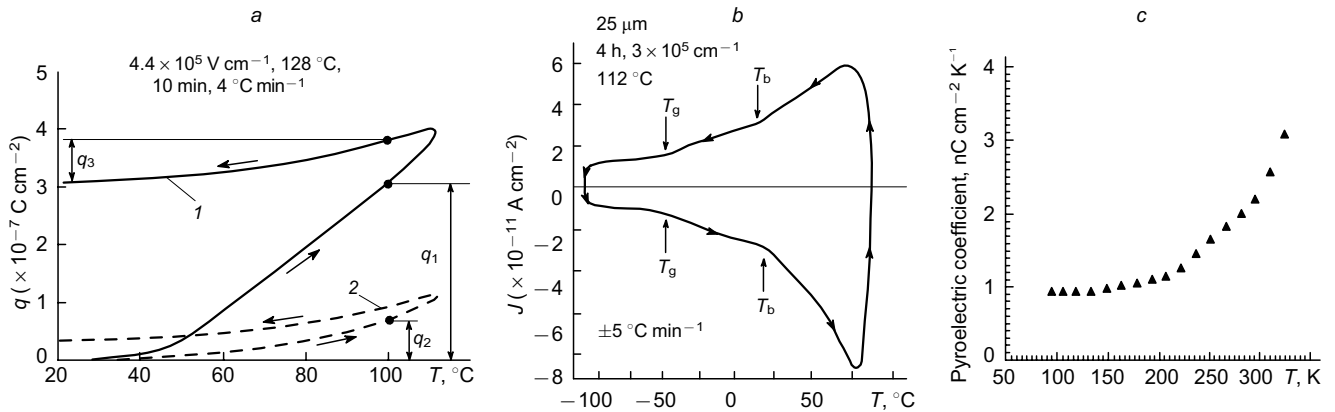


Figure 24. Temperature dependences of the pyroelectric properties of PVDF films. Change in the surface charge density in the first (1) and second (2) heating–cooling cycle (a),¹⁸⁴ pyroelectric current (b)¹⁸⁵ and pyroelectric coefficient (c).¹⁸⁶ T_b and T_g are temperatures corresponding to characteristic points. Published with permission from AIP Publishing.

real part of dielectric permittivity and dielectric loss tangent show anomalous temperature behaviours typical of phase transitions.¹⁸⁶ The presence of these transitions is also indicated by the appearance of low-temperature melting endotherms, which were observed for VDF copolymers with TFE,^{190,191} TrFE¹⁹² and HFP.¹⁹³ Most likely, these endotherms should be attributed to melting of the ordered amorphous regions formed upon secondary crystallization.^{194–200} Thus, both characteristic points are attributable to the amorphous phase in which a fine structure may form.

Other flexible-chain crystalline polymers, polyethylene and isotactic polypropylene (IPP), are also characterized by low-temperature endotherms and anomalies in the structure formation.^{197,201–203} In the case of PE, less perfect hexagonal crystals appear, apart from orthorhombic crystals, while in IPP, less perfect and less closely packed crystals separate to form a mesomorphic phase.^{198,204} X-Ray diffraction data for VDF copolymers with tetrafluoroethylene,^{108,109,205,206} trifluoroethylene^{110,207–210} and hexafluoropropylene,^{88,205,210} in which the indicated comonomers are defects in the VDF backbone attest to similar structurization processes. These processes can be depicted by a scheme shown in Fig. 25 a; transition from the right-hand lamellar crystal to the left-hand one takes place with increasing temperature; this is accompanied by disappearance of imperfect structures formed during the secondary crystallization.

In ferroelectric polymers, low-temperature crystallization from solution gives rise to a non-equilibrium structure. As a result, in addition to the principal reflections for the β -phase crystals, the X-ray diffraction patterns show a halo reflection at smaller angles (Fig. 25 b) corresponding to the reflection of the paraelectric phase, which crystallizes in the hexagonal system.²¹¹ This indicates that crystallization takes place in a mixture of small-sized ferroelectric and paraelectric crystals. The resulting structure is definitely non-equilibrium, as the ferroelectric \rightarrow paraelectric transition takes place at temperatures close to the melting point (150–160 °C). During secondary crystallization, this imperfect crystals can form thermally reversible domains (see Fig. 25 a). In the case of polarized ferroelectric polymers, the destruction of these domains on heating is accompanied by a decrease in the remanent polarization, *i.e.*, gives rise to pyroelectricity.

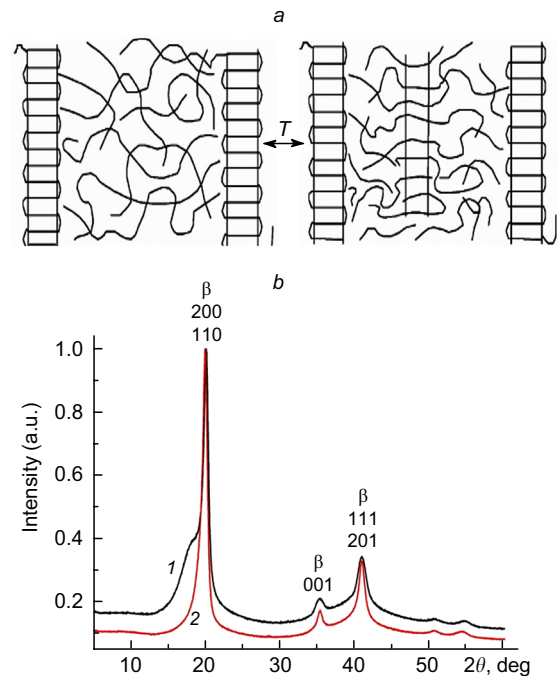


Figure 25. Scheme of the reversible structural rearrangements in the interlamellar layers of crystalline polymers during heating–cooling processes (a) and X-ray diffraction curves for the P(VDF–TrFE) film (70:30) obtained by crystallization from a tetrahydrofuran solution at room temperature (1) and after subsequent annealing at 120 °C (2).¹⁹² Published with permission from John Wiley and Sons.

The experiment on observation of the response of oriented PVDF to a short laser pulse showed the presence of a broad component of pyroelectric response signal (p_y), which was associated with the thermoreversible change in the crystallinity.²¹² Thermodynamic analysis gives the relation

$$\frac{d\phi_c}{dE} = -\frac{d\phi_c}{dT} \frac{dT_m}{dE} = -\frac{\gamma p_y T}{Q_m} \quad (12)$$

where ϕ_c is crystallinity; T_m is the melting temperature; γ is the fraction of pyroelectric response related to the reversible change of crystallinity under the action of temperature; Q_m

is the latent molar heat of melting. Thus, if the hypothesis of a contribution of thermally reversible melting of some crystals to the pyroelectric effect is true, the crystallinity should change with a change in the field. For PVDF this was confirmed by X-ray diffraction.²¹² Later, this fact for fluorinated ferroelectric polymers was noted by many authors (see, for example, references cited in the review⁹⁵).

The technological applications of pyroelectricity have been reviewed in detail by Xiao and Lang;²¹³ we address only some issues and discuss more recent results. Just after the discovery of pyroelectricity in polarized PVDF, the use of pyroelectric detectors based on PVDF to detect IR radiation^{214–218} and to study a wider electromagnetic range from the visible region to 12 μm wavelength²¹⁹ was reported. A very broad range of measurable power (1 mW to 50 W) was established for laser radiation.²²⁰ There are data on the application of these materials for the detection of microwave radiation,²²¹ including that in the millimetre range.²² The microwave absorption (at temperatures above room temperature) should be associated with the presence of an amorphous phase that has an absorption peak precisely in the microwave range.⁷⁵ This feature can be used as a heating method for the measurement of pyroelectricity in PVDF and its copolymers.²²³ In this case, if temperature distribution throughout the sample is uniform,²²⁴ the electromagnetic radiation power can be detected in the radio frequency range. The 5–10 nm-thick films of these polymers can be studied by DSC with a high time resolution.²²⁵ The radiation stability of these polymers accounts for the possibility to detect superheavy nuclei and cosmic-ray particles on the basis of pyroelectric effect.^{226,227} There are interesting publications on the use of pyroelectric detectors in the medical thermometry.^{228,229} Other applications of PVDF-based pyroelectric detectors (light absorption in optical fibre, copying equipment, *etc.*) are described in detail in the review by Xiao and Lang.²¹³

It is of interest to compare characteristics of the pyroelectric responses for the polymers we consider and for other ferroelectric materials. In terms of the voltage sensitivity, PVDF can compete with materials such as PZT and triglycine sulfate.¹⁸⁶ Polyvinylidene fluoride has a low thermodiffusion; therefore, it is used to fabricate vidicons.²³⁰ According to Glass *et al.*,²¹⁴ the noise equivalent power for radiation recorded at 10.6 μm wavelength was 15 $\text{nW Hz}^{-0.5}$ at 100 Hz; according to another publication,²¹⁷ this value was $< 1 \text{ nW Hz}^{-0.5}$ at 4 Hz. The current sensitivity was found^{216,217} to be at a level of 3 $\mu\text{A W}^{-1}$.

It was noted above that polymer films can be textured with controlled chain packing density of the amorphous phase.^{231,232} In this connection, it is of interest to compare the pyroelectric properties of the considered fluorinated polymers in the isotropic and oriented states. At high polarization fields, the pyroelectric response was substantially higher for oriented samples.²³³ Spin-coated thin films can be formed at a high voltage (8–15 kV) between the solution drops and the substrate; the film formation is accompanied by polarization.²³⁴ A correlation was established between the ionic current and the final pyroelectric coefficient, which reached 4 $\text{nC cm}^{-2} \text{ K}^{-1}$ for oriented PVDF films.

The pyroelectric current is usually low (see, for example, Fig. 24*b*). Tien *et al.*²³⁵ used a P(VDF–TrFE) copolymer film as a pyroelectric gate dielectric layer in a field effect transistor based on organic materials. The scheme of this device and the pyroelectric currents obtained after amplifi-

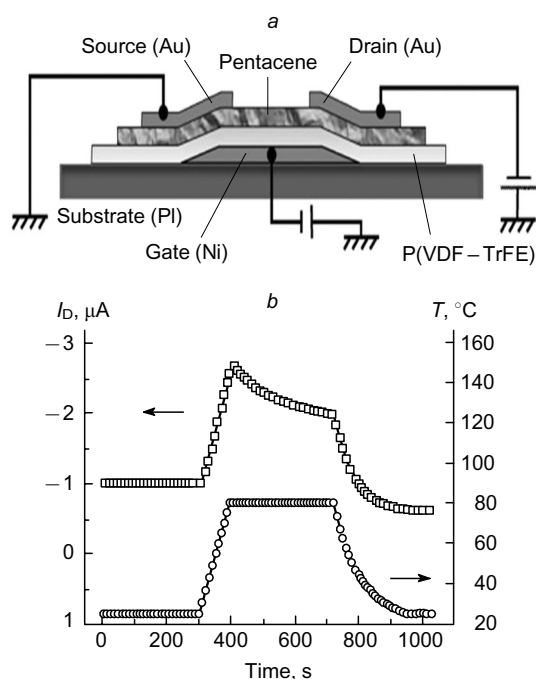


Figure 26. Scheme of operation of a pyroelectric sensor based on P(VDF–TrFE) copolymer used as the gate dielectric layer in an organic field effect transistor (*a*) and time dependences of the temperature and current in the transistor (*b*).²³⁵ Published with permission from John Wiley and Sons.

cation in the transistor are depicted in Fig. 26. The pyroelectric current was several orders of magnitude greater than that obtained by direct measurements.

Characteristics of the pyroelectric detector based on the polymers in question can be improved by forming micrometre-size air cavities in the film bulk.²³⁶ The voltage sensitivity of the film was found to increase after polarization, which can be attributed to decreasing dielectric permittivity and specific heat capacity. It was concluded that this hybrid material is applicable not only as a sensor, but also as a nanogenerator for converting thermal energy into electric energy. When the external load was 41.2 $\text{M}\Omega$, the generated voltage was 3.2 V and the current in the circuit was 52 nA, a unit area of the active element of the P(VDF–TrFE) film generated a power of 151 nW. It is believed that this hybrid film can serve as the basis for a self-powered pyroelectric detector.

Correct measurement of pyroelectricity requires the control of polarization uniformity across the film thickness.^{216,217} This can be done using photopyroelectric spectroscopy,^{237,238} in which the frequency-modulated laser beam is focused on the surface of a polarized ferroelectric material, which is thus heated. The arising pyroelectricity can be used to measure the thermal diffusion.²³⁹ Using a 6 nm-thick thin film of the P(VDF–TrFE) copolymer (70:30) and a high-frequency modulation of laser radiation (beam diameter of 352 nm), a 660 nm resolution was attained.²⁴⁰ Groten *et al.*²⁴¹ used pyroelectric scanning probe microscopy to measure the surface potential rather than the pyroelectric current, which increased the sensitivity of measurements.

The potential distribution upon the local polarization of a film with a bipolar field is shown in Fig. 27. It can be seen that light modulation leads to a periodic change in the

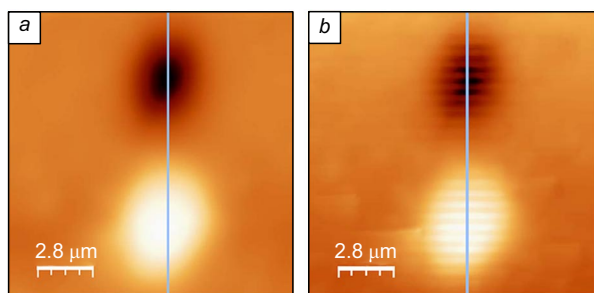


Figure 27. Distribution of the surface potential in an initial P(VDF–TrFE) film (65:35) after its local polarization with a voltage of -100 V (dark area) and $+100$ V (light area) (a) and upon laser modulation (b).²⁴¹ Published with permission from American Physical Society.

potential and, hence, in the pyroelectric response. For the copolymer considered here, switching of a positive voltage to a negative one leads to a pronounced difference between the maximum pyroelectric coefficients, that is, 40 and $25 \mu\text{C m}^{-2} \text{K}^{-1}$, respectively. In our opinion, this is due to the asymmetry of polarization at different signs of the field; this was also shown previously for other VDF copolymers.^{89,94,242} This effect can be attributed to the injection of charge carriers from the electrode. The holes and electrons may have different mobility and be stabilized in the traps of various depths. The space charge fields they form are different, and this affects the final remanent polarization, which determines the pyroelectric coefficient.^{5,6}

The high-voltage polarization of the polymers can be attained by chemical changes in the polymer chain;^{94,95} this is reflected in the final ferroelectric characteristics. Therefore, the research dealing with the preparation methods of self-polarized polymer films deserves attention. Wu *et al.*²⁴³ created a layer containing hydroxyl groups on the glass substrate as a result of chemical treatment. The PVDF film crystallizing on this substrate from a solution had a higher crystallinity and a higher content of the β -phase, which was attributed to hydrogen bonding between the substrate hydroxyl groups and PVDF chains. The film obtained in this way exhibited pyroelectric effect without external polarization. The same study addresses the problem of noise in the pyroelectric sensors formed from these materials. As noted above, the third term in Eqn (11) characterizes the contribution of the piezoelectric effect, which can be conceived as noise, to the pyroelectric response. The authors proposed a method for suppressing

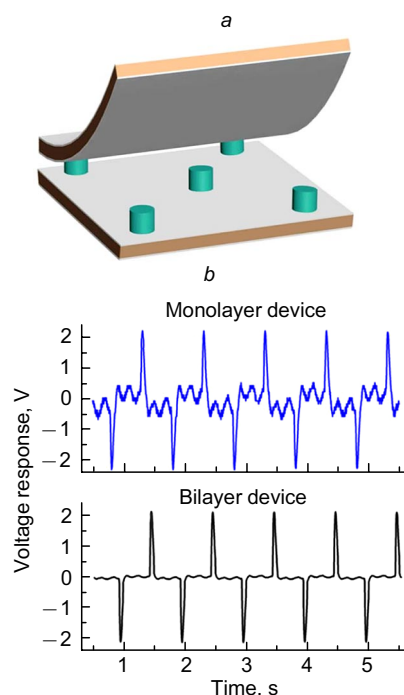


Figure 28. Scheme of formation of a bilayer pyroelectric sensor based on self-polarized PVDF (a) and pyroelectric response signals of the converter based on monolayer and bilayer films upon simultaneous mechanical (5 Hz) and thermal (1 Hz) excitation (b).²⁴³

this noise. This was done by forming a bilayer structure in which neighbouring layers were separated by an acoustic damper, which resulted in an efficient suppression of the piezoelectric noise (Fig. 28); the signal to noise ratio was 18 dB for a monolayer film, while for the bilayer film it reached 38 dB.²⁴³ The methods for contactless measurement of the pyroelectric coefficient discussed in two publications deserve attention,^{244,245} however, no data on the experimental implementation of these methods can be found in the literature.

It was already noted that these polymers are soluble; hence, they can uptake dye molecules from common solvents. The absorbed dye molecules are located near the domains that generate strong electric fields, which affect the electronic spectra of the dyes. A specific feature of ferroelectric materials is that the field from the domains can be controlled by an external source; hence, it is possible to affect the electronic structure of dye molecules. This principle underlies the design of electrochromic devices in which the absorption spectrum of a dye can be controlled by an electric field.²⁴⁶ This idea was implemented in an electrochemical cell in which a membrane made of VDF – hexafluoropropylene copolymer microfibres impregnated with

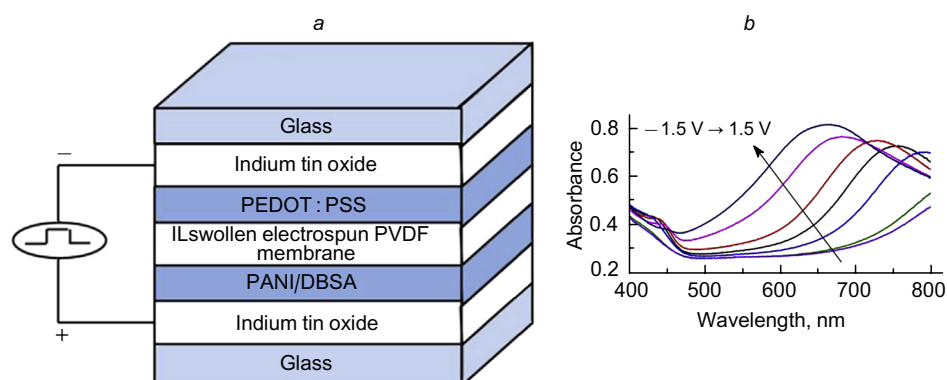


Figure 29. Design of a photochromic cell based on a membrane of cross-linked P(VDF–HFP) fibres (a) and variation of the absorption spectrum in the cell upon variation of the control voltage (b).²⁴⁷ PEDOT is poly(3,4-ethylenedioxythiophene), PSS is poly(styrene sulfonate), DBSA is dodecylbenzenesulfonic acid. Published with permission from Elsevier.

an ionic liquid served as the active element. Using transparent electrodes made of organic semiconductors (see the scheme in Fig. 29 a), light transmittance of $>90\%$ was obtained in such a cell with a $2\ \mu\text{m}$ thick (undoped) active layer.

If a membrane made of microfibrils doped with a definite dye is used, the absorption spectrum exhibits a band that can potentially be controlled by an external electric field (Fig. 29 b). A specific feature is that the absorption spectra are significantly changed even by minor fluctuations of the bipolar control voltage. The optical switching of the absorption can be high: >0.5 at $\lambda = 650\ \text{nm}$. Obviously, the mechanism of this action of the field lies in the conformational rearrangements of copolymer chains, since ionic liquids affect the rotational isomerism of these polymers.²⁴⁸

7. Materials for memory cells

The operation of a ferroelectric-based memory cell is related to the possibility of fast switching of the spontaneous (remanent) polarization by a bipolar external field.^{249, 250} Ferroelectric polymers are characterized by high coercive fields, and for operation of low-voltage circuits, thin films should be used. However, it is known that for film thickness $< 100\ \text{nm}$, the remanent polarization decreases,²⁵¹ and it is necessary to pay attention to the contact phenomena at the electrode/polymer interface. For example, in a $65\ \text{nm}$ -thick P(VDF–TrFE) film, a remanent polarization of $65\ \text{mC m}^{-2}$ was obtained. When an organic electrode was used, polarization in the film was switched by a voltage of $5.2\ \text{V}$ ($80\ \text{MV m}^{-2}$) in $80\ \text{ms}$. In the case of aluminium electrode, the switching time was greater by three orders of magnitude.²⁵² This is due to the fact that reactions of aluminium with copolymer defects displaced to the surface give rise to new functional groups, which affect the switching characteristics. The formation of thinner films for this purpose is hardly possible due to the specific structure and dynamics of crystalline polymers.²⁵³

The use of PVDF oligomers characterized by high remanent polarization is inappropriate, since the coercive fields in them are several times higher than those in polymer films. An adverse role may also be played by the equilibrium space charge,^{191, 254, 255} the formation of which requires a much longer time than switching of the remanent polarization. The composition of the P(VDF–TrFE) thin film

can be modified by epitaxial growth on oriented PTFE.²⁵⁶ However, high-voltage polarization leads to relatively low remanent polarization values ($17\ \text{mC m}^{-2}$); nevertheless, after 5×10^8 switching cycles with $\pm 5\ \text{V}$ control voltage, 88% of the initial polarization value is retained.

One more approach to the application of these materials for the design of memory cells was proposed by Asadi *et al.*²⁵⁷ The authors formed an active element from immiscible components: P(VDF–TrFE) copolymer and an organic semiconductor — poly(3-hexylthiophene) (Fig. 30 a).

Due to high conductivity of the initial film caused by the presence of a semiconductor, this material cannot be used as a usual ferroelectric. Analysis of the current–voltage characteristics after film polarization (Fig. 30 b) demonstrated that the film behaved as a diode. The polarization charge of the copolymer on contact with poly(3-hexylthiophene) changes the concentration of charge carriers in the latter. This results in decreasing barrier for carrier injection from the electrode (Ag), and the current increases. After switching of the control voltage sign ($3\ \text{V}$), the situation symmetrically changes. As can be seen, the difference between the currents may reach more than an order of magnitude; hence, this resistive element is suitable as a memory cell, the more so, because the stability of these currents on an increase in the number of cycles is relatively high (Fig. 30 c).

The engineering application of ferroelectric polymer films for data readout can be performed in the metal–ferroelectric–metal configuration, but the metal–ferroelectric–insulator–semiconductor–metal configuration is more convenient.²⁵⁸ In this case, the task is solved using a ferroelectric film as a control electrode in a field effect transistor, the calculation of which was reported by Miller and McWhorter.²⁵⁹

An important characteristic of the considered devices is the ratio of the transistor currents at switching on and off of the control voltage generated by the polarized ferroelectric polymer. One more important characteristic is the number of switching cycles for which the on/off ratio remains relatively high. Below we analyze some data reflecting the dependence of the indicated parameters on the structure and morphology of the material of the control electrode, represented by a ferroelectric polymer film. Naber *et al.*²⁶⁰ devoted considerable attention to the selection of a solvent for P(VDF–TrFE) that would allow preparation of a defect-free film. In a field effect transistor with a

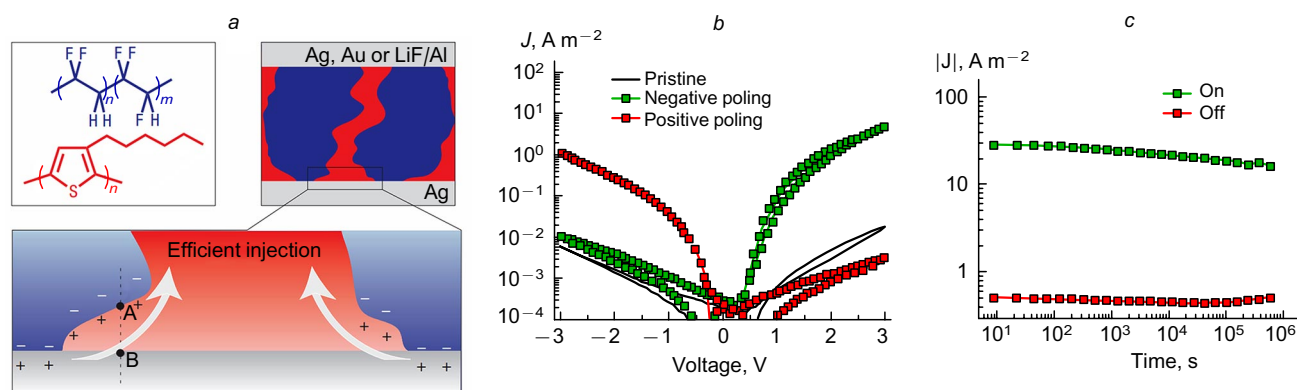


Figure 30. Scheme of formation of a phase-separated mixture of P(VDF–TrFE) copolymer and organic semiconductor, poly(3-hexylthiophene) (a), current–voltage characteristics of the diode formed by this mixture (b) and time stability of the switched current (c).²⁵⁷ Published with permission from Springer Nature.

200 nm-thick film at a control voltage of 15 V, the on/off ratio was $\sim 10^2$.

Kang *et al.*²⁶¹ used a modified pentacene as a single crystal. When the standard spin coating procedure was used, pentacene was formed directly on the film. In the initial state, the field effect transistor had on/off ratio of $> 10^3$, which is higher than in the case of vacuum deposition of pentacene. The characteristics of this device can be improved by orientation of the P(VDF-TrFE) film.²⁶² With all other conditions being equal, this procedure is justified, as this leads to a decrease in the high-voltage conductivity and, hence, to an increase in the remanent polarization;⁸⁹ it was also indicated that the orientation is accompanied by a threefold decrease in surface roughness. The same trend (though in a less explicit form) was also noted by Nguyen *et al.*²⁶² The most important is that the film orientation was accompanied by a twofold increase in the charge carrier mobility in pentacene. The authors²⁶² also attained the on/off ratio at a level of 10^3 .

In the above cited studies, organic semiconductors were used; therefore it is reasonable to compare their results with the data on field effect transistors based on classical inorganic semiconductors. Yamauchi²⁶³ used the Al-SiO₂-P(VDF-TrFE)-SiO₂-Si field effect transistor. Silicon (with a resistivity of 3–5 Ωcm) served as a grounded electrode. The introduction of two layers of the SiO₂ insulator excluded the injection of carriers into the polymer from the electrodes, thus increasing its breakdown characteristics. As the control voltage reaches ~ 190 V, a sharp step appears in the curve of the current in the transistor circuit, with the on/off ratio reaching 10^6 . This is three orders of magnitude higher than that for organic semiconductors, but the switching voltage in the latter is at least an order of magnitude lower. The prospects for decreasing this voltage in the case of silicon may come from decreasing the thickness of the polymer layer and selection of an insulator with a higher dielectric permittivity.

8. Physical grounds for application of polyvinylidene fluoride-based materials in various fields of biomedicine

Currently, biomedical applications of PVDF and other ferroelectric polymers, including implantology, biosensing and harvesting and conversion of biological energy, have

been addressed in numerous reviews (see, for example, Refs 264–274). The application areas are considered in detail in a monograph.²⁷⁵ In this Section, the attention is focused on a new field of medicine that actively uses the main physicochemical properties of PVDF as a piezo- and ferroelectric with acoustic impedance close to that of biological tissues and with a relatively low Q -factor, which provides a broad range of tuning of impact parameters on a biological tissue. This field is regenerative medicine, especially therapeutics, which combines therapy and diagnostics using a common material.

Modulation of the cellular response using sensors based on PVDF and other ferroelectric polymers can be provided simultaneously by their domain structure (presence of β -phase) and piezoelectric, pyroelectric and/or photovoltaic effects as well as by the types of bioelectrochemical and ultrastructural and electrokinetic consequences of these effects in a partially ordered (soft matter) biological medium.²⁷⁶ An important role in these systems is also played by osmosis (electro-osmosis), including the cell volume regulation and the corresponding forms of biological cell signal transduction induced by these factors, electroporation (pore formation in the membrane), modulation of ion channel activity and electrokinetic (including dielectrophoretic) movement of compartments, cell ultrastructure elements and whole cells in the external field of PVDF substrates.

The diagram of electro-osmotic flow induced by a ferroelectric polymer substrate is depicted in Fig. 31. Under the action of an external electric field, ions (Ca²⁺ cations are shown as an example) migrate and some of them approach the cell membrane (solid black arrows in Fig. 31a). The ions have a hydration shell. Free water molecules can be carried along by the electro-osmotic flow, if it is strong enough, and move in the same direction (dashed arrows). The electro-osmotic flow causes displacement of membrane structures such as proteins due to the molecular resistance (Fig. 31b). These structures can transmit cell signals or, as shown in the Figure, can be attached to the cytoskeleton. When the electro-osmosis is stable (white arrows in Fig. 31c), the cellular membrane can be polarized with time (proteins move and accumulate at the pole of the cell). As a consequence, signal transduction is either enhanced or inhibited (signal transduction gradient). Using this effect, it is possible to control, for example, cell migration in certain directions.

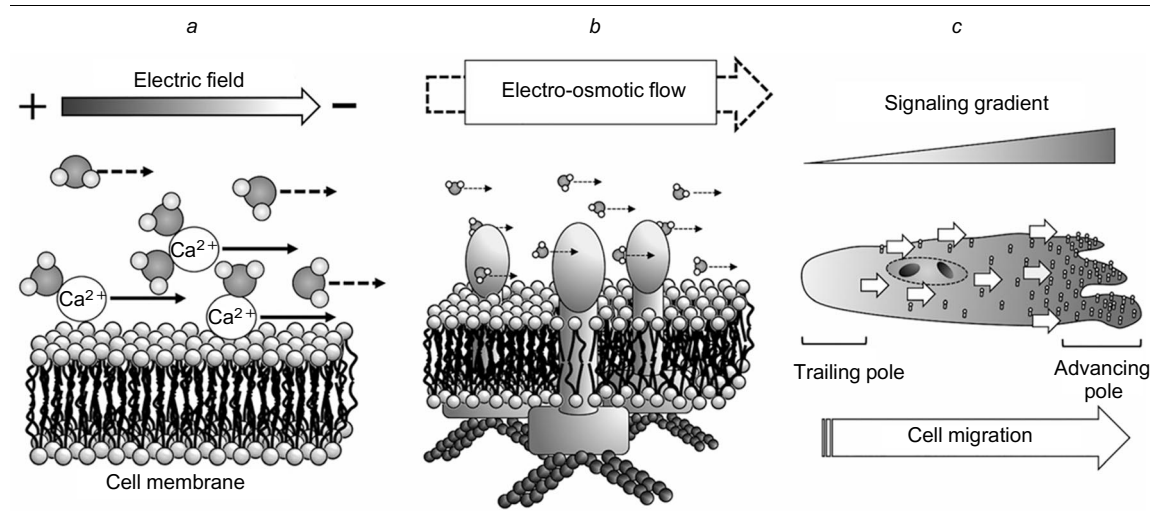


Figure 31. Electro-osmotic process that can take place on a cell membrane under the action of electric field.²⁷⁶ For *a–c*, see text. Published with permission from AIP Publishing.

Molecular crowding induced by an electric field also makes a contribution to modulation of biological activity and is a way of self-organization of biomacromolecular structures in an external electric field.

8.1. Smart scaffolds for non-invasive piezoelectric theranostics

When PVDF-containing hydrogels are used for magnetic and electrical stimulation of tissues²⁷⁷ capable of electrical response to nanomechanical stimuli and response to pulsed electromagnetic field generated by PVDF,²⁷⁸ the performance of the main inductive biophysical functions depends on the electrophysical properties of the β -phase. This phase ensures high pyro- and piezoelectric characteristics of PVDF. For example, dipole alignment provides the maximum dipole moment, which allows considering the β -PVDF scaffolds (3D frameworks for cell growth and tissue regeneration produced by electrospinning²⁷⁹ or, more rarely, by 3D printing²⁸⁰) as both sensors and sonars, that is, actuators capable of electric (electrophysiological) or acoustic (electroacoustic) tissue stimulation and recording of its own signals. This makes the controlled tissue regeneration using PVDF-based materials a special branch of theranostics in which the scaffold itself provides detection of analytical signals from the supported tissue. Whereas PVDF application for bone tissue regeneration^{281,282} is faced with the challenge of intraosteal (intra-bone) signal detection, in the case of excitable soft tissues such as muscle tissue (especially striated cardiac muscle tissue), gland tissue (especially upon electrostimulation)²⁸³ and nerve tissue, detection of the diagnostic signal is not a problem.

The electrophysiological or magnetoelectric²⁸⁴ response of an excitable tissue can be measured by contactless non-invasive methods — electromyography (including the use of cutaneous electrodes), electrocardiography and electroencephalography — and their magnetic analogues — magnetomyography, magnetocardiography, magnetoencephalography. Considering the metrological aspect, this principle is applied rather easily for remote analysis of the tissue response taking account of the reactivity of the smart PVDF scaffold (according to the definition given in the Encyclopedia of Smart Materials,²⁸⁵ PVDF is a smart material). However, this is a challenge for practical theranostics due to multiple feedbacks between the tissue and PVDF.

The diversity of medical applications of PVDF is determined by its unique physical properties inherent in ferroelectric materials providing a versatile energy conversion and, hence, conversion of control or analytical signals. The efficiency of energy conversion in the PVDF matrix depends on the content of polar crystals of the β -phase, which can be controlled during the manufacture of PVDF-based materials.^{286–288} Therefore, it is possible to vary physical stimuli (*e.g.*, acoustic and electric signals) that are transduced to a living cell or a tissue from an electroactive material and back. The morphological difference between the PVDF fibres synthesized under different conditions is illustrated by Fig. 32. The above noted properties of PVDF make it possible to construct various physical algorithms and ways of signal conversion involving PVDF; they could form the basis of new techniques for stimulation, diagnostics, treatment and studying of natural properties of biological tissues in the regenerative medicine. Examples of this type of application of PVDF-based materials are given below.

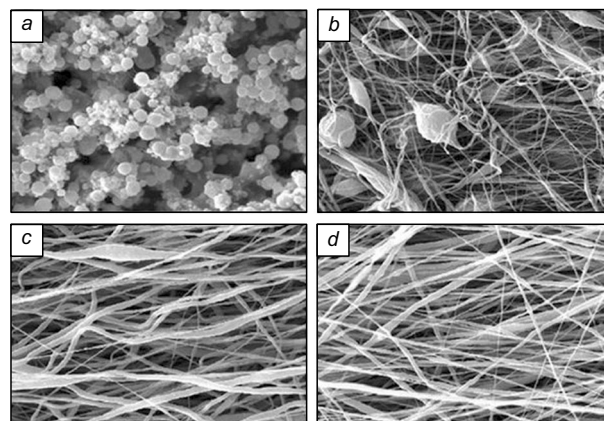


Figure 32. SEM images (SEM is scanning electron microscopy; magnification up to 10 000) of the PVDF fibres of nanofibrillar scaffolds. PVDF concentration in the initial solution (mass %): 10 (a), 20 (b), 25 (c), 30 (d).²⁷⁹

8.2. Scaffolds for nervous tissue regeneration

The PVDF electrospinning technique capable of mimicking the structure and function of the extracellular matrix is a fairly popular biomimetic approach to the design of supporting scaffolds for the development of nervous tissue (Fig. 33). PVDF-based scaffolds implanted into the patient's body provide for the integrated electrophysiological, morphological and functional restoration of the nervous tissue. For example, owing to the electroactivity and biocompatibility inherent in PVDF, these scaffolds can be used as piezoelectric framework for tissue regeneration in the peripheral nervous system.

In view of the considerable increase in the content of the β -phase in the PVDF matrix after electrospinning and the value of ζ -potential of polarized PVDF [close to that of P(VDF-TrFE)], the electrospun PVDF-based scaffolds possessing piezoelectric activity can be considered as promising materials to be used as artificial systems for neural guidance for the restoration of damaged peripheral nerves. When iron-containing magnetic particles are added to the raw material for production of the fibre, the direction of cell growth in an electric field changes, and the ferroelectric polymer is transformed into a composite — a multiferroic. Simultaneously, the cell proliferation trajectory also changes, and even non-neuronal pluripotent stem cells form neural-like structures inherent in the peripheral nervous system. These issues are discussed in the literature in more detail.^{289–295} The development of nervous tissue requires also glial cells. A PVDF-based scaffold promotes adhesion of glial cells (especially Schwann cells) and fibroblasts and active biochemical and physiological functioning of these cells within an implant at the interface with the nervous tissue, as convincingly demonstrated in the literature.^{296–300} The micrographs of neurons and glial cells, that is, astrocytes and oligodendrocytes (more precisely, their precursors) grown on a PVDF scaffold are shown in Fig. 34.

The development of techniques for frequency-selective excitation of ferroelectric materials (*e.g.*, microfibres obtained by electrospinning of PVDF type ferroelectric polymers and acquiring the relevant properties upon polarization during the manufacturing process) implies the existence of conditions providing signal transduction along a

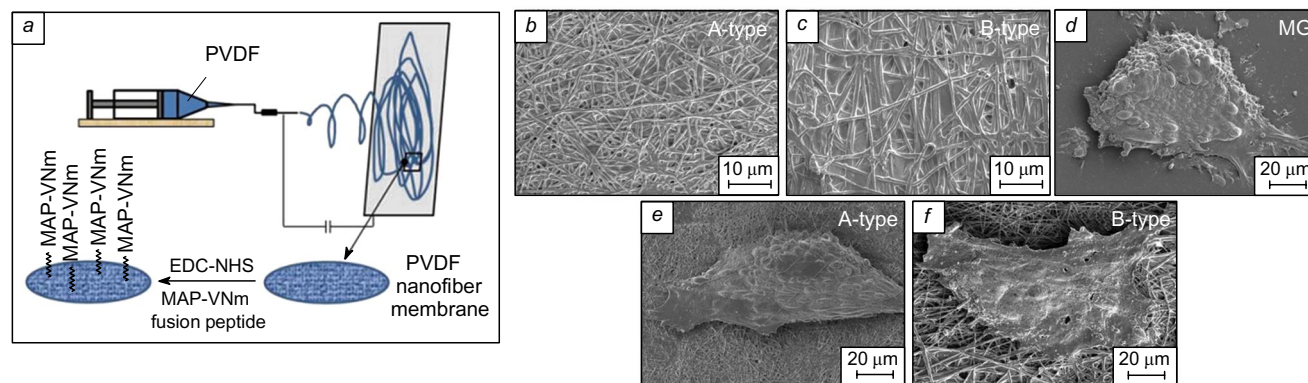


Figure 33. Scheme of formation (a) and SEM characterization (b–f) of PVDF scaffolds.²⁹⁰ Designations: EDC-NHS is activation of the scaffold surface with 1-ethyl-3-(3-dimethylaminopropyl)carbodiimide and *N*-hydroxysuccinimide; MAP-VNm is the subsequent treatment of the scaffold surface with the hybrid recombinant protein promoting the adhesion of stem cells; A-type and B-type are PVDF membranes with fibre diameters of 200 nm and 700 nm, respectively; MG is matrigel.

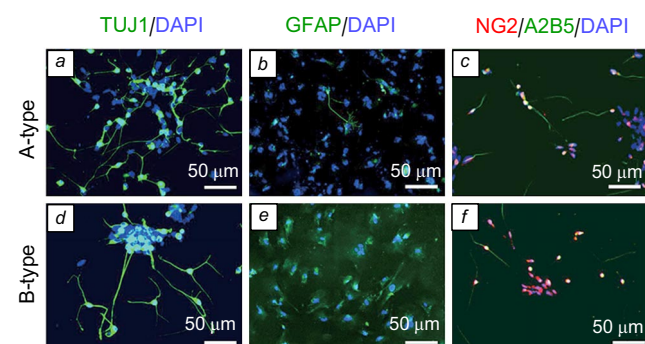


Figure 34. Immunofluorescence images of neurons (a, d), astrocytes (b, e) and oligodendrocyte precursors (c, f) differentiating on PVDF scaffolds of two types.²⁹⁰ A-type: PVDF membranes with fibre diameter of 200 nm, B-type: PVDF membranes with fibre diameter of 700 nm, DAPI (4',6-diamino-2-phenylindole dihydrochloride) is a blue fluorescence dye, TUJ1 is anti-beta III tubulin antibody (class III beta-tubulin is a neuron-specific protein of microtubules), GFAP is anti-gial fibrillary acid protein antibody (the main structural component of astrocytes), NG2 is antibody against the glycoprotein of the chondroitin sulfate proteoglycan family (neuroglia component), A2B5 is antibody against the ganglioside expressed by oligodendrocyte precursor cells.

particular channel (e.g., along a fibre in the case of electrospun materials). Therefore, this may be regarded as a development of targeted systems of biocompatible fibres the excitability of which can be selectively controlled.

8.3 Scaffolds for bone and muscle tissue regeneration

In the modern bone tissue engineering, particular attention is paid to piezoelectric materials based on PVDF, which are able to generate surface charges upon minor mechanical strain. The cells on the surface of piezoelectric PVDF nanofibre scaffolds are readily activated, which is due to the change in ion channel activity and ion transport (especially intracellular calcium transport; the activation of calcium concentration waves is detected by confocal microscopy upon introduction of cells on a PVDF substrate). By utilizing the self-stimulation of cells attached to piezoelectric PVDF fibres, it is possible to manufacture tissue-like functional 3D scaffolds for bone tissue engineering. It is also possible to control the surface potential of PVDF fibres

by means of positive and negative voltage polarity during the electrospinning; this gives rise to two types of scaffolds: PVDF (+) and PVDF (–). It was shown that a pulsed electric field is more efficient for the formation of potential of the fibres. It is also acceptable to introduce mineral components that promote bone tissue regeneration into the composite during the electrospinning; this allows one to control the micromechanical properties of the composite related to the porosity (Fig. 35), together with providing the desired electrophysiological properties. The optimal porosity of the scaffolds ensures an efficient cell in-growth. The percolation parameters of the scaffolds control the permeation and diffusion of biochemical agents. The scaffold grain structure and microroughness, including spherulites (and similar structures) provide efficient cell spreading on the surface, since cells are better distributed over a microheterogeneous surface. These issues are considered in more detail in the literature.^{301–307}

To take full advantage of the properties of PVDF scaffolds, it is expedient to carry out their preliminary mechanical cycling and ferroelectric stimulation by mechan-

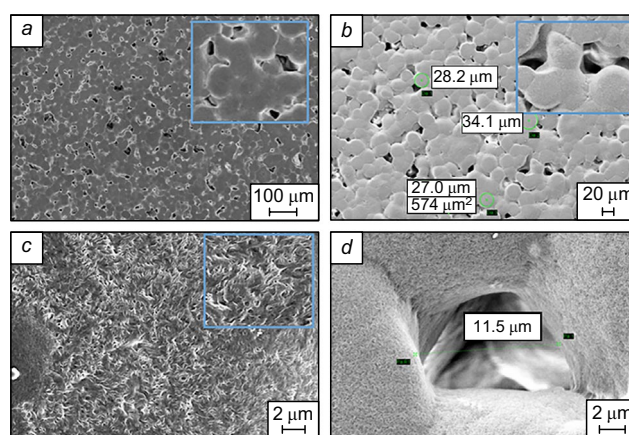


Figure 35. Electron micrographs of the surface of PVDF scaffolds.³⁰¹ The squares in Figs a–c mark characteristic elements of the scaffold texture at large magnification; the numerals in Fig. b indicate the sizes of spherulites (marked in green), and in Fig. d, the transverse dimension of the pore is indicated. Published with permission from Elsevier.

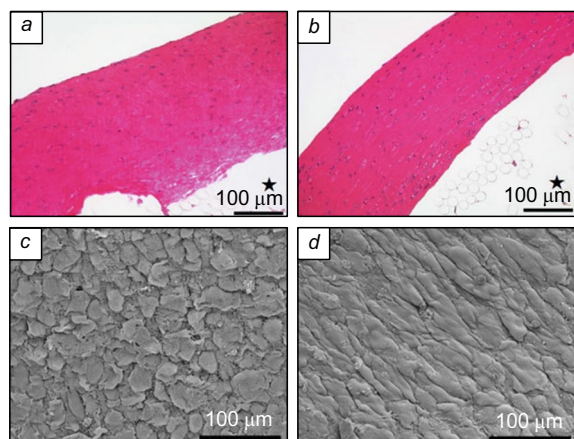


Figure 36. Morphology of pristine (*a, c*) and stimulated (*b, d*) scaffolds.³¹⁶ Figs *a, b* are tissue sections (hematoxylin eosin staining), the asterisk marks the inner space of the channel; Figs *c, d* are SEM images of the surface. Published with permission from Springer Nature.

ical and/or electrical signals. The effect of such treatment on the microstructure needed for cell development is illustrated in Fig. 36, which shows micrographs of the surface of stimulated and pristine scaffolds.

Popkov *et al.*^{308,309} demonstrated the compatibility of PVDF with Ilizarov apparatus (transosseous compression distraction device for osteosynthesis: bone welding and bone fracture healing); this attests to the piezo-active role of mechanical stress and the possibility of using this activity in the design of implants based on piezoelectric PVDF materials. The possibility of fabrication of intramedullary implants^{310–312} the bacteriostatic effect of which is attained *via* magnetron plasma treatment^{313–315} was reported. A possible option is also mechanical piezo-stimulation of muscle tissue development. The appearance of artificial muscles that contract in an electric field and thus stimulate the development of muscle tissue seems to be the near future of regenerative medicine.^{316–318} This is predetermined by the mechanical and morphological features of PVDF as a piezo-active scaffold (Fig. 36 and 37) and by the activity of cells that undergo morphogenesis and differentiation under stimulation conditions on PVDF (Fig. 37, 38).

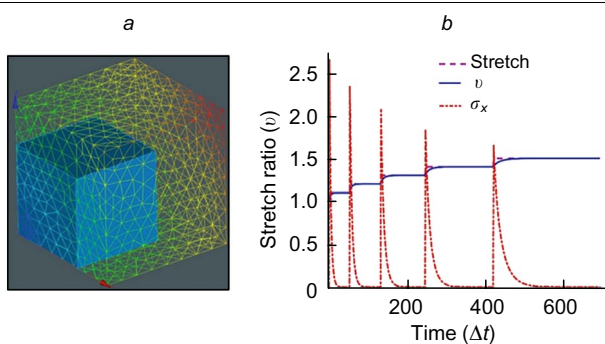


Figure 37. Finite element simulation of the triaxial stretching of a PVDF scaffold.³¹⁶ Fig. *a* shows compressed (shown in blue) and stretched (shown in green) scaffolds; Fig. *b* presents time dependences of stretch, stretch ratio (ν) and mechanical stress (σ_x). Published with permission from Springer Nature.

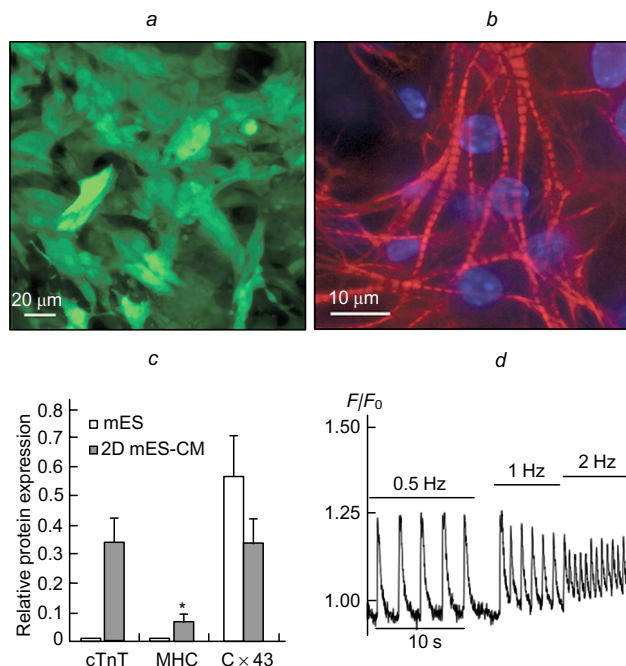


Figure 38. Effect of electrical stimulation of different frequency on the development of cell structure on PVDF scaffolds: (*a*) general view of muscles (cardiomyocytes); (*b*) sarcomeres in cardiomyocytes with actin staining; (*c*) biochemical activity of cardiomyocytes in the expression of various proteins; mES and 2D mES-CM designate various types of cells, cTnT is cardiac troponin T, Cx43 is connexin-43, MHC is heart heavy chain myosin; *d* is amplitude of the electrophysiological response (F/F_0) of cardiomyocytes to various stimulation frequencies.³¹⁹ Published with permission from John Wiley and Sons.

8.4. Materials used in cardiology

Cardiac muscle tissue composed of cardiomyocytes is the most highly organized type of muscle tissue, activated by an electric field and possessing automatic contractile function. Electrospun PVDF and P(VDF–TrFE) scaffolds possess a piezoelectric activity and can generate an electric charge in response to a minor mechanical strain. The myocardium consists of electrically active tissue, and this can be used in tissue engineering of the cardiovascular system. Embryonic stem cell-derived cardiomyocytes and endothelial cells efficiently grow on P(VDF–TrFE) scaffolds; they are adhesively attached to the polymer matrix and are aligned along the fibres. In the case of culturing on P(VDF–TrFE) scaffolds, these cells are spontaneously contracted; this is accompanied by the morphogenesis of sarcomeres and biosynthesis of a number of classical cardiospecific markers. In addition, mesenchymal stem cell cultured on P(VDF–TrFE) scaffolds also actively respond to the exogenous electrical stimulation and demonstrate calcium signalling patterns inherent in developing cardiomyocytes. In view of the above, it is possible to fabricate a cardiac implant with a built-in stimulator based on PVDF. Heart activity signals can be detected from these implants and used for therapeutic feedback. This can be done directly in blood stream, because no overgrowth of the implant takes place and the haemocompatibility of PVDF is rather high. A number of publications^{319–326} address these issues in more detail.

Note also that PVDF and its copolymers can serve for the fabrication of vascular implants³²⁷ and haemocompatible catheters.^{328–330} Devices of this type can influence the

physiological function of the body and serve as detectors (such as needle microphones or applicative detectors) to monitor the function efficiency. The surface microphones and heart rate, blood pressure and flow rate sensors can be easily implemented using PVDF. Cardiac auscultation without the use of hearing or analogue stethoscope can also be accomplished using this type of sensors.^{331,332} From the standpoint of theranostics, analysis of haemodynamics using actuators, sensors and transducers based on PVDF is not limited to the control of endogenous processes; implementation of extracorporeal processes related, for example, to enhancement of blood purification and haemodialysis in a PVDF-generated electrical field is also possible.^{333–337} This is provided by high haemocompatibility and low overgrowth of PVDF membranes at a controlled wettability (in particular, electrical field-controlled surface hydrophobicity during electrowetting). The detection and modification of blood properties can be combined on a real-time basis by using alternating filtration and measurement processes or by spatially separating these processes in distributed systems.

Currently, it appears possible to use PVDF capillary fibres as substitutes for vascular and capillary functions^{338–341} and simultaneously as artificial channels for targeted delivery of pharmacological agents to known targets. This may involve both a laminar flow and a microfluidic flow perturbed on topological singularities (surface irregularities); this enables laminar-to-turbulent transition and change in the flow properties. The properties of the flow depend on the rheology of the components, which is often used in microfluidics.^{342–346} The membrane (membranomimetic) properties of PVDF films, including the controlled porosity (Fig. 39), are also actively utilized for the exchange with the body medium. The developed vascular prostheses and haemodynamic energy converters based on PVDF such as microfluidic biocompatible systems³⁴⁷ (in

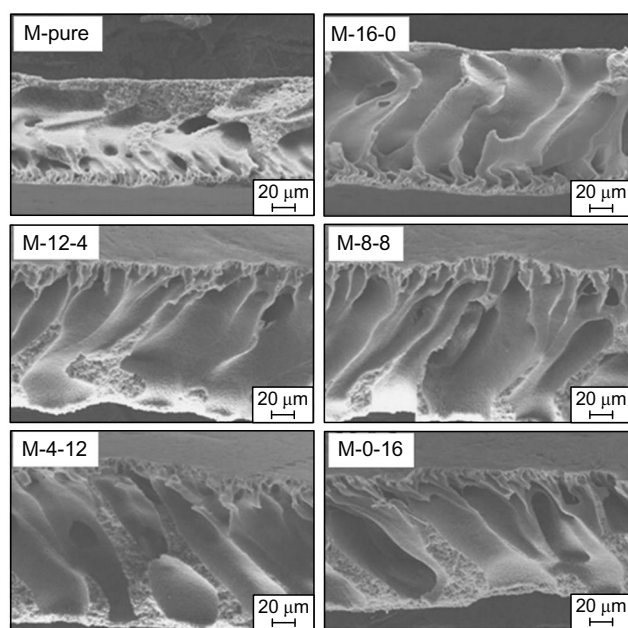


Figure 39. Examples of pores in PVDF membranes used to manufacture vascular prostheses.³⁴¹ In the upper parts of the figures, designations of samples differing in composition are given. Published with permission from Elsevier.

particular those converting the energy of vortex flow arising on surface inhomogeneity into the heat exchange energy)^{348–350} allow the design of energy supply systems for smart prostheses with active elements without controlled energy supply and storage in a peripheral unit^{351–353} located beyond the active implant and interfering with its self-sustained operation.

8.5. Materials used in urology

Many processes in regenerative medicine are based on mesenchymal stem cells, which successfully grow not on any potentially implantable substrate. Stem cell proliferation and differentiation potential can be considerably increased by culturing the cells on PVDF substrates or, to a higher extent, on electrospun PVDF–TGF β (where TGF β is transforming growth factor, a beta-protein that controls proliferation, cell differentiation and other functions in most cells). The efficiency of this approach was demonstrated in relation to bladder wall.^{354–356} From the standpoint of theranostic specialists, PVDF can be used to receive signals of bladder filling. Fast growth of cells on the scaffold resulting in a continuous cell layer (with topological inhomogeneities) is illustrated in Fig. 40.

The renal insufficiency can also be treated by introducing PVDF scaffolds directly into a kidney. Highly efficient values were established for electrospinning parameters and for characteristics of other procedures for the preparation and fabrication of implants for regenerative medicine and renal implantology. For example, it was shown³⁵⁷ that the optimal conditions for the fabrication of an electrospun PVDF scaffold include a voltage of 20 kV, a tip-to-collector distance of 100 mm and a flow rate of 0.5 mL h⁻¹. The resulting fibre diameter was found to be statistically more affected by the tip-to-collector distance and the flow rate, while the pore size in the material depended to a greater extent on the applied voltage. However, the fibre diameter and the pore size in electrospun scaffolds were smaller than those in the native renal tissue. Nevertheless, the approach using PVDF is unique and has no analogues in the electrostimulated renal regenerative therapy.

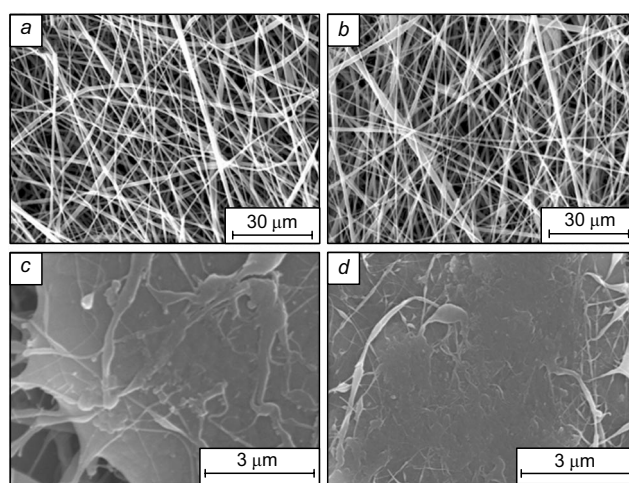


Figure 40. SEM images of the scaffold for bladder prosthesis covered by cells;³⁵⁴ (a, b) initial state of the scaffold; (c, d) after two weeks of cell growth. Published with permission from Elsevier.

8.6. Materials for connective tissue regeneration

Piezo-stimulated regeneration of connective tissue, including derma, is possible. PVDF substrates/carriers have a beneficial effect on the activity of fibroblasts — connective tissue cells that synthesize extracellular matrix and collagen.^{358,359} Therefore, any processes of regenerative medicine involving fibroblasts can be intensified using PVDF. In particular, the β -phase of PVDF was found to accelerate the wound healing.

During electrospinning, the non-piezoelectric α -phase of PVDF is transformed into the piezoelectric β -phase. The fibroblasts cultured on β -PVDF scaffolds are characterized by normal morphology and highly efficient proliferation. The fibroblasts cultured on piezoelectrically excited scaffolds also show enhanced migration, adhesion and secretion. The in-growth of cells into PVDF scaffolds was greater than that for classical polyurethane scaffolds (Fig. 41). The post-surgical and diabetic wounds were healed equally efficiently. More detailed information on this issue can be found in the literature;^{360–365} the most recent studies carried out in Tomsk (Russia) were reported by Tverdokhlebova *et al.*³⁶⁶

8.7. Artificial muscles

The techniques that ensure the introduction of artificial muscle tissue into the human or animal body are currently insufficiently developed to be implemented in practice.^{367–370} However, the advances in the fabrication of artificial muscles and biosimilar actuators for robotic applications suggest the conceptual possibility and promise of using these structures in biomedicine. This is hampered by the absence of a feedback systems or matching of the response parameters between biological tissues and

implanted or applied PVDF-based materials that mimic a muscle; this results in very high (and detrimental for the body and the implant) loads in the contact area of the living tissue and the material.

In view of the above, a relevant trend of PVDF application is related to incorporation into implanted structure of a sort of encoders, or feedback sensors, which would provide for mutual correlation (or even counterbalancing) of excess mechanical stress of an artificial PVDF muscle in proportion with the encoder signal corresponding to the load.^{371–375} An example of such a multilayer design of the PVDF-based sensor actuator and ionic polymer–metal composite (IPMC) is shown in Fig. 42.

A review of special literature demonstrated that currently the PVDF-based pressure, extension and force sensors are used only outside the human or animal body or outside a smart reactive implant.³⁷⁶ This is due to the fact that the possible consequences and physical reliability of such structures on long-term operation in the body are not entirely clear.³⁷⁷ However, one can find numerous examples of using such sensors as artificial skin regulators for robotic purposes and tactile sensors for smart mobile devices.^{378–380}

Not only piezoelectromechanical, but also acoustomechanical, electroacoustic and acoustofluidic PVDF-based techniques may prove to be promising for physical movement of particles and change the positions of structures. The acoustically active ferroelectric polymers are capable of flexible frequency tuning; therefore, they can not only define the modulation, but also serve as (bio)acoustic platforms for the motion of liquids, *i.e.*, as acoustofluidic structures with electroprogrammable frequency tuning and modulation of the efficiency and the direction of (micro)fluidic transport.^{381–384}

The notion acoustofluidics integrates a number of basically different processes and mechanisms of action on liquid or partially ordered (soft matter) media and disperse systems. Using these processes, it is possible to move micro- and nanoparticles,^{385,386} including living cells,³⁸⁷ in an acoustic field; to direct liquid flows^{388,389} using acoustic

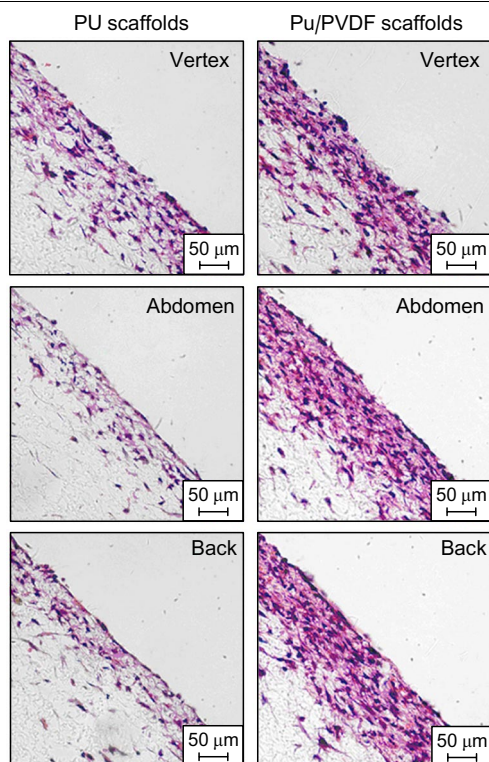


Figure 41. Cell in-growth depth of PVDF scaffolds (on the right) and conventional polyurethane scaffolds (on the left).³⁶⁰ Published with permission from Elsevier.

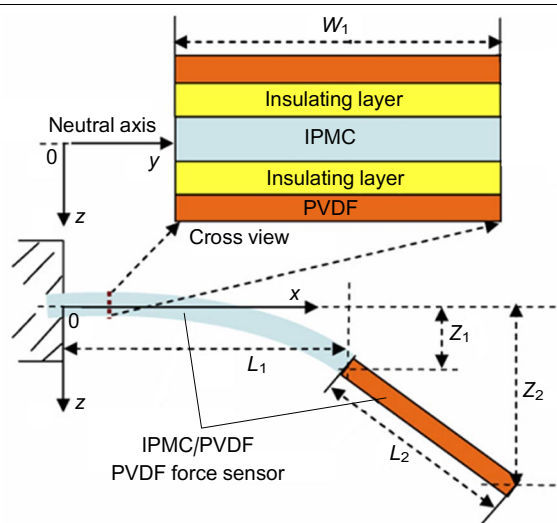


Figure 42. Structure diagram and elastic beam bending of PVDF-based mechanoelectric sensor actuator for biomedical application.³⁷¹ L_1 and Z_1 are the length and displacement of the bending structure, L_2 and Z_2 are the length and displacement of the rigid beam. Published with permission from Elsevier.

pressure^{390,391} or acoustophoresis effects; form cavities,³⁹² envelop particles;³⁹³ transport particles over long distances;³⁹⁴ and synthesize cell spheroids,³⁹⁵ neurospheres^{396–398} and other constructs^{399–405} (which is often used in experimental oncology^{406,407}). By means of acoustofluidics, it is possible to form programmed gradients at the boundaries,⁴⁰⁸ control the time course of reactions,⁴⁰⁹ and to develop the chemical signals and wave generators^{410,411} that regulate the cell behaviour. The processes that occur in acoustofluidic systems may result in formation of many other biologically active compounds, in particular, in threshold nano-quantities, which are still sufficient for the chemostimulation of cells.^{412,413} In addition, acoustofluidics can be used for engineering of systems of ultradispersed particles, controlled aggregation, component enrichment and nanostructural self-organization of both mineral inorganic and polymer structures.^{414–420}

The foregoing suggests that the use of PVDF and principles of acoustofluidics may enable cell sonoporation (and, hence, the targeted delivery of macromolecular pharmaceuticals and genetically engineered constructs)^{421–425} and the targeted drug delivery, in particular, the delivery of diagnostic and theranostic agents.^{426–432} In this regard, PVDF is a unique biocompatible material that is used in acoustofluidics and associated techniques (*e.g.*, electromagnetic materials, multiferroics and metamaterials^{433–435}). Therefore, PVDF can be used on acoustofluidic principles directly in an implanted device in the body (or in contact with tissues), which means the highest degree of connection of biomedicine and acoustofluidics.⁴³⁶ This may benefit the regenerative medicine.

8.8. Fabrication of fully functional tissue prostheses

The fabrication of bioimplantable devices based on PVDF is well fitted in the research area related to the design of fully functional tissue prostheses, *i.e.*, hybrid devices implanted into the body that are able to respond to external stimuli, including the physiological response of the replaced organ and surrounding tissues (for details, see Ref. 417, pp. 69–84). The basic systematic criterion determining the optimal reactivity of the implant is its active adaptability to mechanical and biological factors (Ref. 437, pp. 53–60). In this regard, PVDF as a ferroelectric material possessing biocompatibility, mechanical sensitivity and electrophysiological activity is optimal for the design of implants.^{438,439}

Considering the principles of biomechanics (more precisely, biomimetic mechanics), it seems possible to manufacture PVDF-based cardiac valves, haemodynamic accessories, smooth muscle stimulators, tissue contraction rhythm simulators (*e.g.*, for bladder tissue^{354,355}) and respiratory support systems. According to the concept of fabrication of expandable plastic and elastic implants, which can be used in paediatric surgery, unlike rigid implants (Ref. 437, pp. 15–22), both self-healing prostheses and porous scaffolds and also tissue engineered constructs adaptable to the growing body are in demand.

In this connection, it appears pertinent to discuss the role of PVDF as a possible material for the fabrication of porous, including fibrillar, scaffolds that can maintain plastic and elastic deformation, thus providing biomechanical activity in a growing body. A number of shape memory materials as trainable reactive structures were proposed for this purpose. The active implant should learn to reproduce the dynamics of a normally functioning organ during the human body development rather than to reproduce separate

static states.⁴⁴⁰ The device should also mimic the reversible transition between the states and the adaptive response to the intrinsic (endogenous) state of the organ tissue, the degree of its filling and innervation performed by electrophysical (electrophysiological) pathway. This problem could be perfectly solved using polarizable PVDF.^{441,442} The physical effects inherent in this material open up the possibility of generating multiple feedbacks and maintaining regular dynamics, against the background of the chaotic environmental dynamics, with a selective response to its change affecting a particular feedback stage (electrical, mechanical or acoustic). These issues are considered in detail in a collected book.⁴⁴³

9. Conclusion

Currently, the engineering and biomedical applications of PVDF and its copolymers have passed from the laboratory stage of research to active practical implementation. Whereas before 2009, the PubMed (National Library of Medicine, National Institutes of Health, Bethesda, USA) database indexed not more than a hundred publications dealing with PVDF every year, in 2021, their number was 560. However, some of the most recent biomedical trends (in particular, most of those discussed in this review) and engineering applications have not yet been systematically integrated in the literature. This accounts for the relevance of the material presented here.

A number of reviews published since 2020 address the design of energy storage devices using PVDF,^{444,445} ranging from passive separators for lithium ion batteries^{446,447} to piezoelectric nanogenerators.^{448,449} However, these and some later publications^{450–455} are rather concerned with engineering aspects than with physical aspect analysis. This is due to the fact that most of the authors are not materials scientists, in particular, they do not specialize in the physics of crystalline polymers; therefore, the results they obtained often did not receive a strict physical interpretation. This is especially true for the new state of the materials used as electrospun microfibrils^{456–460} and sensor applications of PVDF for measuring parameters of liquids and gases.^{461–463} Therefore, we set ourselves the task to describe the results that can be interpreted in terms of the hierarchical structure of crystalline polymers. An important role is assigned to the polymers with two forms of heterogeneity, structural and dynamic one. This approach to discussion of experimental data has never been used before.

From this standpoint, it is possible to analyze the material of some parts of the collected book⁴⁴³ published in 2022, which describes a number of PVDF applications addressed also in this review. For instance, part 14 of the book considers composites based on ferroelectric polymers. Section 2 of our review also presents this type of data; however, we discuss the polymers themselves, with attention being focused on the possibility of transforming fluorinated ferroelectric polymers to the relaxor state, which potentially provides for high energy storage capacity. Two key methods for polymer modification are considered, that is, irradiation with high-energy electrons and chemical modification. Examples demonstrating improved energy storage characteristics are given. This review emphasizes for the first time that the power density transferred to the resistive load can reach 200 MW cm⁻³. To explain these values, we took into account the fact that the chains of the amorphous phase of these polymers exist, at room temperature, in the liquid-like

state with a relaxation time of $\sim 1 \mu\text{s}$. This is a new conclusion that shows the necessity of taking account of cooperative dynamics in the amorphous phase chains. A new view of the mechanism of increasing breakdown fields *via* modification of ferroelectric polymers is presented (which is highly important for the capacitive energy storage devices).

Part 15 of the collected book cited above (Ref. 443, p. 503) considers the use of ferroelectric polymers as an alternative to fossil energy sources. The material presented in this review is appropriately supplemented by the results outlined in the book. In particular, we discussed little known studies that experimentally prove the important role of the size of the active element for increasing the efficiency of energy conversion. The design of the energy source operating due to the fact that the piezoelectric coefficients d_{24} and d_{15} (transverse shear piezoelectric modulus) of a polarized textured PVDF film differ from zero. The design simplicity and low flexural moduli make these devices suitable for wind energy engineering. A practically important application of the piezoelectric converter for the control of ship hull biofouling is described, and the results of studies discussing the increase in the area of active element of the converter by switching from a solid film to microfibrils are analyzed in more detail.

In our opinion, the information on the electrocaloric effect discussed in the review well supplements the results given in part 16 of the book. In the collected book (Ref. 443, p. 535), the electrocaloric effect is theoretically predicted in terms of the Landau–Devonshire phenomenological theory by relations (16.5)–(16.7). We used more practically convenient relations (8) and (9), which imply that ferroelectric polymers can potentially have higher ECE parameters than inorganic ferroelectrics. The validity of this conclusion was confirmed by comparing ECE characteristics for polymers and inorganic materials. While considering the mechanisms of this effect, we attempted to elucidate the influence of the amorphous phase (the fraction of which may reach 0.5 or more) on the ECE parameters. This problem is often hushed up and ignored in the literature, although it should be borne in mind that this phase has a liquid-like dynamics at room temperature and above. This circumstance must be taken into account, since the entropy change induced by an external field in this phase may be very high. We present the experimental results that demonstrate how the change in the crystallinity affects the ECE parameters, consider data on the effect of inorganic fillers in ferroelectric polymers on these parameters and analyze more thoroughly the results of experiments (see Fig. 17).

Part 17 of the collected book (Ref. 443, p. 571) addresses the conceptual aspects and biocompatibility criteria of ferroelectric polymers and some their applications in diagnostics and medicine that possess an essential novelty, but are not yet implemented in the clinical practice. In this review, we mainly discuss the applied aspects of the use of ferroelectric polymers in medicine and illustrate the existing or practically implemented biomedical applications of PVDF. Modification of the PVDF structure as applied to biomedical problems is an essentially novel subject of this review, as most reviews on PVDF neglect its structural aspect and do not relate it to the electrophysical activity and reactivity of biological tissues. Therefore, the illustration of the dependence of biomedical applications of PVDF on its structure and (structure-dependent) physical properties is of obvious practical value, which may be appraised by

researchers specializing in the physics and chemistry of polymers and in the fundamental medicine and applied biophysics.

Owing to the multifunctional nature of fluorinated ferroelectric polymers reflected in this review, they can be recommended for the use in various engineering devices. As shown in the review, valuable functional properties of these materials appear after preliminary polarization in an electric field. A specific feature of these polymers is that they possess high coercive fields; therefore, study of the dielectric breakdown mechanisms in the crystalline polymers (in particular, in ferroelectrics) is an important task. The presence of ionogenic impurities in the polymer matrix arising from remainder of the catalyst and admixtures increases the conductivity and decreases breakdown fields. In this connection, the development of a pure polymerization process (*e.g.* induced by radiation) is highly relevant.

The currently used polymerization processes give products with broad molecular-mass distribution. This brings about some inconveniences, *e.g.*, in the film and microfibre preparation from polymer solutions. Thus, the synthesis of polymers with a narrow molecular-mass distribution is also an important task. These ferroelectric polymers are self-organizing systems, which is manifested as self-polarization. During the formation of a film on a substrate, this can be induced by targeted chemical treatment. The functional groups formed in the surface can initiate formation of the surface layer of the polymer in which the polar groups in the planar zigzag conformation would be arranged at right angle to the substrate surface. Studies along this line seem to be highly important and promising.

For electrochromic and photovoltaic applications, the covalent attachment of some chromophore groups to PVDF chains and non-covalent modification of the polymer matrix with various dyes could be fairly useful. For the relaxor polymer dielectrics (with a low remanent polarization), it is reasonable to study in detail both structural (by large and small angle X-ray scattering) and dynamic (by broad-band dielectric spectroscopy and NMR spectroscopy) characteristics.

The development of smart implantable devices using the sensor properties and the capabilities of the multifactorial response of materials based on PVDF and its copolymers is the most promising modern application of PVDF in biomedicine. To achieve this goal, it is necessary to improve the preparation procedures of porous and fibrous materials with a specified type of structure and electrophysical parameters and to develop modification methods for these materials with biologically active components. Research along this line would result in the creation of fully functional prostheses and biomimetic constructs with active response adequately reproducing the properties of biological tissues.

This review was written with the financial support of the Russian Foundation for Basic Research (Project No. 20-12-50344).

10. List of abbreviations and symbols

- BNNS — boron nitride nanosheets,
- BOPP — biaxially oriented polypropylene,
- BST — ferroelectric ceramics ($\text{Ba}_x\text{Sr}_{(1-x)}\text{TiO}_3$),
- CFE — chlorofluoroethylene,
- CTFE — chlorotrifluoroethylene,
- ECE — electrocaloric effect,

HFP — hexafluoropropylene,
 IPP — isotactic polypropylene,
 PE — polyethylene,
 PEMA — polyethylene methacrylate,
 PETF — polyethylene terephthalate,
 PI — polyimide,
 PMMA — polymethyl methacrylate,
 PMN — oxide piezoceramic (PbMnNb),
 PMN-PT — $(1-x)\text{Pb}(\text{Mg}_{1/3}\text{Nb}_{2/3})\text{O}_3-x\text{PbTiO}_3$ ferroelectric,
 PP — polypropylene,
 PPENG — piezo(pyro)electric nanogenerator,
 PS — polystyrene,
 PTFE — polytetrafluoroethylene,
 PVDF — polyvinylidene fluoride,
 PZT — oxide piezoceramic (PbZrTi),
 TENG — triboelectric nanogenerator,
 TFE — tetrafluoroethylene,
 TrFE — trifluoroethylene,
 VDF — vinylidene fluoride,
 C — capacitance,
 C_E — heat capacity,
 d_{ij} , e_{ij} , g_{ij} — piezoelectric coefficients,
 D — electric displacement,
 E — external electric field strength,
 E_b — breakdown field,
 I — current,
 k_{31} — electromechanical coupling coefficient,
 n — number of repeating units between neighbouring cross-links,
 P — polarization,
 P_0 — spontaneous polarization,
 P_r — remanent polarization,
 q — charge,
 Q — heat of reaction,
 Q_m — latent molar heat of melting,
 R — reflection coefficient for a wave that passes from one medium to another with different acoustic impedances,
 S — entropy,
 t — time,
 T — temperature,
 T_C — Curie temperature,
 T_g — glass transition temperature,
 T_m — melting temperature,
 V — voltage,
 v_s — speed of sound,
 W_e — volumetric energy density,
 Y — Young's modulus,
 Z — acoustic impedance,
 α — characteristic field,
 β — coefficient of expansion of the Gibbs energy in terms of the even powers,
 η — energy conversion efficiency,
 γ — fraction of the pyroelectric response related to the reversible change in the crystallinity with temperature,
 ϵ_r — relative dielectric permittivity of the medium,
 ϵ_0 — dielectric permittivity of vacuum,
 ρ — density of the medium,
 λ — wavelength,
 ϕ_c — crystallinity.

11. References

- S.Horiuchi, F.Ishii, R.Kumai, Y.Okimoto, H.Tachibana, N.Nagaosa, Y.Tokura. *Nat. Mater.*, **4**, 163 (2005)
- S.Horiuchi, Y.Tokura. *Nat. Mater.*, **7**, 357 (2008)
- V.V.Kochervinskii, I.A.Malyshkina. In *Organic Ferroelectric Materials and Applications. Woodhead Publishing Series in Electronic and Optical Materials*. (Ed. K.Asadi). (Elsevier, 2022). P. 263
- I.Musevic, R.Blinic, B.Zeks. *The Physics of Ferroelectric and Antiferroelectric Liquid Crystals*. (Singapore, World Scientific, 2002)
- The Application of Ferroelectric Polymers*. (Eds T.T.Wang, J.M.Herbert, A.M.Glass). (Glasgow: Blackie, 1988)
- H.S.Nalva. *Ferroelectric Polymers — Chemistry, Physics and Applications*. (New York: Marcel Dekker, 1995)
- T.Hattori, Y.Takahashi, M.Iijima, E.Fukada. *J. Appl. Phys.*, **79**, 1713 (1996)
- J.-F.Capsal, E.Dantras, J.Dandurand, C.Lacabanne. *Polymer*, **51**, 4606 (2010)
- S.Tasaka, K.Miyasata, M.Yoshikawa, S.Miyata, M.Ko. *Ferroelectrics*, **57**, 267 (1984)
- V.V.Kochervinskii, L.O.Shoranova, S.A.Bondarenko, A.E.Afonkin. *Int. J. Pharm. Technol.*, **8**, 27238 (2016)
- V.V.Kochervinskii. *Polym. Sci., Ser. C*, **48**, 38 (2006)
- V.V.Kochervinskii. *Crystallogr. Rep.*, **48** 649 (2003)
- V.V.Kochervinskii. *Crystallogr. Rep., Suppl.*, **54**, 1146 (2009)
- K.Uchino. *Ferroelectric Devices*. (New York: Marcel Dekker, 2000)
- W.Heywang, K.Lubitz, W.Wersing. *Piezoelectricity: Evolution and Future of a Technology*. (Berlin, Heidelberg: Springer-Verlag, 2008)
- A.Badel, D.Guyomar, E.Lefevre, C.Richard. *J. Intell. Mater. Syst. Struct.*, **16**, 889 (2005)
- M.Ericka, D.Vasic, F.Costa, G.Poulin, S.Tiba. *J. Phys. IV*, **128**, 187 (2005)
- D.Guyomar, A.Badel, E.Lefevre, C.Richard. *IEEE Trans. Ultrason. Ferroelectr. Freq. Contr.*, **52**, 584 (2005)
- Y.B.Jeon, R.Sood, J.H.Jeong, S.G.Kim. *Sens. Actuators, A*, **122**, 16 (2005)
- H.W.Kim, S.Priya, K.Uchino, R.Newnham. *J. Electroceram.*, **15**, 27 (2005)
- S.Kim, W.W.Clark, Q.M.Wang. *J. Intell. Mater. Syst. Struct.*, **16**, 847 (2005)
- S.Kim, W.W.Clark, Q.M.Wang. *J. Intell. Mater. Syst. Struct.*, **16**, 855 (2005)
- E.Lefevre, A.Badel, C.Richard, L.Petit, D.Guyomar. *Sens. Actuators, A*, **126**, 405 (2006)
- G.A.Lesieutre, G.K.Ottman, H.F.Hofmann. *J. Sound. Vibr.*, **269**, 991 (2004)
- P.D.Mitcheson, P.Miao, B.H.Stark, E.M.Yeatman, A.S.Holmes, T.C.Green. *Sens. Actuators, A*, **115**, 523 (2004)
- S.R.Platt, S.Farritor, H.Haider. *IEEE/ASME Trans. Mechatron.*, **10**, 240 (2005)
- H.A.Sodano, D.J.Inman, G.Park. *J. Intell. Mater. Syst. Struct.*, **16**, 799 (2005)
- H.A.Sodano, G.Park, D.J.Inman. *Strain*, **40**, 49 (2004)
- H.S.Yoon, G.Washington, A.Danak. *J. Intell. Mater. Syst. Struct.*, **16**, 877 (2005)
- S.R.Anton, H.A.Sodano. *Smart. Mater. Struct.*, **16**, R1 (2007)
- G.W.Taylor, J.R.Burns. *Ferroelectrics*, **49**, 101 (1983)
- P.Pantelis. *Phys. Technol.*, **15**, 230 (1984)
- G.W.Taylor, J.R.Burns, S.M.Kammann, W.B.Powers, T.Welsh. *IEEE J. Ocean. Eng.*, **26**, 539 (2001)
- P.S.Schwesinger. In *Proceedings of 2004 International Conference on MEMS, NANO and Smart Systems*. (Banff, 2004). P. 480
- X.Li, S.Chen, Y.Jiang, F.E.H.Tay. *J. Polym Sci., Part B*, **47**, 2410 (2009)
- C.R.Bowen, H.A.Kim, P.M.Weaver, S.Dunn. *Energy Environ. Sci.*, **7**, 25 (2014)
- S.Markose, S.S.R.Patange, S.Raja, J.Anjana, B.Elias. *J. Adv. Res. Electr. Electron. Instrum. Eng.*, **2**, 270 (2013)
- M.Latour, P.V.Murphy. *Ferroelectrics*, **32**, 33 (1981)
- M.Latour. *IEEE Trans. Dielectr. Electr. Insul.*, **5**, 40 (1998)

40. R.B.Olsen, D.A.Bruno, J.M.Briscoe, E.W.Jacobs. *J. Appl. Phys.*, **58**, 2854 (1985)
41. G.Cha, Y.S.Ju. *Sens. Actuators, A*, **189**, 100 (2013)
42. J.Xie, X.P.Mane, C.W.Green, K.M.Mossi, K.K. Leang. *J. Intell. Mater. Syst. Struct.*, **21**, 243 (2010)
43. C.R.Bowen, J.Taylor, E.LeBoulbar, D.Zabek, A.Chauhanand, R.Vaish. *Energy Environ. Sci.*, **7**, 3836 (2014)
44. C.Chang, V.H.Tran, J.Wang, Y.K.Fuh, L.Lin. *Nano Lett.*, **10**, 726 (2010)
45. C.M.Wu, M.H.Chou. *Exp. Polym. Lett.*, **14**, 103 (2020)
46. T.Furukawa. *IEEE Trans. Electr. Insul.*, **24**, 375 (1989)
47. V.V.Kochervinskii. *Polym. Sci., Ser. B*, **45**, 326 (2003)
48. U.Khan, R.Hinchet, H.Ryu, S.W.Kim. *Appl. Mater.*, **5**, 073803 (2017)
49. J.W.Lee, B.U.Ye, J.M.Baik. *APL Mater.*, **5**, 073802 (2017)
50. T.Huang, C.Wang, H.Yua, H.Wang, Q.Zhang, M.Zhu. *Nano Energy*, **14**, 226 (2015)
51. X.Li, J.Tao, J.Zhu, C.Pan. *Appl. Mater.*, **5**, 074104 (2017)
52. Y.Zi, L.Lin, J.Wang, S.Wang, J.Chen, X.Fan, P.K.Yang, F.Yi, Z.L.Wang. *Adv. Mater.*, **27**, 2340 (2015)
53. S.Wang, L.Lin, Y.Xie, Q.Jing, S.Niu, Z.L.Wang. *Nano Lett.*, **13**, 2226 (2013)
54. G.Zhu, J.Chen, Y.Liu, P.Bai, Y.S.Zhou, Q.Jing, C.Pan, Z.L.Wang. *Nano Lett.*, **13**, 2282 (2013)
55. C.Y.Chen, C.Y.Tsai, M.H.Xu, C.T.Wu, C.Y.Huang, T.H.Lee, Y.K.Fuh. *Exp. Polym. Lett.*, **13**, 533 (2019)
56. W.J.Sarjeant, J.Zirnheld, F.W.MacDougall. *IEEE Trans. Plasma Sci.*, **26**, 1368 (1998)
57. B.K.P.Scaife. *Principles of Dielectrics*. (Rev. Ed.). (Oxford: Clarendon Press, 1998)
58. I.Burn, D.M.Smyth. *J. Mater. Sci.*, **7**, 339 (1972)
59. L.A.Dissado, J.C.Fothergill. *Electrical Degradation and Breakdown in Polymers*. (London: P. Peregrinus, 1992)
60. C.W.Reed, S.W.Cichanowski. *IEEE Trans. Dielectr. Electr. Insul.*, **1**, 904 (1994)
61. V.V.Kochervinskii, E.V.Chubunova, Yu.Yu.Lebedinskii, N.A.Shmakova, A.Yu.Khnykov. *Polym. Sci., Ser. A*, **53**, 929 (2011)
62. J.L.Nash. *Polym. Eng. Sci.*, **28**, 862 (1988)
63. P.Karanja, R.Nath. *IEEE Trans. Electr. Insul.*, **28**, 294 (1993)
64. M.Rabuffi, G.Picci. *IEEE Trans. Plasma Sci.*, **30**, 1939 (2002)
65. J.Ho, R.Ramprasad, S.Boggs. *IEEE Trans. Dielectr. Electr. Insul.*, **14**, 1295 (2007)
66. N.Zebouchi, D.Malec. *J. Appl. Phys.*, **83**, 6190 (1998)
67. N.Tu, K.Kao. *J. Appl. Phys.*, **85**, 7267 (1999)
68. T.Umemura, D.Coudere, K.Akiyama. *IEEE Trans. Electr. Insul.*, **21**, 137 (1986)
69. S.S.Guo, S.T.Lau, H.L.W.Chan, X.Z.Zhao, C.L.Choy. *J. Appl. Phys.*, **94**, 5566 (2003)
70. A.J.Lovinger. *Macromolecules*, **18**, 910 (1985)
71. Q.M.Zhang, V.Bharti, X.Zhao. *Science*, **280**, 2101 (1998)
72. I.Klier, A.Vokal. *Radiat. Phys. Chem.*, **38**, 457 (1991)
73. V.Bharti, H.S.Xu, G.Shanthi, Q.M.Zhang, K.Liang. *J. Appl. Phys.*, **87**, 452 (2000)
74. Z.Y.Cheng, Q.M.Zhang, F.B.Bateman. *J. Appl. Phys.*, **92**, 6749 (2002)
75. V.V.Kochervinskii. *Russ. Chem. Rev.*, **65**, 865 (1996)
76. B.Chu, X.Zhou, K.Ren, B.Neese, M.Lin, Q.Wang, F.Bauer, Q.M.Zhang. *Science*, **313**, 334 (2006)
77. W.Xia, Z.Zhou, Y.Liu, Q.Wang, Z.Zhang. *J. Appl. Polym. Sci.*, **135**, 46306 (2018)
78. X.Zhou, X.Zhao, Z.Suo, C.Zou, J.Runt, S.Liu, S.Zhang, Q.M.Zhang. *Appl. Phys. Lett.*, **94**, 162901 (2009)
79. L.Zhu, Q.Wang. *Macromolecules*, **45**, 2937 (2012)
80. Z.Y.Cheng, H.S.Xua, T.Maia, M.Chung, Q.M.Zhang. *Proc. SPIE*, **4329**, 106 (2001)
81. F.Guan, Z.Yuan, E.W.Shu, L.Zhu. *Appl. Phys. Lett.*, **94**, 052907 (2009)
82. F.Guan, J.Wang, L.Yang, J.K.Tseng, K.Han, Q.Wang, L.Zhu. *Macromolecules*, **44**, 2190 (2011)
83. J.Li, S.Tan, S.Ding, H.Li, L.Yang, Z.Zhang. *J. Mater. Chem.*, **22**, 23468 (2012)
84. J.Li, X.Hu, G.Gao, S.Ding, H.Li, L.Yang, Z.Zhang. *J. Mater. Chem. C*, **1**, 1111 (2013)
85. J.Li, H.Gong, Q.Yang, Y.Xie, L.Yang, Z.Zhan. *Appl. Phys. Lett.*, **104**, 263901 (2014)
86. M.Rahimabady, K.Yao, S.Arabnejad, L.Lu, V.P.W.Shim, D.C.W.Chet. *Appl. Phys. Lett.*, **100**, 252907 (2012)
87. M.Rahimabady, S.Chen, K.Yao, F.E.H.Tay, L.Lu. *Appl. Phys. Lett.*, **99**, 142901 (2011)
88. V.V.Kochervinskii, I.A.Malyshkina, D.A.Kiselev, T.S.Ilina, N.V.Kozlova, N.A.Shmakova, A.A.Korlyukov, M.A.Gradova, S.A.Bedin. *J. Appl. Polym. Sci.*, **137**, e49235 (2020)
89. V.V.Kochervinskii, D.A.Kiselev, M.D.Malinkovich, N.A.Shmakova. *Colloid Polym. Sci.*, **296**, 1057 (2018)
90. C.Zhao, M.Guo, Y.Lu, Q.Wang. *Macromol. Symp.*, **279**, 52 (2009)
91. K.H.Stark, C.G.Garton. *Nature (London)*, **176**, 1225 (1955)
92. M.Ieda. *IEEE Trans. Electr. Insul.*, **15**, 206 (1980)
93. R.Bartnikas, R.M.Eichhorn. *Electrical Properties of Solid Insulating Materials*. (Philadelphia: American Society for Testing and Materials, 1983)
94. V.V.Kochervinskii, A.S.Pavlov, N.V.Kozlova, N.A.Shmakova. *Polym. Sci., Ser. A*, **56**, 587 (2014)
95. V.V.Kochervinskii. *Crystallogr. Rep.*, **51**, S88 (2006)
96. *Electrocaloric Materials: New Generation of Coolers*. (*Ser. Engineering Materials*). Vol. 34. (Eds T.Correia, Q.Zhang). Springer, 2014
97. M.Lines, A.Glass. *Principles and Applications of Ferroelectrics and Related Materials*. (Oxford: Clarendon Press, 1977)
98. S.G.Lu, B.Rožič, Q.M.Zhang, Z.Kutnjak, X.Li, E.Furman, L.J.Gorny, M.Lin, B.Malič, M.Kosec, R.Blinč, R.Pirc. *Appl. Phys. Lett.*, **97**, 162904 (2010)
99. S.G.Lu, B.Rožič, Z.Kutnjak, Q.M.Zhang. *Ferroelectrics*. (Ed. I.Coondoo). (London: IntechOpen, 2010)
100. A.S.Mischenko, Q.Zhang, J.F.Scott, R.W.Whatmore, N.D.Mathur. *Science*, **311**, 1270 (2006)
101. Ç.M.Correia, J.S.Young, R.W.Whatmore, J.F.Scott, N.D.Mathur, Q.Zhang. *Appl. Phys. Lett.*, **95**, 182904 (2009)
102. M.E.Wood, W.H.Potter. *Cryogenics*, **25**, 667 (1985)
103. A.Kitanovski, J.Tusek, U.Tomc, U.Plaznik, M.Ozbojt, A.Poredos. *Magnetocaloric Energy Conversion: from Theory to Applications*. (Switzerland: Springer International Publishing, 2015)
104. F.Jona, G.Shirane. *Ferroelectric Crystals*. (New York: Dover Publications, 1993)
105. B.Neese, B.J.Chu, S.G.Lu, Y.Wang, E.Furman, Q.M.Zhang. *Science*, **321**, 821 (2008)
106. R.L.Moreira. *Appl. Phys. Lett.*, **100**, 152901 (2012)
107. W.Ulmann, J.H.Wendorff. *Compos. Sci. Technol.*, **23**, 97 (1985)
108. V.V.Kochervinskii, D.A.Kiselev, M.D.Malinkovich, A.S.Pavlov, N.V.Kozlova, N.A.Shmakova. *Polym. Sci., Ser. A*, **56**, 48, (2014)
109. V.V.Kochervinskii, D.A.Kiselev, M.D.Malinkovich, A.S.Pavlov, I.A.Malyshkina. *Colloid Polym. Sci.*, **293**, 533 (2015)
110. V.V.Kochervinskii, D.A.Kiselev, M.D.Malinkovich, A.A.Korlyukov, B.V.Lokshin, V.V.Volkov, G.A.Kirakosyan, A.S.Pavlov. *Crystallogr. Rep.*, **62**, 324 (2017)
111. X.Li, X.S.Qian, H.Gu, X.Chen, S.G.Lu, M.Lin, F.Bateman, Q.M.Zhang. *Appl. Phys. Lett.*, **101**, 132903 (2012)
112. G.Seibald, L.Seveyrat, J.F.Capsal, P.J.Cottinet, D.Guyomar. *Appl. Phys. Lett.*, **101**, 022907 (2012)
113. X.Qian, T.Yang, T.Zhang, L.Q.Chen, Q.M.Zhang. *Appl. Phys. Lett.*, **108**, 142902 (2016)
114. P.F.Liu, J.L.Wang, X.J.Meng, J.Yang, B.Dkhi, J.H.Chu. *New J. Phys.*, **12**, 023035 (2010)

115. X.Z.Chen, X.Li, X.S.Qian, M.Lin, S.Wu, Q.D.Shen, Q.M.Zhang. *Polymer*, **54**, 5299 (2013)
116. Q. Li, G.Z.Zhang, X.S.Zhang, S.L.Jiang, Y.K.Zeng, Q.Wang. *Adv. Mater.*, **27**, 2236 (2015)
117. G.Zhang, Q.Li, H.Gu, S.Jiang, K.Han, M.R.Gadinski, M.A.Haque, Q.Zhang, Q.Wang. *Adv. Mater.*, **27**, 1450 (2015)
118. G.Zhang, X.Zhang, T.Yang, Q.Li, L.Q.Chen, S.Jiang, Q.Wang. *ACS Nano*, **9**, 7164 (2015)
119. F.D.Morrison, Y.Luo, I.Szafraniak, V.Nagarajan, R.B.Wehrspohn, M.Steinhardt, J.H.Wendroff, N.D.Zakharov, E.D.Mishina, K.A.Vorotilov, A.S.Sigov, S.Nakabayashi, M.Alexe, R.Ramesh, J.F.Scott. *Rev. Adv. Mater. Sci.*, **4**, 114 (2003)
120. J.F.Scott. *Ferroelectrics*, **316**, 13 (2005)
121. J.Varghese, R.W.Whatmore, J.D.Holmes. *J. Mater. Chem. C*, **1**, 2618 (2013)
122. P.M.Rorvik, T.Grande, M.A.Einarsrud. *Adv. Mater.*, **23**, 4007 (2011)
123. E.Defay, S.Crossley, S.Kar-Narayan, X.Moya, N.D.Mathur. *Adv. Mater.*, **25**, 3337 (2013)
124. X.Li, S.G.Lu, X.Z.Chen, H.Gu, X.S.Qian, Q.M.Zhang. *J. Mater. Chem., C*, **1**, 23 (2013)
125. B.Lin, V.Giurgiutiu. *Smart Mater. Struct.*, **15**, 1085 (2006)
126. K.Lu, W.Huang, J.Guo, T.Gong, X.Wei, B.-W.Lu, S.-Y.Liu, B.Yu. *Nanoscale Res. Lett.*, **13**, 83 (2018)
127. K.H.Baumgärtel, D.Zöllner, K.L.Krieger. *Proc. Technol.*, **26**, 491 (2016)
128. R.H.Brown. *Sens. Actuators, A*, **21–23**, 729 (1990)
129. P.H.Brown. *Ferroelectrics*, **60**, 251 (1984)
130. M.A.P.Giãõ, N.A.S.Rodrigues, R.Riva, C.Schwab. *Rev. Sci. Instrum.*, **75**, 5213 (2004)
131. J.B.de Matos, N.A.S.Rodrigues. In *Proceedings of the Workshop on Separation Phenomena in Liquids and Gases*. Vol. 12. (France, 2012)
132. J.Xu, M.J.Dapino, D.Gallego-Perez, D.Hansford. *Sens. Actuators, A*, **153**, 24 (2009)
133. H.Xu, J.Hu. *Polymers*, **8**, 299 (2016)
134. A.Bartnik, H.Fiedorowicz, R.Jarocki, J.Kostecki, M.Szczurek, P.W.Wachulak. *Appl. Phys. A*, **106**, 551 (2012)
135. Y.Komaki, S.Ohno, H.Ohtsu, H.Ito, T.Seguchi, M.Iwasaki. *Int. J. Radiat. Appl. Instrum. D*, **11**, 99 (1986)
136. S.Lee, E.V.Bordatchev, M.J.F.Zeman. *J. Micromech. Microeng.*, **18**, 045011 (2008)
137. Y.Zhang. *J. Intell. Mater. Syst. Struct.*, **17**, 843 (2006)
138. R.S.Wagers. *J. Appl. Phys.*, **51**, 5797 (1980)
139. R.Toda, K.Ikenohira. *J. Appl. Phys.*, **51**, 5657 (1980)
140. V.Wilkens, W.Molkenstruck. *IEEE Trans. Ultrason. Freq.*, **54**, 1784 (2007)
141. G.Yan, Z.H.Shen, J.Lu. *J. Test Measur. Technol.*, **21**, 262 (2007)
142. Z.Lu, D.J.Dorantes-Gonzalez, K.Chen, F.Yang, B.Jin, Y.Li, Z.Chen, X.Hu. *Sensors*, **12**, 10500 (2012)
143. M.Schmitt, S.Tietze, W.Liang, G.Lindner. *AIP Conf. Proc.*, **1433**, 133 (2012)
144. R.S.Dahiya, G.Metta, M.Valle, G.Sandini. *IEEE Trans. Robot.*, **26**, 1 (2009)
145. A.A.Schoenberg, D.M.Sullivan, C.D.Baker, H.E.Booth, C.Galway. *Ferroelectrics*, **60**, 239 (1984)
146. J.Dargahi. *Sens. Actuators, A*, **71**, 89 (1998)
147. L.Seminara, M.Capurro, P.Cirillo, G.Cannata, M.Valle. *Sens. Actuators, A*, **169**, 49 (2011)
148. L.Seminara, L.Pinna, M.Valle, L.Basiricò, A.Loì, P.Cosseddu, A.Bonfiglio, A.Ascia, M.Biso, A.Ansaldo, D.Ricci, G.Metta. *IEEE Sens. J.*, **13**, 4022 (2013)
149. C.Li, P.M.Wu, S.Lee, A.Gorton, M.J.Schulz, C.H.Ahn. *J. Microelectromech. Syst.*, **17**, 334 (2008)
150. A.Simaite, F.Mesnilgrete, B.Tondu, P.Souères, C.Bergaud. *Sens. Actuators, B*, **229**, 425 (2016)
151. D.Friedrich, F.Gao, K.Goetz, G.Lindne. In *Proceedings of the 14th International Meeting on Chemical Sensors*. (Nuremberg, 2012). P. 1429
152. R.Marsili. *Int. J. Eng. Sci. Innov. Technol.*, **4**, 75 (2015)
153. D.R.Zilinskis, M.J.Guers, B.R.Tittmann. In *Review of Quantitative Non-destructive Evaluation*. Vol. 27. (Eds D.O.Thompson, D.E.Chimenti). (San Diego, 2008). P. 904
154. T.D.Sullivan, J.M.Powers. *J. Acoust. Soc. Am.*, **63**, 1396 (1978)
155. D.Ricketts. *J. Acoust. Soc. Am.*, **70**, 929 (1981)
156. D.Ricketts. *J. Acoust. Soc. Am.*, **77**, 1939 (1985)
157. D.Ricketts. *J. Acoust. Soc. Am.*, **80**, 723 (1986)
158. H.Ohigashi, K.Koga, M.Suzuki, T.Nakanishi, K.Kimura, N.Hashimoto. *Ferroelectrics*, **60**, 263 (1984)
159. K.Kimura, H.Ohigashi. *J. Appl. Phys.*, **61**, 4749 (1987)
160. K.Ornote, H.Ohigashi. *IEEE Trans. Ultrason. Ferroelectr. Freq. Control*, **43**, 312 (1996)
161. A.Decharat, S.Wagle, S.Jacobsen, F.Melandsø. *Sensors*, **15**, 9210 (2015)
162. R.H.Tancrèll, D.T.Wilson, D.Ricketts. In *Proceedings of IEEE 1985 Ultrasonic Symposium*. (San Francisco, 1985). P. 624
163. B.Granz. *IEEE Trans. Electr. Insul.*, **24**, 499 (1989)
164. G.R.Harris, P.M.Gammell. *J. Acoust. Soc. Am.*, **105**, 725 (1999)
165. P.A.Lewin. *Ultrasonics*, **19**, 213 (1981)
166. R.C.Chivers, P.A.Lewin. *Ultrasonics*, **20**, 279 (1982)
167. H.Crazzolaro, W.von Muench, C.Rose, U.Thiemann. *J. Appl. Phys.*, **70**, 1847 (1991)
168. F.W.Cross, R.K.Aldhahir, P.E.Dyer. *J. Appl. Phys.*, **64**, 2194 (1988)
169. C.Cui, R.H.Baughman, Z.Iqbal, T.R.Kazmar, D.K.Dahlstrom. *Sens. Actuators, A*, **65**, 76 (1998)
170. T.Huang, S.Yang, P.He, J.Sun, S.Zhang, D.Li, Y.Meng, J.Zhou, H.Tang, J.Liang, G.Ding, X.Xie. *ACS Appl. Mater. Interfaces*, **10**, 30732 (2018)
171. F.N.Meyers, K.J.Loh, J.S.Dodds, A.Baltazar. *Nanotechnology*, **24**, 185501 (2013)
172. J.Han, D.Li, C.Zhao, X.Wang, J.Li, X.Wu. *Sensors*, **19**, 830 (2019)
173. I.Graz, M.Krause, S.Bauer-Gogonea, S.Bauer, S.P.Lacour, B.Ploss, M.Zirkel, B.Stadlober, S.Wagner. *J. Appl. Phys.*, **106**, 034503 (2009)
174. V.Bhavanasi, V.Kumar, K.Parida, J.Wang, P.S.Lee. *ACS Appl. Mater. Interfaces*, **8**, 521 (2016)
175. X.Yu, R.Rajamani, K.A.Stelson, T.Cui. *Sens. Actuators, A*, **132**, 626 (2006)
176. J.S.Lee, K.Y.Shin, C.Kim, J.Jang. *Chem. Commun.*, **94**, 11047 (2013)
177. R.Gerhard-Mulhaupt. *Prog. Colloid Polym. Sci.*, **85**, 133 (1991)
178. S.B.Lang, S.Muensit. *Appl. Phys. A*, **85**, 125 (2006)
179. R.Perez, M.Kral, H.Bleuler. *Sens. Actuators, A*, **183**, 84 (2012)
180. T.R.Dargaville, M.C.Celina, J.M.Elliott, P.M.Chaplya, G.D.Jones, D.M.Mowery, R.A.Assink, R.L.Clough, J.W.Martin. In *Space Mirror Concepts*. Sandia National Laboratories Reports, Albuquerque, 2005
181. H.Ohigashi. *J. Appl. Phys.*, **47**, 949 (1976)
182. S.Egusa, Z.Wang, N.Chocat, Z.M.Ruff, A.M.Stolyarov, D.Shemuly, F.Sorin, P.T.Rakich, J.D.Joannopoulos, Y.Fink. *Nat. Mater.*, **9**, 643 (2010)
183. I.Lubomirsky, O.Stafsudd. *Rev. Sci. Instrum.*, **83**, 051101 (2012)
184. G.Pfister, M.Abkowitz, R.G.Crystal. *J. Appl. Phys.*, **44**, 2064 (1973)
185. H.Burkard, G.Pfister. *J. Appl. Phys.*, **45**, 3360 (1974)
186. S.Bauer, B.Ploss. *J. Appl. Phys.*, **68**, 6361 (1990)
187. L.Ibos, A.Bernesa, G.Teyssedre, C.Lacabanne, S.L.Wu, J.I.Scheinbeim. *Ferroelectrics*, **238**, 163 (2000)
188. E.J.Sharp, L.E.Garn. *J. Appl. Phys.*, **53**, 8974 (1982)
189. E.J.Sharp, L.E.Garn. *J. Appl. Phys.*, **53**, 8980 (1982)

190. V.V.Kochervinskii, I.A.Malyshkina, A.S.Pavlov, N.P.Bessonova, A.A.Korlyukov, V.V.Volkov, N.V.Kozlova, N.A.Shmakova. *J. Appl. Phys.*, **117**, 214101 (2015)
191. V.Kochervinskii, N.Kozlova, I.Malyshkina, V.Astakhov. *Ferroelectrics*, **531**, 1 (2018)
192. V.Kochervinskii, I.Malyshkina, S.Bedin, A.Korlyukov, M.Buzin, R.Shakirzyanov. *J. Appl. Polym. Sci.*, **135**, 46186 (2018)
193. V.V.Kochervinskii, I.A.Malyshkina, M.A.Gradova, N.V.Kozlova, N.A.Shmakova, M.I.Buzin, A.A.Korlyukov, S.A.Bedin. *Colloid Polym. Sci.*, **297**, 513 (2019)
194. H.G.Zachmann, H.A.Stuart. *Makromol. Chem.*, **49**, 131 (1960)
195. Z.G.Wang, B.S.Hsiao, B.B.Sauer, W.G.Kampert. *Polymer*, **40**, 4615 (1999)
196. Y.Akpalu, L.Kilehorn, B.S.Hsiao, R.S.Stein, T.P.Russell, J.van Egmond, M.Muthukumar. *Macromolecules*, **32**, 765 (1999)
197. Y.K.Kwon, A.Boller, M.Pyda, B.Wunderlich. *Polymer*, **4**, 6237 (2000)
198. C.De Rosa, F.Auriemma, N.Galotto, R.Di Girolamo. *Polymer*, **53**, 2422 (2012)
199. R.Kolb, C.Wutz, N.Striebeck, G.von Krosigk, C.Riekel. *Polymer*, **42**, 5257 (2001)
200. M.Neidhofer, F.Beaume, L.Ibos, A.Bernes, C.Lacabanne. *Polymer*, **45**, 1679 (2004)
201. R.Androsch. *Polymer*, **40**, 2805 (1999)
202. J.Y.Nam, S.Kadomatsu, H.Saito, T.Inoue. *Polymer*, **43**, 2101 (2002)
203. N.Naga, R.Arai, G.Kikuchi, A.Toyota, K.Noguchi, M.Sone, F.Shirai, T.Gotoh, H.Kurosu. *Polymer*, **52**, 4857 (2011)
204. G.Colombe, S.Gree, O.Lhost, M.Dupire, M.Rosenthal, D.Ivanov. *Polymer*, **52**, 5630 (2011)
205. V.V.Kochervinskii, N.V.Kozlova, A.Y.Khnykov, M.A.Shcherbina, S.N.Sulyanov, K.A.Dembo. *J. Appl. Polym. Sci.*, **116**, 695 (2010)
206. V.V.Kochervinskii, V.A.Astakhov, S.A.Bedin, I.A.Malyshkina, N.A.Shmakova, A.A.Korlyukov, M.I.Buzin, V.V.Volkov. *Colloid Polym. Sci.*, **298**, 1169 (2020)
207. A.J.Lovinger, G.T.Davis, T.Furukawa, M.G.Broadhurst. *Macromolecules*, **15**, 323 (1982)
208. G.T.Davis, T.Furukawa, A.J.Lovinger, M.G.Broadhurst. *Macromolecules*, **15**, 329 (1982)
209. J.L.Lutkenhaus, K.McEnnis, A.Serghei, T.P.Russell. *Macromolecules*, **43**, 3844 (2010)
210. W.Ma, H.Yuan, X.Wang. *Membranes*, **4**, 243 (2014)
211. J.F.Legrand, P.Delzenne, A.J.Dianoux, M.Bee, C.Poinsignon, D.Broussoux, V.H.Schmidt. In *Proceedings of Workshop Grenoble*. (Berlin, 1985). P. 59
212. R.G.Kepler, R.A.Anderson, R.R.Lagasse. *Ferroelectrics*, **57**, 151 (1984)
213. D.-Q.Xiao, S.B.Lang. *IEEE Trans. Electr. Insul.*, **24**, 503 (1989)
214. A.M.Glass, J.H.McFee, J.G.Bergman. *J. Appl. Phys.*, **42**, 5219 (1971)
215. R.J.Phelan, A.R.Cook. *Appl. Opt.*, **12**, 2494 (1973)
216. R.L.Peterson, G.W.Day, P.M.Gruzensky, R.J.Phelan. *J. Appl. Phys.*, **45**, 3296 (1974)
217. G.W.Day, C.A.Hamilton, R.L.Peterson, R.J.Phelan, L.O.Mullen. *Appl. Phys. Lett.*, **24**, 456 (1974)
218. W.R.Blevin, J.Geist. *Appl. Opt.*, **13**, 2212 (1974)
219. G.W.Day, C.A.Hamilton, K.W.Pyatt. *Appl. Opt.*, **15**, 1865 (1976)
220. M.Hammerich, A.Olafsson. *J. Phys. E*, **21**, 80 (1988)
221. T.M.Lee, A.P.Anderson, F.A.Benson. *Electron. Lett.*, **22**, 200 (1986)
222. T.Iwasaki, T.Inoue, T.Nemoto. *IEEE Trans. Instrum. Measur.*, **28**, 88 (1979)
223. H.Sussner, D.E.Horne, D.Y.Yoon. *Appl. Phys. Lett.*, **32**, 137 (1978)
224. B.Rashidian, M.G.Allen. *J. Acoust. Soc. Am.*, **92**, 2353 (1992)
225. H.Coufal, W.Lee. *Appl. Phys. B*, **44**, 141 (1987)
226. J.A.Simpson, A.J.Tuzzolino. *Phys. Rev. Lett.*, **52**, 601 (1984)
227. J.A.Simpson, A.J.Tuzzolino. *Nucl. Instrum. Methods Phys. Res. A*, **236**, 187 (1985)
228. I.Tasaki, K.Iwasa. *Biochem. Biophys. Res. Commun.*, **101**, 172 (1981)
229. I.Tasaki, T.Nakaye. *Science*, **227**, 654 (1985)
230. A.Kaneko, T.Tanabe, T.Fumoto, K.Tomii, J.Nishida. *J. Inst. Telev. Eng. Jpn.*, **40**, 878 (1986)
231. N.Osaka, K.Yanagi, H.Saito. *Polym. J.*, **45**, 1033 (2013)
232. V.V.Kochervinskii, S.A.Bedin, I.V.Razumovskaya, M.A.Shcherbina, M. I. Buzin, I. A. Malyshkina, A.M.Prazdnichnyi, A.S.Pavlov, O.I.Vasilevskii, **58**, 345 (2016)
233. W.Künstler, M.Wegener, M.SeiB, R.Gerhard-Multhaupt. *Appl. Phys. A*, **73**, 641 (2001)
234. J.Sakata, M.Mochizuki. *Thin Solid Films*, **195**, 175 (1991)
235. N.T.Tien, Y.G.Seol, L.H.A.Dao, H.Y.Noh, N.E.Lee. *Adv. Mater.*, **21**, 910 (2009)
236. X.Chen, J.Shao, X.Li, H.Tian. *IEEE Trans. Nanotechnol.*, **15**, 295 (2016)
237. H.Coufal. *Appl. Phys. Lett.*, **44**, 59 (1984)
238. A.Mandelis. *Chem. Phys. Lett.*, **108**, 388 (1984)
239. P.K.John, L.C.M.Miranda, A.C.Rastogi. *Phys. Rev. B*, **34**, 4342 (1986)
240. J.Song, H.Lu, A.Gruverman, S.Ducharme. *Appl. Phys. Lett.*, **104**, 192901 (2014)
241. J.Groten, M.Zirkel, G.Jakopic, A.Leitner, B.Stadlober. *Phys. Rev. B*, **82**, 054112 (2010)
242. V.V.Kochervinskii, E.V.Chubunova, Y.Y.Lebedinskii, A.S.Pavlov, N.I.Pakuro. *Adv. Mater. Res.*, **4**, 113 (2015)
243. Y.Wu, X.Du, R.Gao, J.Li, W.Li, H.Yu, Z.Jiang, Z.Wang, H.Tai. *Nanoscale Res. Lett.*, **14**, 72 (2019)
244. J.Parravicini, J.Safioui, V.Degiorgio, P.Minzioni, M.Chauvet. *J. Appl. Phys.*, **109**, 033106 (2011)
245. D.Ehre, H.Cohen. *Appl. Phys. Lett.*, **103**, 052901 (2013)
246. T.Abidin, Q.Zhang, K.L.Wang, D.J.Liaw. *Polymer*, **55**, 5293 (2014)
247. R.Zhou, W.Liu, J.Kong, D.Zhou, G.Ding, Y.W.Leong, P.K.Pallathadka, X.Lu. *Polymer*, **55**, 1520 (2014)
248. V.V.Kochervinskii, N.V.Kozlova, D.Ponkratov, A.A.Korlyukov, D.A.Kiselev, T.S.Ilina, Yu.S.Terekhova, N.A.Shmakova, A.I.Khorokhorin. *Colloid Polym. Sci.*, **297**, 1275 (2019)
249. J.F.Scott. In *Ferroelectric Memories*. Springer, Heidelberg, 2000. P. 248
250. J.F.Scott, L.D.Bozano. *Adv. Mater.*, **19**, 1451 (2007)
251. R.C.G.Naber, P.W.M.Blom, A.W.Marsman, D.M.de Leeuw. *Appl. Phys. Lett.*, **85**, 2012 (2004)
252. V.Kochervinskii, I.Malyshkina, A.Pavlov, N.Pakuro, N.Bessonova, N.Shmakova, S.Bedin, E.Chubunova, Y.Lebedinskii. *J. Appl. Phys.*, **118**, 244102 (2015)
253. V.V.Kochervinskii. *Vesokomol. Soedin., Ser. B*, **47**, 542 (2005)
254. K.Noda, K.Ishida, A.Kubono, T.Horiuchi, H.Yamada, K.Matsushige. *J. Appl. Phys.*, **93**, 2866 (2003)
255. V.Kochervinskii, N.Shmakova, I.Malyshkina, S.Bedin, V.Astakhov. *Ferroelectrics*, **537**, 173 (2018)
256. Y.J.Park, S.J.Kang, B.Lotz, M.Brinkmann, A.Thierry, K.J.Kim, C.Park. *Macromolecules*, **41**, 8648 (2008)
257. K.Asadi, D.M.de Leeuw, B.de Boer, P.W.M.Blom. *Nat. Mater.*, **7**, 547 (2008)
258. C.W.Choi, A.A.Prabu, Y.M.Kim, S.Yoon, K.J.Kim, C.Park. *Appl. Phys. Lett.*, **93**, 182902 (2008)
259. S.L.Miller, P.J.McWhorter. *J. Appl. Phys.*, **72**, 5999 (1992)
260. R.C.Naber, B.de Boer, P.W.Blom, D.M.de Leeuw. *Appl. Phys. Lett.*, **87**, 203509 (2005)
261. S.J.Kang, I.Bae, Y.J.Park, T.H.Park, J.Sung, S.C.Yoon, K.H.Kim, D.H.Choi, C.Park. *Adv. Funct. Mater.*, **19**, 1609 (2009)

262. C.A.Nguyen, S.G.Mhaisalkar, J.Ma, P.S.Lee. *Org. Electron.*, **9**, 1087 (2008)
263. N.Yamauchi. *Jpn. J. Appl. Phys.*, **25**, 590 (1986)
264. R.A.Surmenev, T.Orlova, R.V.Chernozem, A.A.Ivanova, A.Bartasyte, S.Mathur, M.A.Surmeneva. *Nano Energy*, **62**, 475 (2019)
265. A.Zaszczyńska, A.Gradys, P.Sajkiewicz. *Polymers*, **12**, 2754 (2020)
266. R.A.Surmenev, R.V.Chernozem, I.O.Pariy, M.A.Surmeneva. *Nano Energy*, **79**, 105442. (2021).
267. Y.Xin, C.Guo, X.Qi, H.Tian, X.Li, Q.Dai, S.Wang, C.Wang. *Ferroelectrics*, **500**, 291 (2016)
268. D.M.Shin, S.W.Hong, Y.H.Hwang. *Nanomaterials*, **10**, 123 (2020)
269. J.Li, Y.Long, X.Wang. *Chem. Res. Chin. Univ.*, **36**, 41 (2020)
270. A.Kaur, G.Sapra, A.Gupta. *J. Circ., Syst. Comput.*, **30**, 2130010 (2021)
271. M.N.Hasan, S.Sahlan, K.Osman, M.S.Mohamed Ali. *Adv. Mater. Technol.*, **6**, 2000771 (2021).
272. G.Zhang, M.Li, H.Li, Q.Wang, S.Jiang. *Energy Technol.*, **6**, 791 (2018)
273. Y.Zeng, L.Jiang, Q.He, R.Wodnicki, Y.Yang, Y.Chen, Q.Zhou. *J. Phys. D*, **55**, 013002 (2022)
274. J.Sun, A.Yang, C.Zhao, F.Liu, Z.Li. *Sci. Bull.*, **64**, 1336 (2019)
275. V.V.Kochervinskii. *Primenenie Segnetoelektricheskikh Polimerov v Tekhnike i Meditsine. (Application of Ferroelectric Polymers in Engineering and Medicine)* (Kishenev: PAP, 2021)
276. A.Blázquez-Castro, A.García-Cabañes, M.Carrascosa. *Appl. Phys. Rev.*, **5**, 041101 (2018)
277. B.Hermenegildo, C.Ribeiro, L.Pérez-Álvarez, J.L.Vilas, D.A.Learmonth, R.A.Sousa, P.Martins, S.Lanceros-Méndez. *Colloid. Surf., B*, **181**, 1041 (2019)
278. A.Mirzaei, E.Saburi, S.E.Enderami, M.Barati Bagherabad, S.E.Enderami, M.Chokami, A.Shapouri Moghadam, R.Salarinia, A.Ardeshiryajimi, V.Mansouri, F.Soleimanifar. *Artif. Cells, Nanomed. Biotechnol.*, **47**, 3058 (2019)
279. A.S.Motamedi, H.Mirzadeh, F.Hajiesmaeilbaigi, S.Bagheri-Khoulenjani, M.Shokrgozar. *Prog. Biomater.*, **6**, 113 (2017)
280. B.R.Zineh, M.R.Shabgard, L.Roshangar. *Mater. Sci. Eng. C*, **92**, 779 (2018)
281. M.F.Abazari, F.Soleimanifar, S.E.Enderami, M.Nematzadeh, N.Nasiri, F.Nejati, E.Saburi, S.Khodashenas, B.Darbasizadeh, M.M.Khani, P.Ghoreaeian. *J. Cell. Biochem.*, **120**, 16750 (2019)
282. M.Kitsara, A.Blanquer, G.Murillo, V.Humblot, S.D.B.Vieira, C.Nogués, E.Ibáñez, J.Esteve, L.Barrios. *Nanoscale*, **11**, 8906 (2019)
283. R.Bai, L.Li, M.Liu, S.Yan, C.Miao, R.Li, Y.Luo, T.Liu, B.Lin, Y.Ji, Y.Lu. *Anal. Chem.*, **90**, 5825 (2018)
284. E.Esmaili, M.Soleimani, M.A.Ghiass, S.Hatamie, S.Vakilian, M.S.Zomorrod, N.Sadeghzadeh, M.Vossoughi, S.Hosseinzadeh. *J. Cell. Physiol.*, **234**, 13617 (2019)
285. Q.Zhang, V.Bharti, G.Kavarnos. In *Encyclopedia of Smart Materials*. (Ed. M.Schwartz). (Wiley-Interscience, 2002). P. 1176
286. B.Mazurek, S.Rózecki, D.Kowalczyk, T.Janiczek. *J. Electrostat.*, **51**, 180 (2001)
287. E.Ghafari, X.Jiang, N.Lu. *Adv. Compos. Hybrid Mater.*, **1**, 332 (2018)
288. M.Iqbal, M.M.Nauman, F.U.Khan, P.E.Abas, Q.Cheok, A.Iqbal, B.Aissa. *Electronics*, **9**, 635 (2020)
289. M.Mohseni, S.A.Ahmad Ramazani, F.H.Shirazi, N.H.Nemati. *Int. J. Biol. Macromol.*, **167**, 881 (2021)
290. B.M.Jeon, G.B.Yeon, H.G.Goo, K.E.Lee, D.S.Kim. *Develop. Reprod.*, **24**, 135 (2020)
291. O.V.Gradov. *Geny i Kletki*, **15**, 157 (2020)
292. Y.Cheng, Y.Xu, Y.Qian, X.Chen, Y.Ouyang, W.E.Yuan. *Nano Energy*, **69**, 104411 (2020)
293. O.Gryshkov, F.Al Halabi, A.I.Kuhn, S.Leal-Marín, L.J.Freund, M.Förthmann, N.Meier, S.A.Barker, K.Haastert-Talini, B.Glasmacher. *Int. J. Mol. Sci.*, **22**, 11373 (2021)
294. R.Zhang, S.Han, L.Liang, Y.Chen, B.Sun, N.Liang, Z.Feng, H.Zhou, C.Sun, H.Liu, J.Wang. *Nano Energy*, **87**, 106192 (2021)
295. M.Li, P.Zhang, D.Zhang. *Med. Hypothes.*, **114**, 55 (2018)
296. J.A.Orkwis, A.K.Wolf, S.M.Shahid, C.Smith, L.Esfandiari, G.M.Harris. *Macromol. Biosci.*, **20**, 2000197 (2020)
297. S.Wu, M.S.Chen, P.Maurel, Y.S.Lee, M.B.Bunge, T.L.Arinzeh. *J. Neur. Eng.*, **15**, 056010 (2018)
298. Y.S.Lee, S.Wu, T.L.Arinzeh, M.B.Bunge. *Biotechnol. Bioeng.*, **114**, 444 (2017)
299. Y.S.Lee, S.Wu, T.L.Arinzeh, M.B.Bunge. *J. Visual. Exp.*, **129**, e56077 (2017)
300. C.Defterali, R.Verdejo, S.Majeed, A.Boschetti-de-Fierro, H.R.Méndez-Gómez, E.Díaz-Guerra, D.Fierro, K.Buhr, C.Abetz, R.Martínez-Murillo, D.Vuluga, M.Alexandre, J.-M.Thomassin, C.Detrembleur, C.Jérôme, V.Abetz, M.Á.López-Manchado, C.Vicario-Abejón. *Front. Bioeng. Biotechnol.*, **4**, 94 (2016)
301. R.Arumugam, V.Subramanyam, R.K.Chinnadurai, E.S.Srinadhu, B.Subramanian, S.Nallani. *Mater. Lett.*, **236**, 694 (2019)
302. T.Gong, T.Li, L.Meng, Y.Chen, T.Wu, J.Zhou, G.Lu, Z.Wang. *Ceram. Int.*, **48**, 6461 (2022)
303. M.Kitsara, A.Blanquer, G.Murillo, V.Humblot, S.D.Vieira, C.Nogués, E.Ibáñez, J.Esteve, L.Barrios. *Nanoscale*, **11**, 8906 (2019)
304. P.K.Szewczyk, S.Metwally, J.E.Karbowiczek, M.M.Marzec, E.Stodolak-Zych, A.Gruszczynski, A.Bernasik, U.Stachewicz. *ACS Biomater. Sci. Eng.*, **5**, 582 (2018)
305. Y.Dong, L.Suryani, X.Zhou, P.Muthukumar, M.Rakshit, F.Yang, F.Wen, A.M.Hassanbhai, K.Parida, D.T.Simon, D.Iandolo. *Int. J. Mol. Sci.*, **22**, 6438 (2021)
306. V.N.Gorshenev, A.A.Ol'khov, O.V.Gradov, M.A.Gradova, P.L.Aleksandrov. *Geny i Kletki*, **14**, 69 (2019)
307. P.K.Szewczyk, S.Metwally, Z.J.Krysiak, Ł.Kaniuk, J.E.Karbowiczek, U.Stachewicz. *Biomed. Mater.*, **14**, 065006 (2019)
308. A.V.Popkov, D.A.Popkov, N.A.Kononovich, E.N.Gorbach, S.I.Tverdokhlebov, E.N.Bolbasov, E.O.Darvin. *J. Tissue Eng. Regen. Med.*, **12**, 2248 (2018)
309. A.V.Popkov, N.A.Kononovich, E.N.Gorbach, D.A.Popkov. *Traumadol. Orthoped. Ross. (Traumatol. Orthoped. Russ.)*, **27**, 37 (2021)
310. E.N.Bolbasov, A.V.Popkov, D.A.Popkov, E.N.Gorbach, I.A.Khlusov, A.S.Golovkin, A.Sinev, V.M.Bouznik, S.I.Tverdokhlebov, Y.G.Anissimov. *Mater. Sci. Eng. C*, **75**, 207 (2017)
311. A.M.Aronov, E.N.Bol'Basov, V.V.Guzeev, M.V.Dvornichenko, S.I.Tverdokhlebov, I.A.Khlusov. *Biomed. Eng.*, **44**, 108 (2010)
312. E.N.Bolbasov, D.A.Popkov, N.A.Kononovich, E.N.Gorbach, I.A.Khlusov, A.S.Golovkin, K.S.Stankevich, V.P.Ignatov, V.M.Bouznik, Y.G.Anissimov, S.I.Tverdokhlebov. *Biomed. Mater.*, **14**, 025005 (2019)
313. A.D.Badaraev, A.L.Nemoykina, E.N.Bolbasov, S.I.Tverdokhlebov. *Mater. Today: Proc.*, **22**, 219 (2020)
314. S.I.Tverdokhlebov, E.N.Bolbasov, E.V.Shesterikov, A.I.Malchikhina, V.A.Novikov, Y.G.Anissimov. *Appl. Surf. Sci.*, **263**, 187 (2012)
315. I.V.Lukiev, L.S.Antipina, S.I.Goreninskii, T.S.Tverdokhlebova, D.V.Vasilchenko, A.L.Nemoykina, D.A.Goncharova, V.A.Svetlichnyi, G.T.Dambaev, V.M.Bouznik, E.N.Bolbasov. *Membranes*, **11**, 986 (2021)

316. M.T.Duong, V.Seifarth, A.Artmann, G.M.Artmann, M.Staat. In *Biological, Physical and Technical Basics of Cell Engineering*. (Singapore: Springer, 2018). P. 209
317. K.C.Chinnam, F.Fabriani, I.Giovanna, G.Lanzara. *Proc. ASME*, **51951**, V002T06A006 (2018)
318. M.Nan, D.Bang, S.Zheng, G.Go, B.A.Darmawan, S.Kim, H.Li, C.S.Kim, A.Hong, F.Wang, J.O.Park. *Sens. Actuators, B*, **323**, 128709 (2020)
319. P.Hitscherich, S.Wu, R.Gordan, L.H.Xie, T.Arinzeh, E.J.Lee. *Biotechnol. Bioeng.*, **113**, 1577 (2016)
320. R.Arumugam, E.S.Srinadhu, B.Subramanian, S.Nallani. *Med. Hypothes.*, **122**, 31 (2019)
321. N.Adadi, M.Yadid, I.Gal, M.Asulin, R.Feiner, R.Edri, T.Dvir. *Adv. Mater. Technol.*, **5**, 1900820 (2020)
322. R.Arumugam, R.K.Chinnadurai, B.N.Subramaniam, B.Devaraj, V.Subramaniam, S.E.Sekhar, S.Nallani. *J. Mech. Behav. Biomed. Mater.*, **88**, 270 (2018)
323. S.Kärki, J.Lekkala. *J. Med. Eng. Technol.*, **33**, 551 (2009)
324. K.Y.Shin, J.S.Lee, J.Jang. *Nano Energy*, **22**, 95 (2016)
325. P.Bifulco, G.D.Gargiulo, G.d'Angelo, A.Liccardo, M.Romano, F.Clemente, M.Cesarelli. In *The 20th IMEKO TC4 International Symposium and 18th International Workshop on ADC Modelling and Testing Research on Electric and Electronic Measurement for the Economic Upturn Benevento*, Italy, 2014. P. 786
326. J.J.Im, Y.C.Lim. *J. Inst. Internet, Broadcast. Commun.*, **12**, 57 (2012)
327. Y.Yuriev, S.Goreninskii, A.Runts, E.Prosetskaia, E.Plotnikov, D.Shishkova, Y.Kudryavtseva, E.Bolbasov. *Membranes*, **11**, 690 (2021)
328. T.Sharma, S.S.Je, B.Gill, J.X.Zhang. *Sens. Actuators, A*, **177**, 87 (2021)
329. T.Sharma, K.Aroom, S.Naik, B.Gill, J.X.Zhang. *Ann. Biomed. Eng.*, **41**, 744 (2013)
330. K.Takashima, K.Ota, M.Yamamoto, M.Takenaka, S.Horie, K.Ishida. *ROBOMECH J.*, **6**, 1 (2020)
331. J.P.Tamez, H.Y.Wang, A.Bhalla, R.Guo. *Adv. Electroceram. Mater. II*, **221**, 231 (2010)
332. Y.J.Wang, C.Y.Sue. *J. Automat. Control. Eng.*, **7**, 41 (2019)
333. C.Liu, W.Wang, Y.Li, F.Cui, C.Xie, L.Zhu, B.Shan. *J. Membr. Sci.*, **576**, 48 (2019)
334. F.Ai, H.Li, Q.Wang, W.Z.Yuan, X.Chen, L.Yang, J.Zhao, Y.Zhang. *J. Mater. Sci.*, **47**, 5030 (2012)
335. M.Tenjimbayashi, H.Komatsu, M.Akamatsu, W.Nakanishi, K.Suzuki, J.P.Hill, S.Shiratori, K.Aruga. *RSC Adv.*, **6**, 14261 (2016)
336. V.V.Kochervinskii, O.V.Gradov, M.A.Gradov. *Geny i Kletki*, **14**, 122 (2019)
337. J.Guo, X.Lu, C.Wu, J.Liu, Z.Li, C.Wu, C. In *Materials in Environmental Engineering: Proceedings of the 4th Annual International Conference on Materials Science and Environmental Engineering*. (Ed. H.Haeri). (Berlin, Boston: De Gruyter, 2017). P. 365
338. T.Y.Liu, W.C.Lin, L.Y.Huang, S.Y.Chen, M.C.Yang. *Polym. Adv. Technol.*, **16**, 413 (2005)
339. F.Yalcinkaya, B.Yalcinkaya, A.Pazourek, J.Mullerova, M.Stuchlik, J.Maryska. *Int. J. Polym. Sci.*, 4671658 (2016)
340. A.Park, Y.Song, E.Yi, B.T.Duy Nguyen, D.Han, E.Sohn, Y.Park, J.Jung, Y.M.Lee, Y.H.Cho, J.K.Kim. *ACS Biomater. Sci. Eng.*, **6**, 6424 (2020)
341. Z.An, Y.Li, R.Xu, F.Dai, Y.Zhao, L.Chen. *Appl. Surf. Sci.*, **457**, 170 (2018)
342. H.M.Xia, Z.P.Wang, Y.X.Koh, K.T.May. *Lab Chip*, **10**, 1712 (2010)
343. S.V.Kathuria, O.Bilsel, S.Chakravarthy, C.R.Matthews. *Biophys. J.*, **112**, 61a (2017)
344. J.M.Kim, J.Lim, T.R.Lee, S.Park. *J. Korean Phys. Soc.*, **73**, 60 (2018)
345. J.Guzmán, J.H.Lozano-Parada, W.B.J.Zimmerman, S.Lain. *J. Braz. Soc. Mech. Sci. Eng.*, **43**, 29 (2021)
346. A.I.Shallan, Y.Tavares, M.Navvab Kashani, M.C.Breadmore, C.Priest. *Angew. Chem.*, **133**, 2686 (2021)
347. A.Nanda, M.A.Karami. *Proc. ASME*, **50138**, V003T11A015 (2016)
348. S.A.Isaev, M.S.Gritskovich, A.I. Leontyev, O.O.Milman, D.V.Nikushchenko. *Thermophys Aeromechan.*, (5) (2019)
349. S.A.Burtsev, N.A.Kiselev, A.I.Leontiev. *High Temperature*, **52**, 869 (2014)
350. M.S.Kim, S.E.Jo, H.R.Ahn, Y.J.Kim. *Smart Mater. Struct.*, **24**, 065032 (2015)
351. S.K.Si, S.K.Karan, S.Paria, A.Maitra, A.K.Das, R.Bera, A.Bera, L.Halder, B.B.Khatua. *Mater. Chem. Phys.*, **213**, 525 (2018)
352. A.Sasmal, S.K.Medda, P.S.Devi, S.Sen. *Nanoscale*, **12**, 20908 (2020)
353. M.V.Petrovic, F.Cordero, E.Mercadelli, E.Brunengo, N.Ilic, C.Galassi, Z.Despotovic, J.Bobic, A.Dzunuzovic, P.Stagnaro, G.Canu. *J. Alloys Compd.*, **884**, 161071 (2021)
354. A.Ardeshirylajimi, S.M.H.Ghaderian, M.D.Omrani, S.L.Moradi. *Gene*, **676**, 195 (2018)
355. Z.Mokhames, Z.Rezaie, A.Ardeshirylajimi, A.Basiri, M.Taheri, M.D.Omrani. *Int. J. Polym. Mater. Polym. Biomater.*, **70**, 521 (2021)
356. J.Eom, J.Lee, H.Lee, B.Choi. In *The 6th Biomedical Engineering International Conference*. (Vietnam, 2013). P. 1
357. J.S.Agueda, J.Madrid, J.M.Mondragon, J.Lim, A.Tan, I.Wang, N.Duguran, A.Bondoc. *J. Phys.: Conf. Ser.*, **2071**, 012005 (2021)
358. R.Prusa, S.Krizkova, R.Adam, J.Kukacka, T.Eckschlager, J.Janatova, R.Kizek. *Clin. Chem.*, **55**, A39 (2009)
359. J.Salber, Z.Ademovic, D.Klee, H.Höcker, B.Hafemann, N.Pallua. *Eur. Cells Mater.*, **6**, 103 (2003)
360. H.F.Guo, Z.S.Li, S.W.Dong, W.J.Chen, L.Deng, Y.F.Wang, D.J.Ying. *Colloids Surf., B*, **96**, 29 (2012)
361. A.Venault, K.H.Lin, S.H.Tang, G.V.Dizon, C.H.Hsu, I.V.B.Maggay, Y.Chang. *J. Memb. Sci.*, **598**, 117648 (2020)
362. F.Amini, D.Semnani, S.Karbasi, S.N.Banitaba. *Int. J. Polym. Mater. Polym. Biomater.*, **68**, 772 (2019)
363. M.Ansarizadeh, S.A.Haddadi, M.Amini, M.Hasany, A.Ramazani SaadatAbadi. *J. Appl. Polym. Sci.*, **137**, 48916 (2020)
364. A.A.Hussein, O.H.Sabr. *J. Mech. Eng. Res. Dev*, **42**, 23 (2019)
365. M.Mohseni, F.Delavar, H.Rezaei. *J. Macromol. Sci. A*, **58**, 694 (2021)
366. T.S.Tverdokhlebova, L.S.Antipina, V.L.Kudryavtseva, K.S.Stankevich, I.M.Kolesnik, E.A.Senokosova, E.A.Velikanova, L.V.Antonova, D.V.Vasilchenko, G.T.Dambaev, E.V.Plotnikov. *Membranes*, **11**, 21 (2020)
367. J.D.Helmer, K.E.Hughes. *ASAIO J.*, **19**, 382 (1973)
368. G.Gebert, S.M.Friedman. *J. Appl. Phys.*, **34**, 122 (1973)
369. B.Tondu, N.Bardou, S.Mathé. *Adv. Sci. Technol.*, **76**, 264 (2010)
370. Y.Sun, C.Jin, K.Li, Q.Zhang, L.Geng, X.Liu, Y.Zhang. *Exp. Ther. Med.*, **14**, 5289 (2017)
371. Z.Chen, K.Y.Kwon, X.Tan. *Sens. Actuators, A*, **144**, 231 (2008)
372. G.Yang, S.Wang, Y.Chen. *Sens. Lett.*, **9**, 2078 (2011)
373. Y.Kikushima, K.Yuse, Y.Xu, T.Segawa, N.Tanaka. *Proc. SPIE*, **4946**, 88 (2003)
374. Z.Chen, K.Y.Kwon, X.Tan. *Proc. SPIE*, **6932**, 693210 (2008)
375. J.Feng, S.Xuan, L.Ding, X.Gong. *Composites, Part A*, **103**, 25 (2017)
376. S.Goodrich, M.Tawk, W.C.Orr. *Sleep*, **26**, A405 (2003)
377. J.Cuadri, G.Linan, E.Roca, A.Rodríguez-Vazquez, R.Tetzlaff, C.Niederhofer, P.Fischer. *Proc. SPIE*, **5119**, 1 (2005)
378. C.Guigou, C.R.Fuller. *J. Sound Vibrat.*, **220**, 541 (1999)
379. H.He, Y.Fu, W.Zang, Q.Wang, L.Xing, Y.Zhang, X.Xue. *Nano Energy*, **31**, 37 (2017)
380. B.Mahanty, K.Maity, S.Sarkar, D.Mandal. *Mater. Today: Proc.*, **21**, 1964 (2020)

381. S.A.Pullano, I.Mahbub, S.K.Islam, A.S.Fiorillo. *Sensors*, **17**, 850 (2017)
382. Y.Liu, D.Yang, T.Yu, X.Jiang. *Electrophoresis*, **30**, 3269 (2009)
383. S.Liao, J.Sackmann, A.Tollkötter, M.Pasterny, N.Kockmann, W.K.Schomburg. *Microsyst. Technol.*, **23**, 695 (2017)
384. F.Dehghan. Ph.D. University of Saskatchewan, Saskatoon, 2020
385. S.Zhao, M.Wu, S.Yang, Y.Wu, Y.Gu, C.Chen, J.Ye, Z.Xie, Z.Tian, H.Bachman, P.H.Huang. *Lab Chip*, **20**, 1298 (2020)
386. J.C.Hsu, C.L.Chao. *J. Appl. Phys.*, **128**, 124502 (2020)
387. H.Bruus, J.Dual, J.Hawkes, M.Hill, T.Laurell, J.Nilsson, S.Radel, S.Sadhal, M.Wiklund. *Lab Chip*, **11**, 3579 (2011)
388. J.Lei, P.Glynn-Jones, M.Hill. *Microfluid. Nanofluid.*, **21**, 23 (2017)
389. J.Lei, M.Hill, P.Glynn-Jones. *Phys. Rev. Appl.*, **8**, 014018 (2017)
390. S.Liu, G.Xu, Z.Ni, X.Guo, L.Luo, J.Tu, D.Zhang. *Appl. Phys. Lett.*, **111**, 043508 (2017)
391. R.O'Rorke, D.Collins, Y.Ai. *Biomicrofluidics*, **12**, 024104 (2018)
392. Q.Tang, S.Zhou, L.Huang, Z.Chen. *Micromachines*, **10**, 803 (2019)
393. B.Ayan, A.Ozcelik, H.Bachman, S.Y.Tang, Y.Xie, M.Wu, P.Li, T.J.Huang. *Lab Chip*, **16**, 4366 (2016)
394. S.Li, L.Ren, P.H.Huang, X.Yao, R.A.Cuento, J.P.McCoy, C.E.Cameron, S.J.Levine, T.J.Huang. *Anal. Chem.*, **88**, 5655 (2016)
395. H.Cai, Z.Wu, Z.Ao, A.Nunez, B.Chen, L.Jiang, M.Bondesson, F.Guo. *Biofabrication*, **12**, 035025 (2020)
396. H.Cai, Z.Ao, L.Hu, Y.Moon, Z.Wu, H.C.Lu, J.Kim, F.Guo. *Analyst*, **145**, 6243 (2020)
397. Z.Ao, H.Cai, Z.Wu, J.Ott, H.Wang, K.Mackie, F.Guo. *Lab Chip*, **21**, 688 (2021)
398. H.Cai, Z.Ao, Z.Wu, S.Song, K.Mackie, F.Guo. *Lab Chip*, **21**, 2194 (2021)
399. T.Ren, W.Steiger, P.Chen, A.Ovsianikov, U.Demirci. *Biofabrication*, **12**, 025033 (2020)
400. S.Maramizonouz, X.Tao, M.Rahmati, C.Jia, R.Tao, H.Torun, T.Zheng, H.Jin, S.Dong, J.Luo, Y.Fu. *Int. J. Mech. Sci.*, **202**, 106536 (2021)
401. W.Messaoudi, Z.I.Shaghwf, P.Glynn-Jones, M.Hill. *J. Acoust. Soc. Am.*, **141**, 3504 (2017)
402. H.G.T.Foster. Ph.D. University of Southampton, Southampton, 2019
403. A.Fornell, C.Johannesson, S.S.Searle, A.Happstadius, J.Nilsson, M.Tenje. *Biomicrofluidics*, **13**, 044101 (2019)
404. H.Liu, Z.Ao, B.Cai, X.Shu, K.Chen, L.Rao, C.Luo, F.B.Wang, W.Liu, M.Bondesson, S.Guo. *Nano Futures*, **2**, 025004 (2018)
405. T.Cacace, P.Memmolo, M.M.Villone, M.De Corato, M.Mugnano, M.Paturzo, P.Ferraro, P.L.Maffettone. *Lab Chip*, **19**, 3123 (2019)
406. B.Chen, Y.Wu, Z.Ao, H.Cai, A.Nunez, Y.Liu, J.Foley, K.Nephew, X.Lu, F.Guo. *Lab Chip*, **19**, 1755 (2019)
407. J.A.De Lora, F.A.Fencel, A.D.Macias Gonzalez, A.Bandegi, R.Foudazi, G.P.Lopez, A.P.Shreve, N.J.Carroll. *ACS Appl. Bio Mater.*, **2**, 4097 (2019)
408. J.Park, G.Destgeer, M.Afzal, H.J.Sung. *Lab Chip*, **20**, 3922 (2020)
409. Z.Liu, A.Fornell, M.Tenje. *Biomicrofluidics*, **15**, 034103 (2021)
410. P.H.Huang, C.Y.Chan, P.Li., Y.Wang, N.Nama, H.Bachman, T.J.Huang. *Lab Chip*, **18**, 1411 (2018)
411. D.Ahmed, H.S.Muddana, M.Lu, J.B.French, A.Ozcelik, Y.Fang, P.J.Butler, S.J.Benkovic, A.Manz, T.J.Huang. *Anal. Chem.*, **86**, 11803 (2014)
412. M.Gong, T.Li, L.Wu, Z.Zhang, L.Ren, X.Duan, H.Cao, M.Pei, J.J.Li, Y.Du. *Catalysts*, **10**, 1347 (2020)
413. M.M.Binkley, M.Cui, W.Li, S.Tan, M.Y.Berezin, J.M.Meacham. *Phys. Fluids*, **31**, 082007 (2019)
414. N.Hao, P.Liu, H.Bachman, Z.Pei, P.Zhang, J.Rufo, Z.Wang, S.Zhao, T.J.Huang. *ACS Nano*, **14**, 6150 (2020)
415. Z.Mao, P.Li, M.Wu, H.Bachman, N.Mesyngier, X.Guo, S.Liu, F.Costanzo, T.J.Huang. *ACS Nano*, **11**, 603 (2017)
416. R.Tao, G.McHale, J.Reboud, J.M.Cooper, H.Torun, J.Luo, J.Luo, X.Yang, J.Zhou, P.Canyelles-Pericas, Q.Wu. *Nano Lett.*, **20**, 3263 (2020)
417. P.H.Huang, S.Zhao, H.Bachman, N.Nama, Z.Li, C.Chen, S.Yang, M.Wu, S.P.Zhang, T.J.Huang. *Adv. Sci.*, **6**, 1900913 (2019)
418. M.Akella. Ph.D. Iowa State University, Ames, 2019
419. M.Akella, J.J.Juarez. *ACS Omega*, **3**, 1425 (2018)
420. S.Zhao, P.H.Huang, H.Zhang, J.Rich, H.Bachman, J.Ye, W.Zhang, C.Chen, Z.Xie, Z.Tian, P.Kang. *Lab Chip*, **21**, 2453 (2021)
421. P.Szuromi. *Science*, **368**, 727 (2020)
422. J.N.Belling, L.K.Heidenreich, Z.Tian, A.M.Mendoza, T.T.Chiou, Y.Gong, N.Y.Chen, T.D.Young, N.Wattanatorn, J.H.Park, L.Scarabelli. *Proc. Nat. Acad. Sci. USA*, **117**, 10976 (2020)
423. A.Kamenac, F.L.Schilberth, E.Wagner, A.Wixforth, U.Lächelt, C.Westerhausen. *Processes*, **9**, 913 (2021)
424. Y.Gong. *Mol. Ther.*, **28**, 191 (2020)
425. C.Centner, C.Holton, K.Yaddanapudi, T.Roussel, J.A.Kopechek. *J. Acoust. Soc. Am.*, **148**, 2519 (2020)
426. H.Alsadiq, K.Tupally, R.Vogel, G.Kokil, H.S.Parekh, M.Veidt. *Phys. Eng. Sci. Med.*, **44**, 79 (2021)
427. R.K.Patel, M.Priddy, E.Murphy, B.Stamp, C.Centner, P.Bates, K.Yaddanapudi, J.A.Kopechek. *J. Acoust. Soc. Am.*, **148**, 2801 (2020)
428. C.S.Centner, E.M.Murphy, B.F.Stamp, M.C.Priddy, J.T.Moore, P.J.Bates, M.A.Menze, K.Yaddanapudi, J.A.Kopechek. *J. Visual. Exp.*, **167**, 62035 (2021)
429. N.Bose, X.Zhang, T.K.Maiti, S.Chakraborty. *Biomicrofluidics*, **9**, 052609 (2015)
430. Y.Gong, J.Belling, J.Park, T.T.Chiou, N.Chiang, S.De Oliveira, P.S.Weiss, S.Jonas. *Abs. Papers Am. Chem. Soc.*, **258** (2019)
431. I.K.Zervantonakis, C.D.Arvanitis. *Small*, **12**, 2616 (2016)
432. A.Salari, S.Appak-Baskoy, I.R.Coe, J.Abousawan, C.N.Antonescu, S.S.Tsai, M.C.Kolios. *Lab Chip*, **21**, 1788 (2021)
433. V.Revathi, S.D.Kumar, V.Subramanian, M.Chellamuthu. *Eur. Phys. J., Appl. Phys.*, **72**, 20402 (2015)
434. P.Saha, T.Debnath, S.Das, S.Chatterjee, S.Sutradhar. *Mater. Sci. Eng. B*, **245**, 17 (2019)
435. M.Saadatz, M.N.Saadatz, S.Banerjee. *Proc. ASME*, **59438**, V006T06A015 (2019)
436. T.J.Huang. *J. Acoust. Soc. Am.*, **145**, 1786 (2019)
437. *National Research Council. Smart Prosthetics: Exploring Assistive Devices for the Body and Mind: Task Group Summaries*. (Washington: National Academies Press, 2007)
438. O.V.Gradov, M.A.Gradova, I.A.Maklakova, S.N.Kholuiskaya. *Mater. Res. Proc.*, **21**, 370 (2022)
439. O.V.Gradov, M.A.Gradova, S.N.Kholuiskaya, A.A.Olkhov. *IEEE Trans. Plasma Sci.*, **50**, 178 (2022)
440. K.Jorner, A.Tomberg, C.Bauer, C.Sköld, P.O.Norrby. *Nat. Rev. Chem.*, **5**, 240 (2021)
441. C.Adams, D.Tate. *IFIP Adv. Inform. Commun. Technol.*, **304**, 27 (2009)
442. D.Y.Shi, S.Liu. *Key Eng. Mater.*, **450**, 145 (2011)
443. *Organic Ferroelectric Materials and Applications (WP Ser. in Electronic and Optical Materials)*. (Ed. K.Asadi). (Duxford, Cambridge: Elsevier; Woodhead Publishing), 2022
444. S.Sukumaran, S.Chatbouri, D.Roussel, E.Tisserand, F.Thiebaud, T.Ben Zineb. *J. Intell. Mater. Syst. Struct.*, **32**, 746 (2021)

445. X.Zhang, L.Zhang, M.Li, W.Chen, J.Chen, Y.J.Liu, Y.Wang. *Membranes*, **12**, 274 (2022)
446. C.M.Costa, S.Lanceros-Mendez. *Curr. Opin. Electrochem.*, **29**, 100752 (2021)
447. K.Bicy, A.B.Gueye, D.Rouxel, N.Kalarikkal, S.Thomas. *Surfaces Interfaces*, **31**, 101977 (2022)
448. C. Lee, H.Park, J.H.Lee. *Actuators*, **9**, 57 (2020)
449. Y.Wang, L.Zhu, C.Du. *Micromachines*, **12**, 1278 (2021)
450. H.H.Gong, Y.Zhang, Y.P.Cheng, M.X.Lei, Z.C.Zhang. *Chin. J. Polym. Sci.*, **39**, 1110 (2021)
451. A.Gebrekrstos, T.S.Muzata, S.S.Ray. *ACS Appl. Nano Mater.*, **5**, 7632 (2022)
452. H.Abriyanto. *J. Memb.Mater.*, **1**, 1 (2021)
453. L.Wu, Z.Jin, Y.Liu, H.Ning, X.Liu, N.Hu. *Nanotechnol. Rev.*, **11**, 1386 (2022)
454. L.Xie, G.Wang, C.Jiang, F.Yu, X.Zhao. *Crystals*, **11**, 644 (2021)
455. P.Saxena, P.Shukla. *Adv. Comp. Hybrid Mater.*, **4**, 8 (2021)
456. G.Kalimuldina, N.Turdakyn, I.Abay, A.Medeubayev, A.Nurpeissova, D.Adair, Z.Bakenov. *Sensors*, **20**, 5214 (2020)
457. A.Sanyal, S.Sinha-Ray. *Polymers*, **13**, 1864 (2021)
458. K.Reshma, B.Indumathy, R.Gunasekhar, A.P.Arun. *ECS Trans.*, **107**, 13289 (2022)
459. V.H.Malini, B.Indumathy, R.Gunasekhar, A.A.Prabu. *ECS Trans.*, **107**, 14675 (2022)
460. Z.He, F.Rault, M.Lewandowski, E.Mohsenzadeh, F.Salaün. *Polymers*, **13**, 174 (2021)
461. S.A.Pullano, C.D.Critello, M.G.Bianco, M.Menniti, A.S.Fiorillo. *IEEE Trans. Ultrason. Ferroelectr. Freq. Control*, **68**, 2324 (2021)
462. M.A.Al-Harhi, M.Hussain, H.Afzal. *Polymer-Plastics Technol. Mater.*, **60**, 1719 (2021)
463. D.Zou, Y.M.Lee. *Prog. Polym. Sci.*, **128**, 101535 (2022)